NASA CR-134728

BELL AEROSPACE COMPANY DIVISION OF TEXTRON
P. O. Box One Buffalo, New York

CONTRACT NAS3-16798

DEVELOPING A GAS ROCKET PERFORMANCE PREDICTION TECHNIQUE

FINAL REPORT

J. H. Morgenthaler
L. F. Moon
W. R. Stepien

Research and Engineering Department

Period of Performance:

June 1, 1973 to May 30, 1974

Date of Publication:

October 28, 1974

Prepared for NASA-Lewis Research Center
Cleveland, OH 44135

(NASA-CR-134728) DEVELOPING A GAS ROCKET PERFORMANCE PREDICTION TECHNIQUE Final Report, 1 Jun. 1973 - 30 May 1974 (Bell Aerospace Co.) 138 p HC $5.75 CSCL 21H

N75-13927

Unclas
06508

G3/20

1. Report No.	2. Government Accession No.	3. Recipient's Catalog No.
NASA CR-134728		

4. Title and Subtitle	5. Report Date
Developing a Gas Rocket Performance Technique	October 28, 1974
	6. Performing Organization Code

7. Author(s)	8. Performing Organization Report No.
J. H. Morgenthaler, L. F. Moon, W. R. Stepien	D9203-953001
	10. Work Unit No.

9. Performing Organization Name and Address	11. Contract or Grant No.
Bell Aerospace Company P. O. Box One Buffalo, New York 14240	NAS3-16798
	13. Type of Report and Period Covered
	Contractor Report

12. Sponsoring Agency Name and Address	14. Sponsoring Agency Code
National Aeronautics and Space Administration Lewis Research Center Cleveland, OH 44135	

15. Supplementary Notes

Final Report

16. Abstract

A simple, semi-empirical performance correlation/prediction technique applicable to gaseous and liquid propellant rocket engines is presented. Excellent correlations were attained for over 100 test firings by "adjusting" the computation of the gaseous mixing of an unreactive, coaxial jet using a Correlation Factor, F, which resulted in prediction of the experimental combustion efficiency for each firing.

Static pressure, mean velocity and turbulence intensity in the developing region of non-reactive coaxial jets, typical of those of coaxial injector elements were determined. Detailed profiles were obtained at twelve axial locations (extending from the nozzle exit for a distance of five diameters) downstream from a single element of the Bell Aerospace H_2/O_2 19-element coaxial injector. These data are compared with analytical predictions made using both eddy viscosity and turbulence kinetic energy mixing models and available computer codes. Comparisons were disappointing, demonstrating the necessity of developing improved turbulence models and computational techniques before detailed predictions of practical coaxial free jet flows are attempted.

17. Key Words (Suggested by Author(s))	18. Distribution Statement
Combustor Correlation Rocket Performance Prediction Coaxial Jet Mean Velocity Data Turbulence Intensity Data Turbulent Mixing	Unclassified - Unlimited

19. Security Classif. (of this report)	20. Security Classif. (of this page)	21. No. of Pages	22. Price*
Unclassified	Unclassified	138	

* For sale by the National Technical Information Service, Springfield, Virginia 22151

ACKNOWLEDGMENT

The authors are indebted to Dr. Richard J. Priem, NASA-Lewis, and Professor James G. Skifstad, Purdue University, for many helpful discussions and suggestions concerning this Rocket Engine Performance/Prediction Technique and its presentation. They also are indebted to Mr. Owen Fortune, Consultant, who programmed and debugged the computer program for the correlation, and to Sue Feyl, Bell Electronic Data Processing, who made the program operational on the IBM 7090. They are especially indebted to Mr. Lou Montanino, Bell Combustion Devices/Propulsion Systems and Components, who selected and assisted in reducing the performance data correlated herein.

CONTENTS

CONTENTS

TABLES

ILLUSTRATIONS

ILLUSTRATIONS (CONT)

ILLUSTRATIONS (CONT)

ILLUSTRATIONS (CONT)

ABSTRACT

A simple, semi-empirical performance correlation/prediction technique applicable to gaseous and liquid propellant rocket engines is presented. Excellent correlations were attained for over 100 test firings by "adjusting" the computation of the gaseous mixing of an unreactive, coaxial jet using a Correlation Factor, F, which resulted in prediction of the experimental combustion efficiency for each firing.

Static pressure, mean velocity and turbulence intensity in the developing region of non-reactive coaxial jets, typical of those of coaxial injector elements were determined. Detailed profiles were obtained at twelve axial locations (extending from the nozzle exit for a distance of five diameters) downstream from a single element of the Bell Aerospace H_2/O_2 19-element coaxial injector. These data are compared with analytical predictions made using both eddy viscosity and turbulence kinetic energy mixing models and available computer codes. Comparisons were disappointing, demonstrating the necessity of developing improved turbulence models and computational techniques before detailed predictions of practical coaxial free jet flows are attempted.

1. SUMMARY

A simple, semi-empirical performance correlation/prediction technique applicable to gaseous and liquid propellant rocket engines is presented. Excellent correlations were attained by "adjusting" the computation of the gaseous mixing of an unreactive, coaxial jet using a Correlation Factor, F, which resulted in prediction of the experimental combustion efficiency for each firing. The technique was successfully applied to Rocketdyne, Aerojet, TRW, and Bell Aerospace gaseous H_2/O_2 rocket engines utilizing coaxial, triplet, trislot, premix, and reverse flow injector elements, and to Bell's 6000 lb-thrust Orbital Maneuvering and 600 lb-thrust Reaction Control Engines, which utilize triplet and unlike doublet injector elements, respectively, and liquid monomethylhydrazine and nitric oxide propellants.

Test data from over 100 firings, representing a wide range of engine sizes and flow conditions, were compressed when the Correlation Factor, F, times the Chamber Length, L, divided by the "effective" radius, R_1, was plotted versus the ratio of the injection velocity of the fuel divided by the injection velocity of oxidizer. The resulting correlations are useful for comparing the effectiveness of different injectors at the same velocity ratios (which are proportional to the mass flux ratios), for predicting optimum operating conditions for a given injector geometry, and for assessing the consistency of test data. Before liquid rocket and Space Shuttle Main Engine performance predictions can be made with confidence, additional liquid rocket data, covering a wider range of conditions must be correlated.

Static pressure, mean velocity and turbulence intensity in the developing region of non-reactive coaxial jets, typical of those of coaxial injector elements, are presented. Detailed profiles were obtained at twelve axial locations (extending from the nozzle exit for a distance of five diameters) downstream from a single element of the Bell Aerospace H_2/O_2 19-element coaxial injector. Measurements of mass-flux per unit area (using a constant temperature anemometer); total pressure, and local temperature were used in the determination of local static pressure and velocity. These data show a low pressure region exists near the nozzle exit. Although this pressure reduction is small (0.34 psi), it substantially altered the flow development. Comparison of results shows that velocity near the nozzle exit decreased initially (there was no central velocity core) as a result of both pressure gradients and viscous mixing. These data are compared with analytical predictions made using both eddy viscosity and turbulence kinetic energy mixing models and available computer codes. Comparisons were disappointing, demonstrating the necessity of developing improved turbulence models and computational techniques before detailed predictions of practical coaxial free jet flows are attempted.

II. INTRODUCTION

Background

As combustors become more complex and mission considerations require maximum delivered performance, the need for quantitative prediction of performance of advanced propulsion systems becomes increasingly important. In the past, the design and optimization of rocket and ramjet combustors has been accomplished primarily using trial-and-error procedures. Although this approach can be very costly and time consuming, the extremely complex processes - for example, injection, mixing, and combustion - that occur in a practical combustor, and their interactions, have defied detailed analysis leaving little alternative. That is, the turbulent mixing reacting flow field within practical combustors, which consists of unsteady, three-dimensional flows, recirculation regions (at least in the immediate vicinity of the injector), and significant radial and axial pressure gradients, cannot be predicted in detail, e.g., Ref. 1. Therefore, a semi-empirical approach must be used if predictions of the performance of practical combustors are to be made utilizing current limited analytical capabilities, and existing turbulence models, e.g., Ref. 2.

Recent success in the development of a simple empirical eddy viscosity model (3,4,5) suggested that it might be used in a semi-empirical correlation technique based on the rational assumption that the turbulent mixing of reactants is the rate controlling process in combustors employing diffusion flames. If such a correlation technique could be made to work, it would produce design guidance years before the extremely sophisticated computational techniques that are needed to characterize, in detail, the turbulent reacting flows of practical combustors - if indeed they can be! The development of a semi-empirical correlation/prediction technique was the subject of this contract; to assist in the development, various turbulence models were evaluated by comparison of predictions with hot-wire anemometry data.

Objective

The objective of this contract was to obtain a semi-empirical technique for predicting combustor performance (C* efficiency) for gaseous propellants. In order to accomplish this objective, a large number of actual rocket test data, covering a wide range of test conditions and injector geometries, first had to be successfully correlated.

Program Description

The program consisted of applying an existing technique, previously developed at Bell Aerospace Company, Ref. 6, for the prediction of combustion efficiency of gaseous H_2/O_2 rocket

engines utilizing the following types of injectors: coaxial, triplet, trislot, premix, and reverse flow.

In order to better characterize the coaxial injector element, which formed the basis of the technique, detailed flow measurements were made during cold-flow tests of simulated, coaxial injectors using hot-wire instrumentation. These measurements for a coaxial jet in which the outer jet velocity was 700 ft/sec and the central jet velocity 250 ft/sec demonstrated that conventional modeling techniques will not apply; reductions in static pressure of over 0.3 psi occurred in the vicinity of the injection station, and that significant and unexpected radial and axial pressure gradients were present.

Computations also were made using the new Spalding (BRASS) and the Bell Aerospace jet mixing programs, and compared with the data. Agreement with the actual data was not at all good.

A binary (machine language) deck compatible with the 7090/7094 Data Processing System at NASA-LeRC has been prepared for NASA-LeRC.

Because the correlation technique is based on actual experimental data using a semi-empirical approach, it appeared likely that liquid, and liquid/gaseous-fueled rocket engine performance also could be correlated, and ultimately predicted through its application. The technique was successfully applied to the liquid-fueled Bell Aerospace Orbital Maneuvering and Reaction Control Engines, and the liquid/gaseous-fueled Rocketdyne Space Shuttle Main Engine. Although beyond the scope of this contract, results of these analyses are included in this report because of their potential importance.

III. ANALYSIS

Basis for Correlation

The correlation technique was based on the assumption that turbulent mixing alone is the rate controlling process; therefore, the rate of chemical reactions that occur in combustors was assumed to be very fast compared to the mixing rate. Since almost all practical combustors are fueled with extremely reactive propellants, this assumption appears plausable; making it permits engine performance, i.e., combustion efficiency, to be computed without considering the finite-rate chemical kinetics, and resulted in an enormous savings in computer time. A final simplification, which also appeared justified since only an empirical correlation was being sought, was that the stagnation temperature remains constant and equal to the initial (unreacted) propellant temperature before combustion, rather than using a computed temperature based on the extent of the mixing and reaction.

For the practical gaseous H_2/O_2 injectors analyzed, excess hydrogen, required for cooling and performance optimization, was used in each of the injector elements. In such configurations, most of the oxygen ultimately should react with hydrogen from the same element; therefore, the interaction between injector elements could be neglected as a first approximation. Using this assumption permitted the axisymmetric mixing model and numerical integration procedure (discussed below) to be applied directly for the computation of combustor performance; that is, the calculation of the mixing for a single coaxial injector element (or "equivalent" coaxial element for other injector types) could be assumed indicative of each of the injector elements, thereby permitting correlation and prediction of the performance of the overall combustor to be made based on the mixing of a single element.

Of course, performance computed using a mixing model applicable to nonreactive coflowing free jets, without pressure gradients, could not be expected to predict actual rocket engine performance without modification. The approach selected herein was to empirically adjust the values of the eddy viscosity predicted using the mixing model of Ref. 3 (discussed below) by multiplying it by a Correlation Factor, F, which remained constant in each performance calculation, that is, the value of the turbulent mixing coefficient (eddy viscosity) used for the performance calculation became

$$\varepsilon_\eta = F\varepsilon_{model} \tag{1}$$

The value of F was obtained by iteration for a particular set of performance data until

$$\eta_{pred} \approx \eta_{exp} \tag{2}$$

The linearity between F and η_{pred} assisted greatly in obtaining the desired value of η_{pred} which satisfied the inequality

$$\left| \frac{\eta_{pred}}{\eta_{exp}} - 1 \right| \leq 0.001 \tag{3}$$

That is, the value of η_{pred} was within 0.1% of the value of η_{exp} for all the correlations reported herein.

Because the Correlation Factor, F, was empirically determined, it includes a variety of "real-world" effects such as the influence of multiple-jet interaction, heat losses, the interaction of mixing and combustion, and local temperature and density variations. For example, computation of the detailed chemical kinetics requires instantaneous (molecular) concentrations, rather than the time-averaged concentrations. Therefore, even if time-averaged concentrations could be accurately computed, they could not be expected to yield appropriate reaction rates without some empirical modification to either the mean concentration or the chemical kinetic rate constant. Unfortunately, such sophisticated modeling is beyond current capabilities, e.g., Ref. 7.

The important feature of this approach is that it retained the nonlinear effects of both the partial differential equations (shear layer equations), and the mixing model. Using it, correlations applicable over a wider range of combustor variables were anticipated than when using purely empirical correlations alone - for example, data fitting techniques. In particular, better scaling was anticipated using the proposed technique than with previous techniques because the size of the individual injector elements and actual chamber length is used in the calculations rather than, for example, the overall chamber diameter. Note, that the eddy viscosity mixing model upon which the correlation technique is based has been demonstrated to be applicable for conditions covering a reasonably wide range of geometries and velocities; data were used in the model development in which jet areas and velocities varied by factors of 90,000 and 2,500, respectively, Refs. 4, 5.

Of course, a technique in which correlation of an experimentally determined, lumped performance parameter like combustion efficiency is obtained assuming mixing alone to be the rate controlling process, will not predict details of the complex mixing and reacting flow field, such as local velocity, composition, and temperature. Such details only can be computed when each of the processes important in a combustor are included in extremely sophisticated analyses that are beyond current capabilities. Certainly as a minimum in such analyses, the simultaneous turbulent mixing and chemical kinetics and their interactions must be considered, as well as the influences of multiple elements; in addition, recirculation effects also must be considered in such analyses since they provide the source of ignition once combustion has been initiated.

Empirical Axisymmetric Mixing Model

Details of the development of an empirical, mass defect, eddy-viscosity-type, turbulent mixing model that resulted in

correlation of both mean quantities and turbulence parameters has been reported, Refs. 3 to 5. Because an empirical Correlation Factor, F, was to be applied for combustor correlations, the simpler model of Ref. 3 was selected. This model permits prediction of the shear stress at the velocity half width of the jet, which is the point at which the turbulent shear stress approximately reaches its maximum value, and is*

$$\varepsilon_{model} = 0.018 D_{\rho}(1+2f) \frac{\int_0^{\infty} |\rho U - \rho_e U_e| r dr}{r_u + (D-r_u)\exp(-0.115\bar{z})} \qquad (4)$$

The more complex version of the model in Refs. 4 and 5 which predicts radial shear stress distributions as well, was not required in the semi-empirical correlation technique. As a further simplification, no effort was made to model the core region of the coaxial jet separately from the transition region (Figure 2), even though such a distinction must be made in detailed flow analyses, Ref. 4. The relatively simple mass defect model of Eq. (4) was considered adequate for these correlations since a Correlation Factor, F, to be determined empirically, would compensate for the model's lack of generality, as long as the general functional form of the model was valid and mixing is indeed the rate controlling process in combustors employing diffusion flames. That is, all the complex effects which are present in an actual combustor and influence its performance, such as pressure gradients and heat losses, as well as the chemical kinetics, are lumped empirically in the single Correlation Factor, F.

Combustion Efficiency Calculation

In the correlation procedure, the combustion efficiency was computed by considering only the non-reactive mixing of the H_2 and O_2 propellants; no chemical reaction nor change in stagnation temperature was considered. In order to compute the combustion efficiency, η_{pred}, the assumption was made that whenever H_2 and O_2 were mixed locally, the H_2O formed at that point could be computed directly from the limiting constituent. The total mass flow rate of H_2O that resulted from this assumption was determined by numerical integration at each axial station; its division by the maximum mass flow rate of water that could be formed when all

*Symbols are defined in NOMENCLATURE

the O_2 was reacted (since H_2 always was in excess), yielded the predicted combustion efficiency, η_{pred}. Using these assumptions, η_{pred} will increase with axial length, until ultimately it approaches 100%. Although this assumption obviously is not valid in actual combustors, since chemical equilibrium and heat losses prevent attainment of complete reaction (and hence 100% combustion) even for very long chambers, the assumption that η_{pred} increases with increasing chamber length appears reasonable for practical combustors which always are reasonably short. As demonstrated below, these simplifying assumptions, while precluding computation of detailed flow conditions such as local concentration or velocity, do not adversely affect the prediction of combustion efficiency.

The combustion efficiency was computed in the following manner. The local mass fraction of H_2O, Y_{H_2O}, that would have occurred as a result of mixing was computed as

$$Y_{H_2O} = \frac{9}{8} Y_{O_2}, \text{ when } Y_{O_2}/Y_{H_2} \leq 8 \tag{5}$$

$$Y_{H_2O} = 9 Y_{H_2}, \text{ when } Y_{O_2}/Y_{H_2} > 8 \tag{6}$$

For the cases considered, in which H_2 was always in excess, the maximum quantity of water formed was proportional to the initial flow rate of O_2; that is, all the O_2 would ultimately react to form H_2O, so that

$$(\dot{m}_{H_2O})_{max} = \frac{9}{8} (G_{O_2}) \tag{7}$$

Therefore, the overall combustion efficiency at any axial station was computed as

$$\eta_{pred} = \frac{2\pi}{(\dot{m}_{H_2O})_{max}} \int_0^{r_\infty} \rho U Y_{H_2O} r dr \tag{8}$$

where r_∞ is the freestream boundary which defines the extent of the shear layer, i.e., mixing region.

In the computation for η_{pred}, the governing equations of change, which are the shear layer equations, were solved

numerically in von Misses coordinates using a standard explicit finite difference method, similar to that described in Ref. 8. For simplicity, the outer (external) H_2 stream was assumed to be infinite in extent (Figure 2) which was consistent with the assumption of excess H_2. Of course, this meant that the velocity at the outer edge of the hydrogen stream (freestream) always remained constant, and equal to its initial value, which is <u>not</u> the case in an actual coaxial injector element, as demonstrated in the next section of this report. Numerical integration was continued until the length (distance from injector to throat) of the actual combustor being modeled was attained. Mean values of velocity, mass fractions, and static temperature were computed at each grid point in the flows and the value of η_{pred} was computed from these profiles by summation at each axial station using Eq. (8). Computed and measured combustion efficiencies were then compared and an appropriate adjustment of the correlating parameter, F, made, and the entire numerical procedure repeated (starting again at the injection station) until the desired agreement was attained; agreement of 0.1% in η was found to be quite satisfactory for good correlation. Linear interpolation of initial results of η_{pred} versus F reduced the number of iterations needed. The simple computer program used for the correlation required only about one minute on the IBM 360/65 per iteration; four iterations were generally sufficient for convergence. Additional details of the computational procedure are presented in APPENDIX A.

IV. RESULTS AND DISCUSSION

A. Gas Rocket Performance Predictions

The first task of the contract required that 100 data points be selected from Refs. 9 to 13 and correlated as described in the preceding section. The data selected, and approved by the NASA-LeRC Project Manager, are presented in Tables 1 to 5. The data in the tables designated A were taken directly from the various reports (except for the central jet radius R_1 which was computed). The data in the tables designated B summarize the correlation obtained for each case.

The injection velocities for the H_2 and O_2 were computed using the continuity equation and the perfect gas law, e.g., U_{O_2}, the injection velocity of the gaseous O_2 propellant was computed from the relation

$$U_{O_2} = \frac{(GO_2)(R)(T_{O_2})}{(P_c)(MWO_2)(\sum A_{O_2})} \tag{9}$$

A similar computation was made to calculate the injection velocity of the gaseous H_2, U_{H_2}. The velocity ratio, V_R, was simply computed as

$$V_R = \frac{U_{H_2}}{U_{O_2}} \tag{10}$$

The effective radii R_1 and R_2 were computed from the relations

$$R_1 = \left[\frac{(\sum A_{O_2})}{\pi(EL)}\right]^{1/2} \tag{11}$$

$$R_2 = \left[\frac{(\sum A_{H_2})}{\pi(EL)} + R_1^2\right]^{1/2} \tag{12}$$

Note the thickness of the splitter plate was not considered in the computation of R_2 because the coaxial jet (shear layer) computer program cannot handle the recirculation that would be generated in the immediate vicinity of the splitter plate.

Correlation of Data

Applying the correlation technique discussed in ANALYSIS using the Gaseous Hydrogen/Oxygen Rocket Performance Correlation and Prediction Computer Program described in APPENDIX A, resulted in the values of the Correlation Factor, F, and the Correlation Function, $F(L/R_1)$, [which is written $F \cdot L/R_1$] tabulated in the last two columns of the tables designated B. Values of the experimental efficiency were predicted to within ±0.1% using these tabulated values.

The experimentally determined energy release efficiency (or combustion efficiency) is plotted versus the velocity ratio, V_R, in Figs. 3A to 9A for all of the data. The points in these plots show considerable scatter, which was not unexpected, since many different engine geometries and flow conditions were correlated. The scatter of these data illustrates the magnitude of the correlation challenge.

Since an empirical adjustment of the mixing was to be employed in the correlation technique by varying the Correlation Factor, F, computation of the exact experimental combustion efficiency for each particular case always can be achieved. Of course, such agreement is not at all significant unless useful correlation of a reasonably wide range of experimental data is attained - that is, a useful correlation must result in a smooth, continuous Correlation Factor, F, over a range of test conditions at least for similar geometries. Therefore, the value of the proposed correlation technique could not be assessed until a considerable quantity of experimental results had been correlated.

Figures 1B to 9B are plots of the Correlation Factor, F, obtained for each of the injector types again plotted versus V_R. These figures clearly demonstrate that the chamber length, L, (injector to nozzle throat) is an important parameter in this correlation technique. Note, it is not possible to determine whether the velocity ratio or the mass flux ratio are the more basic correlating parameters since these quantities are directly proportional. When the pressure at the injector exit (i.e., P_c) and the temperature of each propellant is equal, the constant of proportionality is merely the molecular weight ratio.

Figure 3C to 9C are plots of the final value of the turbulent viscosity, or turbulent mixing coefficient, ε_η, [defined in Eq. (1)] used in the computation of the combustion efficiency; detailed discussion of the calculations are presented in APPENDIX A. Values of ε_η in these plots vary widely, i.e., from 0.1 to 6 × 10^{-4} lbf-sec/ft^2 (values of $F \cdot L/R_1$ vary only from 3 to 17). Also, the ε_η's exhibit rather irregular, erratic behavior, which clearly illustrates that they would be completely unsatisfactory correlation or prediction parameters. Comparison of values of ε_η with corresponding values of F (Figs. 3B to 9B), and specifically the

Bell Coaxial Injector results of Fig. 9C for L = 4.24 in., conclusively prove their unsuitability. It would be impossible to interpolate with confidence between any of these values in Fig. 9C even in the immediate vicinity of existing points. Note however, that it is the magnitude of the Turbulent Viscosity ε_n, (synonymous with Eddy Viscosity and Turbulent Mixing Coefficient) which is the measure of the mixing that occurs in the actual rocket engine, not F, which merely indicates the extent of the "adjustment" required in ε_{model}, e.g., see Eq. (1).

The general similarity of the shape of the plots of F versus V_R (Figs. 3A to 9A) is very surprising when the great differences in injector geometry and operating conditions are considered. Only a very few points do not seem to correlate consistently, e.g., one of the 6-in. length Rocketdyne Coaxial injector points in Fig. 3B. However, the Energy Release Efficiency of this point, 31H, is considerably higher (2.3 and 4.2%) than adjacent points 25H and 33H, (Table 1A) although conditions for all three of them are nearly identical; therefore, the validity of this data point is questionable. One advantage of this correlation technique is it permits a simple assessment of the consistency of the experimental performance data.

General Correlations

Consideration of the Aerojet Coaxial Injector Data in Fig. 5B suggested that F is inversely proportional to the chamber length, L. The correlation F·L versus V_R was applied to all the data and is presented in Figs. 10A and 10B. However, the values of F·L for the Bell Reverse Flow Injector are almost 10 times as high as for the other four types of injectors (Fig. 10A) and so had to be plotted on a separate figure (Fig. 10B). Nevertheless, considerable consolidation occurred when the parameter F was replaced by F·L. The TRW Triplet Injector Correlation Factor, F, was considerably smaller than the others, as was its "effective" central jet radius, R_1. Comparison of these results with those of the Coaxial Injectors suggested that F is directly proportional to R_1. Results of the F/R_1 correlation of the entire set of data is presented in Fig. 11; again considerable consolidation occurs. In fact, the curve for the TRW Triplet (R_1 = 0.0256 in.) and that of the Rocketdyne Trislot (R_1 = 0.105 in.) both of which have nearly the same length, are practically continuous in Fig. 11; whereas, there is no indication of any correlation of these data in Fig. 10A. Results obtained with the Bell Reverse Flow Injector (R_1 = 0.713 in.) also demonstrate the effectiveness of the F/R_1 parameter. The maximum value of F for this injector is 2.2 as compared with a high of 0.32 for the other four types of injectors; however, values of F/R_1 are only slightly higher for the Reverse Flow Injector than for the others, e.g., 3.0 vs 2.6 $in.^{-1}$, validating the usefulness of the F/R_1 parameter.

The final non-dimensional Correlation Function, $F \cdot L/R_1$ plotted versus V_R, for all the Gaseous H_2/O_2 Rocket Engine performance Data analyzed was presented in Fig. 1. It consists of Correlation Factor F multiplied by L, the chamber length and divided by R_1, the "effective" radius of the central oxygen jet, and is a combination of the F·L and F/R_1 parameters. This function compressed the performance data for all of the injectors including the Bell Reverse Flow injector; it allows direct comparison of the effectiveness of various injector types at a given value of V_R. Of course, values of $F \cdot L/R_1$ at different V_R's cannot be used as a measure of the effectiveness of the mixing any more than can F and for the same reasons.

Figure 1 shows that no single type of injector is best over the entire range of velocity ratios. Also, the functional form of $F \cdot L/R_1$ suggests that within the range of parameters covered by the data, chamber length, L, is directly proportional to the effective radius of the central jet, R_1, for a given level of performance. This tentative conclusion is extremely important and should be verified experimentally. Nevertheless, it is certainly reasonable that improved mixing occurs as R_1 is decreased. In fact, this effect is currently utilized in chemical laser designs, which utilize microjet nozzles to obtain extremely short mixing and reaction lengths.

The role of the Correlation Function appears to be similar to that of the drag coefficient for flow around bodies of various shapes, which predicts the shapes that will exhibit the highest drag at a particular set of flow conditions, i.e., Reynolds number. The Correlation Function, $F \cdot L/R_1$, permits similar comparison of the relative effectiveness of various injector types at a particular V_R because injector geometry is eliminated by this simple non-dimensional parameter. Note, the Reverse Flow correlations were surprisingly consistent with the others in Fig. 1, despite the fact that a single oxygen injector was used with R_1 28 times as large as in the TRW Triplet.

Discussion of General Correlation

One unexpected result is the sharp break in the Correlation Function that occurs at V_R between 8 and 10, which very interestingly occurs very close to the overall stoichiometric ratio of 8 at which the H_2/O_2 completely reacts to form water. This behavior is most evident in Fig. 3B (Rocketdyne Coaxial Injector) in which this transition region is spanned by cases having the same geometry and very similar flow conditions. The most likely reasons for this behavior are:

1) Failure of the mass-defect eddy viscosity mixing model to adequately predict details of the turbulent mixing reacting

flow. The model predicts mixing to be proportional to the quantity,

$$\text{Mass Defect} \equiv \int_0^{r_\infty} |\rho U - \rho_e U_e| r dr \qquad (13)$$

It is unlikely that a complex phenomena such as turbulent mixing will increase linearly with mass defect over the entire range of flow conditions from V_R = 1 to 25. In addition, the density of the propellants at the injection station are proportional to their molecular weights (the molecular weight ratio is 16), and the velocity of the hydrogen is always greater than that of the oxygen (i.e., $V_R > 1$), so that a range of velocity ratios exists (near 16) for which very small mass defect integrals will be computed over a considerable length of the chamber. The singularity that occurs when this integral is zero illustrates a deficiency in the model. Of course, the extent of the mixing that has occurred at a particular axial station influences both the local mean molecular weight, and hence the density, which both decrease with length, as well as the local mean velocity, which increases with length. Analysis of results plotted in Figs. 3C to 9C show that the values of the turbulent or eddy viscosity, ε_η, used in the actual mixing computation are generally near their minimum at $V_R \approx 8$, inspite of the fact that the Correlation Factors, F, are near their maximum. Since $\varepsilon_{model} = \varepsilon_\eta / F$ [Eq. (1)], it is clear that ε_{model} is computed to be far too small in the range $8 < V_R < 10$; hence, F must be sufficiently large to compensate for this defect in the model. The plots of ε_{model} vs axial station, z, presented in APPENDIX A further illustrate this point.

2) The hydrogen stream was assumed to be infinite in extent (see ANALYSIS and APPENDIX A) in the correlation calculation, which means that the velocity of the hydrogen stream at its outer edge (freestream condition) remains constant throughout the calculations. Clearly, such a condition does not exist in a thin coannular jet typical of a coaxial injector in which the velocity decays rapidly, as demonstrated by the experimental velocity data presented herein. The persistence of this high-velocity outer stream in the computation causes the mixing to be over predicted; however, the factor F, must compensate for this effect, since the performance of actual combustors (with a thin annular hydrogen jet) is being computed.

Although the relative importance of each of these effects is uncertain, it is not necessary to understand them in detail, since accurate predictions of the engine performance (combustion efficiency) is obtained with the existing Correlation Function. The fact that practical results can be attained without detailed understanding of all of the physical processes involved is one of the major advantages of a practical semi-empirical approach such as the one presented herein.

Evaluation of Design Parameters

The success attained with the Correlation Function when plotted versus the Velocity Ratio (Fig. 1), suggests that only those quantities explicitly included in these parameters are of major importance, and that all others are of only secondary importance in the prediction of gaseous rocket engine performance. Two of the secondary effects discussed below are the chamber pressure and the film coolant level. Note, variables such as the injector element spacing chamber diameter, nozzle configuration, heat losses, etc., do not appear to be of prime importance, but their significance cannot be assessed directly because they generally are constant for each particular engine, so that there is no simple means for differentiating between them when comparing completely different engines. A test program designed specifically to evaluate these secondary effects would be beneficial. Because of the demonstrated insensitivity of the correlation technique to size, this program could be conducted almost exclusively with small-scale engines.

Those design parameters for which definite conclusions appear justified are summarized below:

1. Velocity Ratio, V_R, has been demonstrated to be the most important parameter in the correlation (e.g., Fig. 1). Note that the mass flux ratio, $(\rho U)_{H_2}/(\rho U)_{O_2}$, is directly proportional to V_R and that the constant of proportionality is $(MW_{H_2})/(MW_{O_2})$ when the static pressure and temperature of each propellant is the same at the injection station. The fact that these ratios are important rather than the magnitude of the actual velocities is initially surprising. Examination of the mass-defect mixing model used in the correlation [Eq. (4)], and consideration of the Species Diffusion, Axial Momentum, and Continuity Equations (APPENDIX A) yields the explanation. If the initial values of both U_{O_2} and U_{H_2} are increased (or decreased) by the same factor, V_R will remain constant; however, the Mass Defect and hence ε_{model}, [Eqs. (4) and (13)], also will be increased (or decreased) by this same factor (as long as the static temperature does not vary significantly). The Continuity Equation requires that the transverse derivative of the radial velocity, and hence the radial velocity itself, increase (or decrease) by the same factor, because the axial and transverse derivatives of the axial velocity, U, both increase (or decrease) by the factor. Therefore, when U_{O_2} and U_{H_2} are varied simultaneously holding V_R constant, every term in the Species Diffusion Equation is multiplied by the factor since the turbulent mass mixing coefficient is computed as $\varepsilon_n/0.7$, and identical concentration profiles are obtained for all species in each case, which yield the same value of η_{pred}. However, every term in the Shear Layer Momentum Equation (when $\partial P/\partial z = 0$) is multiplied by

the square of the factor, because the velocity throughout the flow field is increased (or decreased) by the factor as well as ε_n. Comparison of computer results demonstrated these explanations to be valid.

Therefore, the Velocity Ratio, V_R, rather than the velocity of the individual streams is the critical parameter influencing the computation of η_{pred}. The fact that reasonable correlation of actual rocket test data was achieved with these computations, suggests that they adequately approximate the actual complex processes that occur in combustors employing gaseous fuels when used in conjunction with the empirical Correlation Factors.

2. The Correlation Function, $F \cdot L/R_1$, suggests that the ratio of the chamber length, L, to the "effective" central jet radius, R_1, is the critical geometric parameter in the design of gaseous fueled rocket injectors. This ratio implies that similar performance can be expected from "scaled" combustors of various sizes as long as this ratio remains constant. Of course, such scaling can be expected to apply only over reasonable ranges of combustor dimensions, i.e., those within the range of the test data correlated herein.

3. Chamber Pressure, P_c, was shown to have little influence on the Correlation Factor, F, e.g., Figs. 3B to 9B. In Fig. 9B, a single curve correlated the Bell 9.5-in. length coaxial injector for P_c's ranging from 90 to 260 psia. The overall success of the Correlation Function, $F \cdot L/R_1$ (Fig. 1) implies there is no P_c effect, at least over the range of P_c's from 15 to above 450 psia. The computations are not affected by pressure because when pressure gradients are neglected, the Species Diffusion Equations, Shear Layer Momentum Equation, and Continuity Equation are all independent of pressure, as long as a mass-defect mixing model and the perfect gas law are used to compute ε_{model}. Note, if the flow is assumed to be isoenergetic, the momentum equation is not completely independent of the static temperature (as it is of the pressure), since static temperature depends on the local velocity. However, for subsonic injection velocities, static temperature variation is small and density variations are caused primarily by the molecular weight variation.

4. The Film Coolant was shown to have little effect on the correlations in Figs. 1 and 3B to 9B. In fact, only in Fig. 6B does the Film Coolant Level appear to influence the value of F. As explained in ANALYSIS, all correlations were made neglecting the hydrogen fuel injected in the film barrier, focusing on only a "typical" injector element. Of course, if the combustor design were such that a significant portion of the film coolant were ingested into the combustion zone and reacted, this assumption no longer would be valid. Apparently, such an effect occurred in the Aerojet Premixed Combustor.

In Fig. 1 the solid squares designated Aerojet Premixed (No Coolant) correlate more poorly than any of the other 100 points. Interestingly, the Aerojet Coaxial and the Premix cases in which 20 to 30% of the total hydrogen was injected as film coolant, all correlate reasonably well with a single straight line. Assuming no errors in the reported data, the most reasonable explanation appears to be that high levels of coolant increase mixing (yielding higher values of $F \cdot L/R_1$ at a given V_R) in the Premixed Injector geometry, by causing some of the coolant to react, than occurs in cases in which no film coolant is present. In the Premixed Injector, H_2/O_2 is presumably mixed prior to injection and the likelihood of the hydrogen coolant reacting with the oxygen present in its immediate vicinity (near the wall) is obviously far greater than when each oxygen injector element is completely surrounded (and hence "protected") by an excess of hydrogen, as is the case for most of the other types of injectors. Apparently, without the film coolant to enhance mixing, the Premixed Injector is less effective than the Coaxial Injector. Clearly, additional data should be correlated to confirm the above hypothesis.

Application of Prediction Technique for Performance Optimization

The ultimate application of the Performance Prediction Technique would be for design guidance in the selection of optimum combustor geometries and flow conditions. The Correlation Function, $F \cdot L/R_1$, in Fig. 1 permits an assessment of the H_2/O_2 injector configuration expected to yield the highest performance at the design velocity ratio. Of course, the selection of most efficient injector configuration can only be made from those specific injectors for which correlations already are available. For example, there is no means for determining whether changing the angle of impingement of a Trislot Injector element would improve its effectiveness - unless such an injector were test fired and its combustion efficiency determined experimentally for at least a few velocity ratios (mixture ratios).

Once the type of injector element to be used for a particular application has been selected, the flow conditions that will yield the highest performance and the anticipated overall efficiency are of interest to the designer. The Prediction Technique presented herein may be used to select the flow conditions, e.g., V_R, expected to yield the highest performance. Subsequent hot firings would confirm the predictions and yield additional performance data, that when correlated, would allow refinement of subsequent predictions. Of course, once the velocity of each propellant was selected, the effective radius, R_1, of the central injector could be chosen to achieve the desired mixture ratio.

An example of this procedure, using the Rocketdyne Coaxial Injector and 5-in. chamber is presented in Fig. 12, in which predicted Energy Release Efficiency is plotted versus V_R. In these predictions all input parameters including R_1 were held constant at those values indicated in the figure, except for U_{O_2} which was varied from 118 to 205 ft/sec and the Correlation Factor F, which was taken from the curve of Figs. 3B in which 10 points were very consistently correlated for the Rocketdyne Coaxial Injector with L = 5 in. These data were selected for use in this illustration because the correlation curve contained a maximum, and the effect of this type of correlation on the prediction was of interest. The results in Fig. 12 indicated both a minimum and a maximum in performance is predicted, and that η_{pred} varies between 92 to 96% - a very significant variation in performance. The "S" shape of the curve is undoubtedly caused by the fact that the Correlation Factor was double valued. It would be extremely interesting to test fire this particular engine to determine whether or not both the maximum and minimum performance levels do indeed occur.

Sensitivity of Predictions

The Correlation Factor, F, is the only input parameter not readily determined when making performance predictions (see APPENDIX A). The results presented in Fig. 1 showed that as anticipated in any correlation of experimental data, some scatter occurred about each of the correlation curves. Therefore, it was of interest to determine the significance of a perturbation in F on the predicted value of η. A specific test was made using the Coaxial Injection Data of Rocketdyne Case 12H by changing F ± 4% from the value of 0.185 reported in Table 1B. The ± 4% variation in F resulted in only a ± 0.6% variation in the predicted value of η (ETA PRED), indicating that the variation in η was only about 1/6 the magnitude of the perturbation in the predicted value of η.

These results were typical of those obtained for all the other cases, i.e., the magnitude of the slope $\Delta F/\Delta\eta$ was very nearly constant for all the cases except for the Reverse Flow Injectors. These results demonstrate that reasonably accurate performance predictions can be expected when realistic estimates of the magnitude of F are possible, and that F does not have to be known precisely if estimates of η to within ± 1% are adequate.

Space Shuttle Main Engine

Although there is little interest at present in gaseous H_2/O_2 rocket engines, there is considerable interest in LOX/gaseous H_2 engines since these propellants are used for the Space Shuttle Main Engine (SSME). The SSME is not only very much larger than any of the Reaction Control Engines, i.e., 600 injection elements, 8.9 in. chamber diameter and 14 in. length, but initial designs operated at pressures as high as 3000 psia. Therefore, applying the Performance Correlation/Prediction Technique to this engine was a considerable challenge. Mr. Klaus W. Gross, NASA Marshall Space Flight Center supplied several sets of performance data for various engines in various stages of development. Each data set was correlated by applying the identical technique used for the gaseous H_2/O_2 engines, but the injection velocity of the oxygen was computed assuming the oxygen to be gaseous rather than liquid (see LIQUID ROCKET PERFORMANCE PREDICTIONS).

Detailed results will not be presented because extremely limited test data were available at the time the correlations were made. However, values of F, $F \cdot L$, F/R_1, and $F \cdot L/R$, were all within the range of the data plotted in Figs. 1, 10, and 11. Obviously, definite conclusions cannot be drawn from these preliminary data; however, it is clear that SSME data can be successfully correlated, and meaningful predictions made, once a data base has been established. The fact that P_c and the number of injection elements both were increased nearly an order of magnitude from previous maximum values made little difference in the magnitude of the correlation parameters.

B. Liquid Rocket Performance Predictions

The successful application of the semi-empirical correlation/prediction technique to gaseous H_2/O_2 rockets suggested that it might be applied as well to liquid rockets. Of course, in liquid/liquid rocket engines, droplet formation, injection, penetration, spreading, mixing, burning, and vaporization occur as well as gaseous mixing. Therefore, the magnitude of the "equivalent mixing" of a cold-flow, coaxial gas/gas injector element would be expected to be considerably smaller when applied to liquid/liquid injectors than when applied to gas/gas injectors. However, the correlation/prediction technique, because of its semi-empirical nature, still should be applicable.

To demonstrate this capability, Bell Aerospace Reaction Control Engine (RCE), Ref. 14, and Orbital Maneuvering Engine (OME), Ref. 15, test data were correlated; in each case, the fuel was monomethyl-hydrazine (MMH) and the oxidizer was nitric oxide (N_2O_4). However, two very different types of injector configurations were used in these engines; the RCE elements were unlike doublets, while the OME elements were triplets (two MMH jets impinging at 32° on a central N_2O_4 jet).

In order to demonstrate the applicability of the correlation/prediction technique to liquid propellants as simply as possible (without <u>any</u> modification of the computer program), the calculation of propellant "injection velocities" were made assuming that the propellants were completely vaporized, so that the injection velocities U_{MMH} and $U_{N_2O_4}$ could be calculated combining the Continuity Equation and Perfect Gas Law as in Eq. (9), but using the appropriate molecular weights. Therefore, the velocities computed in this manner are referred to as "pseudo" velocities, since they are purely fictitious. Of course, the actual injection velocity of liquid propellants depends on the density of the liquid and not their molecular weights; however, computation of "pseudo" velocities was the simplest way to apply the technique to liquid rocket data. Since the demonstration calculations were made with the same computer program used for the H_2/O_2 propellants, <u>incorrect</u> molecular weights (i.e., 2.016 and 32.0) and thermodynamic properties were associated with MMH and N_2O_4 in the η_{pred} computations. Nevertheless, because these computations all were made in a consistent manner, the Correlation Factor, F, "adjusted" the mixing [Eq. (1)] to the appropriate level for each experimental firing and excellent correlation of all 21 cases was obtained.

The experimental combustion efficiency data, η_{pred}, is plotted versus the Mixture Ratio, N_2O_4/MMH, in Fig. 13a. The

Mixture Ratio was plotted from right to left so that trends would correspond roughly to the previous plots in which V_R was used as the independent variable. Clearly, attempting to correlate such widely scattered data was a considerable challenge for the correlation/prediction technique. Resulting correlations are presented in Fig. 13b in which the Correlation Factor, F, is also plotted versus the Mixture Ratio, N_2O_4/MMH; these correlations were unexpectedly good. All the points for each type of injector fall on a smooth continuous curve, suggesting that meaningful predictions may be made for liquid propellants as well as for gaseous propellants. Of course, each of the injectors has a very different correlation characteristic because two very different configurations were used. Naturally, a great deal of additional liquid rocket performance data must be correlated for various types of injectors and ranges of flow conditions before predictions can be made except within the rather limited range of the Bell OME and RCE data. Nevertheless, these results suggest that the relative merits of the unlike doublet and triplet be carefully evaluated in subsequent engine development programs.

The final values of the Turbulent Viscosity, ε_η, computed at x = L for the Liquid/Liquid Rocket data are presented in Fig. 14. These results confirm the conclusions concerning Figs. 3C to 9C, i.e., the mixing coefficient itself cannot be used for correlation or prediction of rocket performance data. Of course, some of the variation in Fig. 14 is probably caused by the fact that "pseudo" velocities rather than actual liquid velocities were used. For this same reason, it is not possible to compare the magnitude of the F's for gaseous and liquid injectors and draw any definite conclusions.

C. EXPERIMENTAL COAXIAL JET FLOW CHARACTERIZATION

The Gaseous Rocket Performance Correlation/Prediction Technique presented herein is based on the ability to predict, at least approximately, the non-reactive turbulent mixing that occurs in a coaxial jet. Therefore, it was of considerable interest to characterize such a flow in detail, and to compare the results with predictions made using available computational techniques. In this task, the Bell 19-element Coaxial Injector, which had been previously tested during hot firings was selected to insure that this investigation would be relevant to practical rocket combustors. For simplicity, all elements except for the central element, were masked so that the complex 3-D interaction between elements need not be considered. A photograph of this injector is presented in Fig. 15. A schematic diagram showing the dimensions of the element is shown in Fig. 16. Note, that the splitter plate separating the central and annular jets was recessed 0.03 in. from the injector face.

The motivation for this investigation was twofold: First, because coaxial elements form the basic injection mechanism for many combustors, it was of interest to better characterize the initial flow region of such elements. Second, since computations for reactive systems in the past have often been based on the ability to predict the non-reactive turbulent mixing, it was of interest to characterize such a flow in detail and compare the results with predictions made using available computational techniques.

The measurements presented herein are applicable to the developing region of a coaxial jet in which the injection velocity of the central jet is significantly less than that of the external annular jet. That is, an effort was made to characterize the classical core and transition regions (Fig. 2) of a practical Coaxial Injector Element, in which the velocity ratio, V_R, was 2.8, a value typical of the Coaxial Injectors for which the Correlation/Prediction Technique was applied, e.g., Fig. 1 and Tables 1, 2, and 5.

Several previous experimental investigations have been conducted to characterize the flow field of coaxial jets. Determinations of the mean velocity field obtained using pitot probes are discussed in Refs. 16 to 18. Two more recent investigations have been conducted using hot wire anemometers in which both the mean and turbulence structure of the flow were determined, Refs. 19 and 20. One assumption, which seems to be common to these investigations was that static pressure gradients in the developing region of the flow are small and could be neglected. However, as demonstrated herein, when the velocity ratios, U_o/U_i, are greater than one, and area ratios, A_L/A_i, greater than zero (typical of real combustors), neglecting differences in static pressure in the vicinity of the injector may not be a valid assumption. When using total and static pressure data to calculate mean velocity for incompressible flows, even extremely small changes in static pressure can cause large errors in the velocity determined. These small changes in static pressure do not, however, cause large errors in velocity measured using a hot wire. Using hot wire anemometry, both Champagne and Wygnanski, (19) and Durao and Whitelaw, (20), investigated incompressible coaxial flows where the velocity ratios were greater than one. The measurements of Champagne and Wygnanski were concerned with the developing region of coaxial jets where the initial flows were nearly fully potential and separated by a very thin splitter plate. In contrast, the measurements of Durao and Whitelaw were for fully developed flows with a significant splitter plate thickness.

The present study was concerned with the flow from a coaxial injector element from an actual combustor. As with most practical flow hardware, the nozzle and annulus flows were neither fully potential nor fully developed and the separation distance (splitter plate) was relatively large. Measurements were made for a velocity ratio greater than one and in contrast to previous investigations the velocities were in the compressible range. As noted earlier, these higher velocities are typical of real combustors.

Experimental Procedure

In this experimental investigation, a Bell 19-element coaxial injector, which had been previously tested during hot firings, was selected and all elements except the central one were masked, (13). A photograph of this injector was presented in Fig. 15 and geometrical shape and physical size are shown in Fig. 16. Note, that the splitter plate separating the central jet and annulus was recessed 0.03 in. from the injector face. The constant area inlet length was about 6 diameters for the central nozzle and about 7 nozzle thicknesses for the annulus. Therefore, fully developed turbulent flow conditions were not expected at the injector exit. The area ratio between the outer and inner nozzles, A_o/A_i, was 1.48 and between the splitter plate and central nozzles, A_L/A_i, was 1.02. The ratio of the annulus velocity ($\bar{U}_o$ = 700 ft/sec) to that of the central jet ($\bar{U}_i$ = 250 ft/sec) was equal to 2.8 for all tests. These velocities and dimensions correspond to Reynolds numbers of 3.8 x 10^5 based on diameter for the inner jet and 2.0 x 10^6 based on annulus height for the outer jet and are approximately an order of magnitude larger than those investigated in Ref. 19 and 20.

In these experiments, clean, dry compressed air was supplied at constant pressure and temperature to the two plenum chambers. Plenum pressure was measured on a mercury manometer for the high velocity outer jet and on a precision pressure indicator (T.I.-145) for the low velocity inner jet. Both plenum and room temperature were maintained at 70± 1°F during all tests.

Measurements of mean velocity and turbulence intensity were made using a linearized constant temperature anemometer (TSI-1050). The hot film probe (TSI-1270-10) was calibrated and linearized to 2% of reading over the range 100 to 700 ft/sec. Below 100 ft/sec the error increased becoming about 4% at 50 ft/sec. To assure calibration accuracy, the zero and maximum velocity points were checked before measurements were made at each axial station. The mean value of the linearized signal was determined using a true integrator (DISA-52B30) and displayed on a digital voltmeter (Fluke-8200A). The rms signal was obtained from a true rms meter (TSI-1060).

Total pressure measurements were made using a pitot probe fabricated from a 0.020 in. outside diameter by 0.004 in. wall stainless steel tube with the tip flattened to 0.006 in. inside and ground to 0.010 in. outside height. Pitot pressure was sensed using a precision pressure indicator (TI-145) which was calibrated and shown to have inaccuracies less than ±0.001 psid at the 3 sigma level of confidence. Atmospheric pressure was measured using a similar instrument which had inaccuracies less than ±0.004 psia at the 3 sigma level.

Surveys of the flow field were made by mounting the coaxial injector on a translating table (mill bed) and moving the injector relative to a fixed probe position. By driving the gears of the translating table in only one direction, the displacement of the test nozzle was known accurately to ±0.001 in. Initial location of the probes relative to the coaxial injector was determined using a theodolite.

Detailed velocity and pressure measurements were made along the jet centerline beginning 0.010 in. downstream of the nozzle exit and continuing for 2.50 in. Axial stations at which velocity profiles were obtained are 0.010, 0.030, 0.075, 0.15, 0.25, 0.50, 0.75, 1.00, 1.25, 1.50, 2.00, and 2.50 inches. Pressure profiles were obtained at three axial stations: 0.010, 0.10, and 0.25 inches.

Qualitative Description of Coaxial Jet Mixing

It is helpful in understanding these results to form a picture of the developing flow field. Some of the flow parameters which must be considered are Reynolds numbers, velocity and area

ratios, and state of the flow, i.e., fully viscous or potential like flow. In forming a picture of the flow, first consider conditions where the Reynolds numbers and velocity ratio are high ($Re_o > Re_i > 10^4$, $U_o/U_i > 1$) and where the area of the splitter plate to that of the central nozzle is extremely small, i.e., where the thickness of the plate separating the inner from the outer flow can be neglected, $A_L/A_i \approx 0$. For these conditions and completely viscous flow at the injector exit, velocity at the nozzle centerline must increase due to viscous mixing between the high velocity outer jet and the low velocity inner jet. However, for a condition of potential like flow at the injector exit, velocity along the centerline will remain constant until viscous mixing at the boundary between the two jets has had time to reach the centerline. In other words, a potential core will initially exist the length of which is dependent on both velocity and area ratios as well as the initial thickness of the boundary layers at the nozzle exit. An example of this type flow is discussed in the paper by Champagne and Wygnanski (19).

Now consider for a moment the same flow conditions as above except let the splitter plate have a finite thickness, $A_L/A_i \approx 1$. The flow must now expand to fill the region immediately downstream of this plate. Therefore, a recirculation region will develop which contains two vortices of opposite direction of rotation, see Fig. 17. This recirculation region has approximately the same thickness as the splitter plate at the nozzle exit and tapers to zero at some downstream point. For the condition of a thick splitter plate, as opposed to a negligible one, the momentum transfer is initially from both jets into the recirculation region instead of from the high speed outer jet directly to the low speed inner one. Thus, for completely viscous flow at the nozzle exit the centerline velocity will decrease. Downstream where the recirculation zone ends, the momentum exchange is again from the outer to the inner jet and the centerline velocity will now begin to increase. An example of fully developed jet mixing with a finite splitter plate is discussed in the paper by Durao and Whitelaw (20).

The velocity decay in the early developing region of the flow, the region contained within the recirculation zone, is caused by at least two separate mechanisms: viscous mixing and pressure gradients. To help in understanding the separate effects each of these mechanisms has on the flow development, consider again the flow condition shown in Fig. 17, but in contrast to the earlier example consider the flow at the nozzle exit to be potential with only a thin viscous region at its boundary. If the static pressure were constant everywhere downstream of the nozzle, as in a free jet, then viscous mixing would cause a decrease in velocity near the jet edge but a potential core would exist near the center, i.e., the centerline velocity would remain constant for a short distance downstream. The static pressure is, however, not constant throughout the flow. For conditions where the splitter plate is not negligible, the recirculation zone forms a pseudo-diffuser, causing a low pressure region to exist near the nozzle exit. Within this region lines of constant mass diverge and even for potential like flow velocity decreases almost uniformly across the jet. Viscous effects, which are always present, cause a slightly more rapid decrease in velocity at the jet boundary. For potential flow, where the viscous mixing region at the jet boundary has not spread to the centerline by the time the flow reaches the end of the recirculation zone, the velocity at the centerline will after leaving the zone, remain constant until viscous effects reach the center.

Experimental Results

Due to physical limitations, flows in practical injectors are neither completely potential nor fully developed at the nozzle exit. Experimentally determined initial velocity profiles for one element of the Bell 19-element injector are shown in Fig. 18. Shown in this same figure are power law curves representing a state of fully viscous initial flow. Empirical fits, using experimental data, show that a 1/7th power law gives the best agreement for Reynolds numbers near 3.8×10^5 and that a 1/10th power works best for Reynolds numbers near 2.0×10^6, (21).

A comparison of these curves with the measurements indicates that the flow was not fully developed. Note that a small potential flow region exists near the center of each jet.

An overlay of velocity profiles measured at twelve axial locations is shown in Fig. 19a. Before discussing these data, several comments should be made regarding the hot film used and its sensitivity. First, the power dissipated by the air passing over the heated film depends on both the mass flow rate past the sensor and the temperature difference between the sensor and fluid. Where this temperature difference is held constant, as it was during these measurements, the hot film is primarily sensitive to the fluid mass flow per unit area ρU. For measurements made at the same flow conditions for which a sensor is calibrated, velocity can be determined directly; however, for measurements made at conditions other than those for which it was calibrated, a correction for density must be made. The actual velocity is thus equal to the indicated velocity times the density during calibration divided by the density of the flow being measured, $U = V\rho_c/\rho$. Second, cylindrical hot films are sensitive to flow velocity normal to their axis and almost insensitive to any velocity components along their axis. These films are, however, not sensitive to the direction of flow normal to their axis, i.e., the magnitude of the velocity component normal to the axis is measured and not its direction. Thus, measurements in regions of flow recirculation will be incorrect.

The profiles presented in Fig. 19a show a rapid velocity decrease in the initial region of the central jet owing to both viscous and pressure effects. Since the initial velocity at the nozzle centerline can be considered potential, see Fig. 18, the decrease in velocity between stations z = 0.010 in. and 0.075 in. must be to a large extent due to pressure effects. Evidence of strong viscous effects can also be seen by noting the much more rapid decrease in velocity at the jet boundary when going from z = 0.01 to 0.15 in. This figure indicates that for $z \leq 0.25$ in. the momentum exchange is from both the inner and outer jets into the recirculation zone behind the splitter plate. Somewhere between z = 0.25 and z = 0.50 in. the recirculation zone ends and the momentum transfer is from the high velocity annulus flow directly to the lower velocity inner jet. Also, illustrated by this figure is the tendency for the higher speed annulus flow to collapse around the central jet. A comparison of the peak velocity at z = 0.15, 0.25, and 0.50 in. shows these peaks to be moving toward the nozzle centerline. Figure 19b shows this trend to continue until the flow becomes jet-like somewhere between z = 1.5 and z = 2.0 in. It is also evident from this figure that the velocity near the outer edge of the outer flow, $r \approx 0.22$ in., remains almost constant until the flow becomes jet-like, at which time the velocity across the entire flow field decays with distance. This is seen by noting that the profiles measured at all stations except z = 2.5 in., cross at approximately the same point.

In order to quantify the importance of pressure gradients in the initial regions of the flow, a measure of static pressure was needed. Because direct measurements of static pressure are difficult, if not impossible to make near the exit of such a small injector, an indirect measure was made. In contrast to static pressure, total pressure can be accurately measured for the flow conditions considered here. Measurements of total pressure, P_o, in addition to mass flux per unit area, $\rho\bar{U}$, and total temperature, T_o, are sufficient to evaluate local static pressure. Static pressure at a point can for an ideal gas be written in terms of the local total pressure and Mach number as

$$\frac{P_o}{P} = \left(1 + \frac{\gamma-1}{2} M^2\right)^{\frac{\gamma}{\gamma-1}} \qquad (14)$$

where Mach number is defined by

$$M^2 = \frac{\rho\bar{U}^2}{\gamma P}$$

Mach number can be rewritten in terms of velocity measured using the hot film, $\overline{U} = \rho_c \overline{V}/\rho$, and static pressure as

$$M^2 = \frac{\overline{V}^2}{\gamma R T_o}\left(\frac{P_c'}{P}\right)^2 \left(1 + \frac{\gamma - 1}{2} M^2\right) \tag{15}$$

where the flow temperature is equal to the temperature during calibration. Equations 14 and 15 can now be simultaneously solved for static pressure.

The effect of experimental error when evaluating static pressure can most easily be seen by expanding Eq. 14 for small Mach number.

$$\frac{P_o}{P} = 1 + \frac{\gamma M^2}{2} + \frac{\gamma M^4}{8} + \cdots \tag{16}$$

By substituting Eq. 15 for M^2 one gets a quadratic equation for static pressure, which when solved becomes

$$P = \frac{1}{2}\left\{P_o + \sqrt{P_o^2 - \frac{2P_c'^2}{RT_o}\overline{V}^2\left(1 + \frac{\gamma - 1}{2} M^2\right)\left(1 + \frac{\gamma M^4}{8} + \cdots\right)}\right\} \tag{17}$$

During this investigation, the central jet Mach number was always less than 0.23, therefore, the terms $(\gamma-1)\,M^2/2$ and $\gamma M^4/8$ were neglected and the above equation differentiated to give a simple expression relating static pressure error to errors in measurements of mean velocity and total pressure.

$$\frac{dP}{P} = \left[\frac{|dP_o|}{P_o} + \frac{|d\overline{V}|}{\overline{V}}\right]\left[1 - \frac{2P_c'^2\overline{V}^2}{P_o' RT_o}\right]^{-1/2} - \frac{|d\overline{V}|}{\overline{V}} \tag{18}$$

Evaluation of Eq. 18 for errors of 2% in $\overline{V}$ and 0.25% in P_o show the expected error in static pressure to be less than 0.4%.

Using the hot film and pitot tube data and Eq. 14 and 15, static pressure was determined. The data plotted in Fig. 20 shows static pressure to be approximately 2.5% below ambient at the nozzle exit (14.30 psia compared to 14.64 psia), to increase rapidly and become equal to ambient just beyond z = 0.25 in. (approximately one inner nozzle diameter). Shown in Fig. 21 are three radial pressure profiles The profiles measured at z = 0 01, 0 10 and 0.25 in show static pressure across the central jet to be practically constant. There does appear to be a very slight decrease in pressure near the jet boundary for r = 0.01 in. These figures show axial pressure gradients to be much stronger than the radial ones for the flow contained within the central jet. However, outside this region, in the recirculation zone, radial pressure gradients must be very steep because it is across this very narrow region that the pressure increases to become ambient.

Discussion

Figure 22 has been prepared to show that the static pressure measured at the nozzle exit is of the magnitude one should expect. Shown in this figure is a plot of inner nozzle exit pressure as a function of annulus plenum pressure. With no flow in the central jet, increasing velocity in the annulus causes a nearly linear decrease in pressure at the nozzle exit. Also shown in this figure is one static pressure point measured for a inner jet velocity of 250 ft/sec and an annulus velocity of 700 ft/sec (plenum pressure $\approx$ 10 in. Hg). As expected, the pressure was lowest with no flow in the nozzle and increased with increasing velocity.

Going back to the idea that flow downstream of the splitter plate forms a pseudo-diffuser, one can be integration of the data given in Figs. 19 and 20 establish contours (lines) within which mass is constant and equal to the total flow through the central nozzle. Doing this, one finds that the flow expands approximately 60% of the distance across the splitter plate at the location at which pressure gradients disappear.

Effects of neglecting pressure gradients when evaluating velocity from hot film and pitot tube data can be seen in Fig. 23. Three separate curves of centerline velocity are shown. The velocity curve indicated by open circles is evaluated from hot film data directly while the curve indicated by solid circles is the same data corrected for changes in density (true velocity). Comparison of these curves shows the maximum error in velocity due to neglecting density variations to be less than 3%. The third curve, indicated by diamonds, shows the velocity calculated directly from the total pressure data assuming static pressure everywhere equal to ambient (as is often done in reduction of pitot tube data for coaxial jets). Determination of velocity in this way can result in tremendous errors, e.g., the 2.5% difference in static pressure results in a difference of approximately 40% in calculated velocity. This large error results from taking the difference between pressure ratio and one in contrast to hot wire errors which results from pressure ratio only.

Figure 23 shows not only a rapid decrease in centerline velocity due to both viscous and pressure effects ($z < 0.35$ in.), it also indicates a short region beyond the recirculation zone where the velocity remains constant (0.35 in. $< z <$ 0.55 in.). The reason for this, as has already been explained, is that the growing viscous region has not spread to the centerline before the flow leaves the recirculation zone. The sharp increase in velocity for $z > 0.55$ in. shows that viscous effects have finally reached the centerline. Beyond $z \approx 0.35$ in. and until the flow becomes jet like at $z \approx 2.0$ in., the momentum exchange is directly from the high velocity annulus flow to the lower velocity nozzle flow. There is, of course, during the entire flow development, a viscous region growing at the outer edge of the annulus. Where the ratio of annulus area to central nozzle area, A_O/A_i, is less than one, this viscous mixing region will have a large effect on the flow development.

For $A_O/A_i > 1$, which is the condition considered in this paper, the effect of this viscous region is to cause the flow to become jet-like more rapidly (19).

To demonstrate the accuracy of the velocity measurements, momentum was calculated at each axial measuring station. The percent deviation in momentum from the mean of all measuring stations is shown as a function of axial displacement in Fig. 24. The maximum error over the entire measuring region is less than 2%. Two factors contributing to this small error are the nonlinearity of the hot film response and the finite region over which the momentum integral could be evaluated (the region over which measurements were made). Using this same data, the rate of mass entrainment was determined. It is apparent from Fig. 25 that the rate of entrainment remains almost constant with downstream distance. Comparing this rate with that of a free jet, e.g., see Spalding (22), the coaxial injector corresponds to a free jet with a nozzle diameter of 0.27 in. This

is smaller than the annulus diameter (0.44 in.) and larger than the central nozzle diameter (0.24 in.), thus, the measured entrainment rate is within the expected range.

In addition to mean velocity, axial turbulence intensity was determined at each measuring station. Figure 26 shows an overlay of turbulence intensity profiles measured at seven axial stations. During the early development, three intensity peaks exist, two corresponding to the mixing regions between the recirculation zone and the jets and one corresponding to the mixing region at the outer edge of the annulus. The two peaks downstream of the splitter plate rapidly merge and become one at the end of the recirculation zone. Note that beyond this zone the inner peak decays and moves towards the centerline, becoming jet-like between $z = 1.5$ and 2.0 in. In contrast the outer peak remains at a fixed position, $z \approx 0.22$ in., while decreasing in magnitude (as for a free jet). The change in magnitude of turbulence intensity along the jet centerline can best be seen from Figure 27. Turbulence intensity increases almost linear with distance from the nozzle exit to the end of the region of recirculation, $z < 0.25$ in. For a short distance outside this region, $0.25 < z < 0.45$ in., the intensity remains fairly constant then increases similar to the mean velocity. These regions of similarity, between the centerline velocity and turbulence intensity, do not coincide with one another as can be seen from Figure 28. Shown in this figure are three curves - one for turbulence intensity, one for mean velocity and a third for the ratio of turbulence intensity and mean velocity (relative turbulence intensity). Each of these curves show regions of rapid change in the flow properties with axial displacement. Notice, however, that these regions are different in length as well as being slightly displaced from curve to curve. This is not surprising since turbulence and mean time scales are different.

Figure 29 has been prepared to summarize in a concise way some of the key features of coaxial jet flows where the splitter plate has a finite thickness and where the annulus velocity is greater than the central jet velocity. Shown in this figure are measured velocity profiles plotted as a function of distance from the injector exit. The key features illustrated by this two-dimensional representation of the flow field are: first, the recirculation zone downstream of the splitter plate, second the rapid decrease in velocity of the central jet in this recirculation region owing to both viscous and pressure effects, and third, the eventual collapsing of the annulus flow around the central jet.

D. Analytical Coaxial Jet Flow Characterization

The ability to make meaningful calculations of the performance of rockets and ramjets has been an important goal of Propulsion Engineers for many years. Within the past five years, Chemical Lasers have reinforced this interest, because it has become increasingly apparent that adequate laser design requires the ability to predict in detail both laminar and turbulent flows (including recirculation regions), together with the chemical kinetics, and their complex interactions. At present, adequate design calculations cannot be made using existing computational and modeling techniques, e.g., Ref. 2.

Historically, investigators have been concerned with very simple flows such as single-component, non-reacting boundary layers, and axisymmetric free jets. Of course, when the complexities of turbulence must be included in analyses, the prediction of even such relatively simple flows becomes a formidable computational task. These complexities are compounded when boundary conditions applicable to actual hardware must be considered.

In the Analytical Coaxial Jet Flow Characterization phase of the contract, computations were made using state-of-the art computational and modeling techniques. A simple coaxial geometry was being computed in which no significant density variations occurred. There are two different approaches generally followed for such analyses of turbulent flows: a) an eddy viscosity turbulence model, e.g., Refs. 5, 23, 24, and b) a turbulence kinetic energy turbulence model, e.g., Refs. 25 to 27 and 29. Because operational computer programs were available at Bell Aerospace which used the eddy viscosity model of Ref. 5 and the turbulence kinetic energy approach of Spalding et al, e.g., Ref. 29, these specific models were used for the prediction of the detailed axial velocity distributions for direct comparison with the experimental data previously presented (Section C). Note that the eddy viscosity model of Ref. 5 had been specifically developed for predicting axisymmetric coflowing streams and, therefore, was expected to make predictions as good as any such model.

The computational technique used for the numerical integration of the continuity, momentum, and energy equations was similar to the method used by Zeiberg and Bleich, Ref. 8, i.e., the equations were simplified using boundary layer approximations, the radial velocity was eliminated through use of the von Mises coordinate transformation, and the resulting equations solved by employing an explicit finite difference method. The turbulence kinetic energy (TKE) program and TKE model had been developed by Spalding and coworkers for predicting flows bounded by walls, Refs. 28 and 29. In applying this program to predict coaxial free jet flows, the walls were moved from the coaxial element as

far as possible to minimize their effect on the computations. The predictive technique used, was to transform the separate conservation equations (mass, momentum and energy) into a "standard" set of nonlinear, elliptic, partial differential equations, Ref. 28. The resulting coupled equation set was solved by a finite-difference procedure, using the Gauss-Seidel interactive technique.

Comparison of the predictions obtained with each of these mixing models and the experimental data (Section C) are presented in Figs. 30 to 41. For the eddy viscosity model, predictions were available at the identical axial stations for which data were taken; however, because of the aspect ratio constraints of the grid in the "Spalding" analysis, Ref. 28, identical stations were not available in all cases. In such cases, the axial station closest to that desired was presented as indicated in the figures. Clearly, the agreement obtained with the TKE model and the data would not have been improved by a minor adjustment of the grid spacing.

Both type of predictions were made assuming initial slug (step) profiles at $z=0$ using bulk mean velocities, as discussed in Ref. 4. These comparisons clearly demonstrate that neither type of mixing model is applicable to the coaxial jet flow of a practical coaxial injector. (Features of this flow were discussed in some detail in Section C.) In this particular instance the eddy viscosity mixing model does a far better job than the TKE model, although the mixing rate is underpredicted somewhat by the eddy viscosity model but drastically overpredicted by the TKE model. Note that neither of the analyses account for the transverse pressure gradients that occur in the actual flow which are in part responsible for their failure to predict the detailed behavior.

The eddy viscosity model made no adjustment for the core region, as was found necessary in predicting the data presented in Ref. 4. Had a decreased value of the eddy viscosity been used in the core, a decrease in the predicted rate of mixing would have occurred, and agreement with the experimental data would have been even poorer than presented in Figs. 30 to 41.

Two important features of the eddy viscosity predictions are: 1) The decrease in the central jet velocity at $z < 0.5$ in. is not predicted. Since only momentum transfer between the low-velocity central jet and high-velocity outer jet is considered, no velocities less than that of the original central jet can be computed, and 2) Mixing in the vicinity of the centerline is not sufficiently fast for the velocity maximum to reach the centerline between $z = 1.5$ and 2.0 in. as occurs in the data. In fact, the predictions do not even exhibit a local maximum at the centerline at the 2.5 in. station. The eddy viscosity model of

Ref. 5 had to be multiplied by a factor of 1.7 before the maximum velocity occurred at the centerline at z = 2.5 in. However, in these predictions mixing at most radial positions were much too fast, and jet spreading was predicted to be considerably too great.

Another eddy viscosity model that was operational at Bell was that of Ref. 30. Therefore, it was of interest to compare predictions of this model with that of the model of Ref. 5, that had been under development for several years, e.g., Ref. 3. The predictions made with the model of Ref. 30 were considerably poorer than those using the original model; mixing rates were still further underpredicted; therefore, detailed results are not presented. At the z = 2.5 in. station, the velocity profile still exhibited a local maximum (511 ft/sec) at a radial position of 0.12 in. while the velocity at the centerline was 163 ft/sec lower (348 ft/sec). Therefore, none of the profiles shapes were as valid as those obtained using the model of Ref. 5. Clearly, the model of Ref. 30 is not an improvement over that of Ref. 5 as originally forecast, at least for predicting these coaxial jet data.

The mixing rates predicted with the TKE model and computational technique designated by Spalding as BRASS are much too fast resulting in very rapid velocity decays. The relative influence of the walls which could not be moved out beyond about 3.5 in. without computational instability resulting, and the influence of the TKE model which overpredicted the mixing drastically could not be assessed.

"Adjustment" of the velocity field, i.e., the profile shapes, no doubt could have been made by further modification of the constants of the models. However, such modification was beyond the scope of this work, which had as its objective an evaluation of existing models. Results clearly demonstrate that a new mixing model, or at least drastic revision of existing models, is required before computation of practical coaxial jet flows in which the velocity of the outer jet is significantly greater than that of the central jet, and which contain a splitter plate, can be made with confidence.

V. CONCLUSIONS

A simple, semi-empirical performance correlation/prediction technique applicable to gaseous and liquid propellant rocket engines was presented. Correlations were attained by "adjusting" the computation of the gaseous mixing of an unreactive, coaxial jet using a Correlation Factor, F, which resulted in prediction of the experimental combustion efficiency to within 0.1% for each firing. The technique was successfully applied to Rocketdyne, Aerojet, TRW, and Bell Aerospace gaseous H_2/O_2 rocket engines utilizing coaxial, triplet, trislot, premix, and reverse flow injector elements, and to Bell's 6000 lb-thrust Orbital Maneuvering and 600 lb-thrust Reaction Control Engines, which utilize triplet and unlike doublet injector elements, respectively, and liquid monomethylhydrazine and nitric oxide propellants.

The range of conditions over which the gaseous H_2/O_2 rocket engines were correlated is: Injector elements 7 to 96, Chamber length 3.7 to 8.3 in., L* 7.7 to 57, Chamber pressure 28 to 470 psia, "Effective" radius (R_1) 0.026 to 0.71 in., U_{O_2} 90 to 580 ft/sec, U_{H_2} 520 to 3720 ft/sec, V_R 1.04 to 22.6, η_{exp} 81.6 to 99.5%, Film-coolant level 0 to 30%, O_2/H_2 mass ratio 1.9 to 7.5, F 0.029 to 2.2, and $F \cdot L/R_1$ 3 to 17. For these test data, F was essentially independent of η_{exp}, number of injector elements, chamber pressure, and (except in one injector) film-coolant level.

Predictions of rocket engine performance using the simple unreactive (cold flow), H_2/O_2 mixing calculation require as input: chamber pressure (P_C), length from injector to nozzle throat (L), number of injector elements (EL), and the mass flow rate, injector area, and total temperature of each propellant. An additional input required is the Correlation Factor, F, which can be estimated from plots of $F \cdot L/R_1$ versus velocity ratio, V_R, for the injector configuration of interest.

The success achieved with these simple correlations suggests that key rocket design parameters are: 1) injector configuration, 2) chamber length divided by the "effective" radius of the central oxidizer jet, L/R_1, 3) velocity ratio, V_R, (rather than the actual velocities themselves), and 4) propellant type. The correlation/prediction technique is useful for predicting optimum operating conditions for a given injector geometry, and for assessing the consistency of test data. Before liquid rocket and Space Shuttle Main Engine performance predictions can be made with confidence, additional liquid rocket data, covering a wider range of conditions, must be correlated.

Static pressure, mean velocity and turbulence intensity profiles in the developing region of a non-reactive (air-air) coaxial jet were presented in which $U_o/U_i = 2.8$, typical of

coaxial injector elements. Detailed data were obtained at twelve axial locations (extending from the nozzle exit for a distance of five diameters) downstream from a single element of the Bell Aerospace H_2/O_2 19-element coaxial injector. Measurements of mass-flux per unit area (using a constant temperature anemometer), total pressure, and local temperature were used in the determination of local static pressure and velocity.

Results showed the static pressure decreases in the vicinity of the nozzle exit. Although the pressure reduction was only 0.34 psi, it substantially altered the flow. Velocities in the central jet near the nozzle exit, decreased initially (there was no central velocity core) as a result of both pressure gradients and viscous mixing.

The experimental results were compared with analytical predictions made using eddy viscosity and turbulence kinetic energy mixing models and available computer codes. Comparisons were disappointing, the eddy viscosity model underpredicted the extent of the mixing, especially in the region within the radius of the central jet; whereas, Spalding's TKE model drastically overpredicted the extent of the mixing throughout the flow field. In sum, in practical coaxial injectors: 1) the effects of pressure gradients can significantly influence the mixing and combustion, and 2) present turbulent mixing models and computational techniques are not adequate for predicting the flow in the developing region.

TABLE 1A

ROCKETDYNE PERFORMANCE DATA (REF. 9)

REPORT	INJECTOR TYPE	TEST NO	P_c psia	INJECTOR MIXTURE RATIO O/F	GO_2 FLOW lb/sec	INJECTOR GH_2 FLOW lb/sec	% GH_2 FILM FLOW	TOTAL GH_2 FLOW lb/sec	TOTAL MIXTURE RATIO O/F	ENERGY RELEASE EFF. η	COMB. LENGTH INJ-TH. in.	COMB. L* in.	$\sum A_{O_2}$ CONE IN/OUT $in.^2$	$R_1(O_2)$ CONE IN/OUT in.	$\sum A_{H_2}$ $in.^2$	COMMENTS
NAS CR-120805 Table XXVIII pp. 185-186 Rocketdyne	Concentric, H_2 Annulus-54 Elements (CT-A) Nominal Design Conditions V_f/V_o=8 O/F=6.47 GH_2 Film=18% $T_{O_2}=T_{H_2}$=540°R	1H	310.1	4.84	2.897	.597	0	.597	4.84	95.4	5	14.5	.590/1.182	.0590/.0835	.373	Reference Data for 0% Film (CT-A)
		2H	300.7	6.09	3.025	.497	0	.497	6.09	92.6	5	14.5	.590/1.182	.0590/.0835	.373	
		3H	317.0	5.32	3.007	.565	0	.565	5.32	93.9	5	14.5	.590/1.182	.0590/.0835	.373	
		4H	298.7	3.74	2.448	.655	0	.655	3.74	97.4	5	14.5	.590/1.182	.0590/.0835	.373	
		11H	278.0	4.04	2.245	.556	20.9	.701	3.20	96.5	5	14.5	.590/1.182	.0590/.0835	.373	
		14H	274.8	5.19	2.390	.461	27.3	.634	3.77	95.2	5	14.5	.590/1.182	.0590/.0835	.373	
		15H	277.2	4.41	2.398	.544	9.3	.600	4.00	96.0	5	14.5	.590/1.182	.0590/.0835	.373	
		18H	280.8	3.64	2.269	.624	9.6	.690	3.29	96.8	5	14.5	.590/1.182	.0590/.0835	.373	
		12H	276.0	6.25	2.564	.410	27.8	.568	4.51	92.6	5	14.5	.590/1.182	.0590/.0835	.373	Closer to Design Injector O/F of 6.47
		16H	443.9	6.71	4.162	.621	23.7	.814	5.11	94.2	5	14.5	.590/1.182	.0590/.0835	.373	
		21H	282.1	5.66	2.553	.451	18.7	.555	4.60	95.6	5	14.5	.590/1.182	.0590/.0835	.373	
		23H	280.5	5.68	2.569	.452	17.0	.545	4.72	95.4	5	14.5	.590/1.182	.0590/.0835	.373	
		25H	281.4	6.32	2.608	.413	30.2	.592	4.41	93.1	6	19	.590/1.182	.0590/.0835	.373	
		31H	282.1	5.72	2.570	.450	17.9	.547	4.70	97.3	6	19	.590/1.182	.0590/.0835	.373	
		33H	283.4	5.65	2.564	.454	18.7	.558	4.59	95.0	6	19	.590/1.182	.0590/.0835	.373	
													Equivalent Dimensions*			
pp. 186-187	Trislot Inj. 18 Elements (TS-A) Nominal Design Conditions V_f/V_o=4.2 O/F=6.47 GH_2 Film=18% $T_{O_2}=T_{H_2}$=540°R	46H	294.1	4.47	2.502	.560	19.2	.692	3.62	95.5	5	14.5	.619	.105	.366	
		48H	295.9	6.30	3.003	.477	10.7	.534	5.62	91.4	5	14.5	.619	.105	.366	
		49H	294.8	6.44	2.788	.434	28.9	.608	4.58	91.9	5	14.5	.619	.105	.366	
		50H	294.9	5.16	2.548	.494	30.7	.712	3.58	94.3	5	14.5	.619	.105	.366	
		51H	297.5	7.08	3.016	.426	23.5	.556	5.42	89.6	5	14.5	.619	.105	.366	
		53H	295.7	7.26	3.062	.422	22.2	.542	5.65	89.6	5	14.5	.619	.105	.366	
		59H	299.0	6.65	2.840	.427	30.2	.612	4.64	92.1	6	19	.619	.105	.366	
		60H	298.6	5.30	2.591	.489	32.3	.722	3.59	94.2	6	19	.619	.105	.366	
		64H	301.9	6.47	3.044	.471	10.2	.524	5.81	92.5	6	19	.619	.105	.366	
		65H	299.2	5.32	2.807	.528	10.2	.588	4.78	93.7	6	19	.619	.105	.366	
		67H	304.1	7.48	3.152	.475	16.2	.503	6.26	92.2	6	19	.619	.105	.366	
		69H	301.9	7.23	3.050	.422	21.3	.537	5.68	91.9	6	19	.619	.105	.366	
		62H	293.3	5.99	2.986	.500	0	.500	5.99	93.8	6	19	.619	.105	.366	Reference Data for 0% Film (TS-A)
		76H	294.5	3.51	2.434	.693	0	.693	3.51	97.4	6	19	.619	.105	.366	
		77H	295.2	4.46	2.698	.605	0	.605	4.46	95.4	6	19	.619	.105	.366	
		78H	294.9	5.47	2.913	.532	0	.532	5.47	94.0	6	19	.619	.105	.366	

*Trislot Injector Geometry

	Inner Row (6 elements)	Outer Row (12 elements)	Total (18 elements)
$\sum A_{O_2}$ $in.^2$	.124	.495	.619
$\sum A_{H_2}$ $in.^2$	.073	.293	.366
R_1 in.	.081	.115	.105

TABLE 1B

ROCKETDYNE PERFORMANCE DATA ANALYSIS*

INJECTOR TYPE	TEST NO.	P_c psia	U_{O_2} ft/sec	U_{H_2} ft/sec	V_R	ENERGY RELEASE EFF. η	R_1 in.	R_2 in.	F	$\frac{F \cdot L}{R_1}$
Concentric, H_2 Annulus-	1H	310.1	205	2144	10.450	95.4	.08350	.09572	.19205	11.5000
	2H	300.7	221	1841	8.302	92.6	.08350	.09572	.18469	11.0593
54 Elements	3H	317.0	209	1985	9.495	93.9	.08350	.09572	.19645	11.7635
(CT-A)	4H	298.7	181	2443	13.521	97.4	.08350	.09572	.16268	9.7413
Nominal										
Design	11H	278.0	178	2228	12.515	96.5	.08350	.09572	.16888	10.1126
Conditions	14H	274.8	192	1869	9.747	95.2	.08350	.09572	.20259	12.1311
V_f/V_o = 8	15H	277.2	191	2186	11.464	96.0	.08350	.09572	.17982	10.7677
O/F = 6.47	18H	280.8	178	2475	13.898	96.8	.08350	.09572	.15378	9.2204
GH_2 Film = 18%	12H	276.0	205	1655	8.081	92.6	.08350	.09572	.18545	11.1048
$T_{O_2} = T_{H_2}$ = 540°R	16H	443.9	207	1558	7.540	94.2	.08350	.09572	.18893	11.3132
	21H	282.1	199	1781	8.927	95.6	.08350	.09572	.21140	12.6587
	23H	280.5	202	1795	8.891	95.4	.08350	.09572	.20974	12.5593
	25H	281.4	204	1635	8.003	93.1	.08350	.09572	.15280	10.9796
	31H	282.1	201	1777	8.848	97.3	.08350	.09572	.19202	13.7978
	33H	283.4	199	1784	8.948	95.0	.08350	.09572	.16549	11.8915
Trislot Inj.	46H	294.1	358	2153	6.009	95.5	.10462	.13198	.20489	9.7921
18 Elements	48H	295.9	427	1823	4.264	91.4	.10462	.13198	.11466	5.4798
(TS-A)	49H	294.8	398	1665	4.179	91.9	.10462	.13198	.11541	5.5157
Nominal	50H	294.9	364	1894	5.205	94.3	.10462	.13198	.15679	7.4933
Design	51H	297.5	427	1619	3.792	89.6	.10462	.13198	.09574	4.5756
Conditions	53H	295.7	436	1614	3.700	89.6	.10462	.13198	.09463	4.5226
V_f/V_o = 4.2										
O/F = 6.47	59H	299.0	400	1615	4.036	92.1	.10462	.13198	.09282	5.3233
GH_2 Film = 18%	60H	298.6	365	1852	5.067	94.2	.10462	.13198	.12335	7.0742
$T_{O_2} = T_{H_2}$ = 540°R	64H	301.9	425	1764	4.154	92.5	.10462	.13198	.09692	5.5584
	65H	299.2	395	1995	5.050	93.7	.10462	.13198	.12043	6.9067
	67H	304.1	437	1567	3.590	92.2	.10462	.13198	.08686	4.9815
	69H	301.4	426	1583	3.714	91.9	.10462	.13198	.08705	4.9924
	62H	293.3	429	1928	4.495	93.8	.10462	.13198	.10951	6.2804
	76H	294.5	348	2661	7.643	97.4	.10462	.13198	.26668	15.2942
	77H	295.2	385	2317	6.020	95.4	.10462	.13198	.16808	9.6395
	78H	294.9	415	2040	4.903	94.0	.10462	.13198	.12014	6.8901

*NASA CR-120805, Table XXVIII, pp. 185-186 and pp. 186-187 (Ref. 9)

TABLE 2A

AEROJET INJECTOR PERFORMANCE DATA (REF. 10)

REPORT	INJECTOR TYPE	TEST NO.	P_c psia	INJECTOR MIXTURE RATIO O/F	GO_2 FLOW INC. $\dot{W}_{IGN.}$ lb/sec	INJECTOR GH_2 FLOW INC. $\dot{W}_{IGN.}$ lb/sec	% GH_2 FILM FLOW	TOTAL GH_2 FLOW lb/sec	TOTAL MIXTURE RATIO O/F	ENERGY RELEASE EFF. η	COMB. LENGTH INJ-TH. in.	COMB. L* in.	$\sum A_{O_2}$ CONE IN/OUT $in.^2$	$R_1(O_2)$ CONE IN/OUT in.	$\sum A_{H_2}$ $in.^2$	T_{O_2} °R	T_{H_2} °R	COMMENT
NASA-CR-120895, Vol. I Aerojet pp. V49-V52	Concentric, H_2 Annulus-42 Elements, In Copper Chamber with Spark Igniter	135	313	3.71	4.733	.736	0	.736	3.71	97.1	8.3	25	.898/2.290	.0825/.132	.616	498	508	r series, 0% Film
		136	319	4.95	3.845	.615	0	.615	4.95	97.5	8.3	25	.898/2.290	.0825/.132	.616	498	507	
		137	316	6.05	3.4	535	0	.535	6.05	97.4	8.3	25	.898/2.290	.0825/.132	.616	501	506	
		138	346	5.19	062	.590	30	.836	3.67	97.5	8.3	25	.898/2.290	.0825/.132	.616	496	505	Eval. % H_2 Film
		139	338	5.13	07	.598	20	.740	4.14	97.5	8.3	25	.898/2.290	.0825/.132	.616	497	506	
		142	311	3.88	2.736	.705	0	.705	3.88	96.6	5.5	15	.898/2.290	.0825/.132	.616	498	507	Eval. L* - No. H_2 Film
		143	311	6.21	3.235	.521	0	.521	6.21	96.0	5.5	15	.898/2.290	.0825/.132	.616	498	507	
p. V53	e-Mix S/N5 3" Triplet 72 Elements in Copper Chamber with Spark Igniter	159	310	3.82	2.719	.712	0	.712	3.82	97.5	5.5	15	.8412	.061	.288	492	505	r series, 0% Film
		160	314	4.87	2.984	.613	0	.613	4.87	97.1	5.5	15	.8412	.061	.288	499	506	
		161	313	5.89	3.178	.539	0	.539	5.89	96.7	5.5	15	.8412	.061	.288	507	508	
		167	318	2.97	2.566	.866	0	.866	2.96	98.2	5.5	15	.8412	.061	.288	499	513	
		169	298	4.21	2.612	.621	30	.880	2.97	97.2	5.5	15	.8412	.061	.288	356	519	Eval. % H_2 Film, O_2 Temp.
		170	295	4.24	2.668	.630	20	.780	3.42	97.8	5.5	15	.8412	.061	.288	371	519	
		174	297	5.02	2.786	555	30	.785	3.55	98.0	5.5	15	.8412	.061	.288	365	522	
		171	467	4.72	4.255	.900	30	1.276	3.34	97.8	5.5	15	.8412	.061	.288	341	513	Hi P_c
		175	99	4.91	0.938	.191	30	.271	3.47	99.5	5.5	15	.8412	.061	.288	359	523	Lo P_c
		176	288	4.42	2.675	.606	20	.746	3.59	97.3	5.5	15	.8412	.061	.288	347	289	Low Prop. Temp. @ 20% H_2 Film
		177	284	5.21	2.771	.532	20	.656	4.22	97.8	5.5	15	.8412	.061	.288	363	353	

TABLE 2B

AEROJET PERFORMANCE DATA ANALYSIS*

INJECTOR TYPE	TEST NO.	P_c psia	U_{O_2} ft/sec	U_{H_2} ft/sec	V_R	ENERGY RELEASE EFF. n	R_1 in.	R_2 in.	F	$\frac{F \cdot L}{R_1}$
Concentric, H_2 Annulus- 42 Elements, In Copper Chamber with Spark Igniter	135	313.0	92	1486	16.210	97.1	.13174	.14841	.12367	7.7916
	136	319.0	100	1216	12.133	97.5	.13174	.14841	.17932	11.2347
	137	316.0	108	1066	9.841	97.4	.13174	.14841	.21345	13.4480
	138	346.0	93	1071	11.576	97.5	.13174	.14841	.19000	11.9705
	139	338.0	95	1114	11.714	97.5	.13174	.14841	.18605	11.7217
	142	311.0	92	1430	15.480	96.6	.13174	.14841	.23143	9.6619
	143	311.0	109	1057	9.675	96.0	.13174	.14841	.32032	13.3730
Pre-Mix S/N5 "I" Triplet 72 Elements in Copper Chamber with Spark Igniter	159	310.0	248	3086	12.461	97.5	.06098	.07066	.10185	9.1862
	160	314.0	272	2629	9.658	97.1	.06098	.07066	.13407	12.0922
	161	313.0	295	2328	7.879	96.7	.06098	.07066	.14672	13.2332
	167	318.0	231	3718	16.086	98.2	.06098	.07066	.05432	4.8993
	169	298.0	179	2878	16.070	97.2	.06098	.07066	.09306	8.3934
	170	295.0	193	2949	15.315	97.8	.06098	.07066	.09857	8.8859
	174	297.0	197	2596	13.209	98.0	.06098	.07066	.11938	10.7673
	171	467.0	178	2631	14.753	97.8	.06098	.07066	.10723	9.6714
	175	99.0	195	2685	13.753	99.5	.06098	.07066	.12310	11.1028
	176	288.0	185	1618	8.748	97.3	.06098	.07066	.14245	12.8481
	177	284.0	203	1760	8.656	97.8	.06098	.07066	.15306	13.8050

*NASA CR-120895, Vol. I, Aerojet, pp. V49-V52 and p. V53 (Ref. 10)

TABLE 34

BELL AEROSPACE PERFORMANCE DATA - REVERSE FLOW CHAMBER (REF.11)

REPORT		TEST NO.	P_c psia	MIXTURE RATIO O/F	TOTAL FLOW lb/sec	GO_2 FLOW lb/sec	GH_2 FLOW lb/sec	COMB. EFF. η	COMB. LENGTH, INJ-TH. in.	COMB. L* in.	T_{O_2} °R	T_{H_2} °R	$\sum A_{H_2}$ in.^{2}	V_{H_2} ft/sec	COMMENTS
NASA CR-120881 (Bell 8636-950004)	Reverse Flow, O_2 Swirl Cup	1022	301.5	4.02	3.433	2.749	0.684	94.4	5.66	32	540	540	.445	2100	Baseline Tests at L*=32
	D_1=1.900 in.*	1024	308.0	2.52	3.350	2.398	0.952	96.9	5.66	32	540	540	.445	2100	
		1025	304.1	5.41	3.531	2.980	0.551	97.0	5.66	32	540	540	.445	2100	
	D_2=1.427 in.	1034	302.7	3.05	3.461	2.606	0.855	95.7	6.42	42	540	540	.445	2100	To Evaluate L*=42
	A_s=0.421 in.^{2}	1036	307.3	4.03	3.623	2.902	0.721	94.7	6.42	42	540	540	.445	2100	
	α =28°	1037	294.9	4.43	3.586	2.925	0.661	92.8	6.42	42	540	540	.445	2100	
	C.F.=5% $\dot{W}_{O_2}$	1055	299.4	3.01	3.435	2.579	0.856	93.3	5.54	22	540	540	.445	2100	To Evaluate L*=22
		1056	301.6	4.08	3.500	2.811	0.689	93.4	5.54	22	540	540	.445	2100	
		1058	299.4	4.57	3.533	2.899	0.634	93.6	5.54	22	540	540	.445	2100	
		1064	284.1	3.04	3.594	2.704	0.890	95.7	5.66	32	540	540	.398	2400	To Evaluate M_{H_2}=0.56 @ L*=32
		1065	297.5	4.02	3.856	3.088	0.768	95.2	5.66	32	540	540	.398	2400	
		1067	298.5	4.40	3.863	3.147	0.716	96.4	5.66	32	540	540	.398	2400	
		1069	304.3	2.52	3.820	2.736	1.084	95.8	5.66	32	540	540	.560	1700	To Evaluate M_{H_2}=0.40 @ L*=32
		1070	305.0	3.72	3.924	3.093	0.831	94.7	5.66	32	540	540	.560	1700	
		1071	303.9	4.07	3.959	3.179	0.780	94.3	5.66	32	540	540	.560	1700	

H_2 Injection Station:
40 Slots
0.292 in. wide × .034 (M=.56)
0.292 in. wide × .038 (M=.50)
0.292 in. wide × .048 (M=.40)
@ A_c/A_T=4:1

*Parameters are defined in Fig.7D; C.F. is the center flow

TABLE 38

BELL AEROSPACE PERFORMANCE DATA ANALYSIS**

INJECTOR TYPE	TEST NO.	P_c psia	U_{O_2} ft/sec	U_{H_2} ft/sec	V_R	COMB. EFF. η	R_1* in.	R_2* in.	F	$\frac{F \cdot L}{R_1}$
Reverse Flow,	1022	301.5	149	2110	14.19	94.4	.71343	.80661	1.6330	12.9554
O_2 Swirl Cup	1024	308.0	127	2874	22.64	96.9	.71343	.80661	0.5750	0.4562
D_1 = 1.900 in.*	1025	304.1	160	1685	10.55	97.0	.71343	.80661	2.2078	17.5154
D_2 = 1.427 in.	1034	302.7	140	2627	18.71	95.7	.71343	.80661	0.6658	5.9917
A_s = 0.421 in.^{2}	1036	307.3	154	2182	14.17	94.7	.71343	.80661	1.4280	12.8503
	1037	294.9	162	2085	12.89	92.8	.71343	.80661	1.4108	12.6962
α = 28°	1055	299.4	140	2659	18.93	93.3	.71343	.80661	0.6846	5.3159
C.F. = 5% $\dot{W}_{O_2}$	1056	301.6	152	2125	13.98	93.4	.71343	.80661	1.6162	12.5503
	1058	299.4	158	1969	12.47	93.6	.71343	.80661	1.7540	13.6208
	1064	284.1	155	3257	20.99	95.7	.71343	.79729	0.0578	4.5879
	1065	297.5	169	2684	15.86	95.2	.71343	.79729	1.1255	8.9295
	1067	298.5	172	2494	14.5	96.4	.71343	.79729	1.6650	13.2093
	1069	304.3	147	2633	17.96	95.8	.71343	.82899	0.8645	6.8585
	1070	305.0	165	2013	12.18	94.7	.71343	.82899	1.7872	14.1787
	1071	303.9	171	1897	11.12	94.3	.71343	.82899	1.8820	14.9324

*Computed assuming a single coaxial injector element

**NASA CR-120881 (Bell 8636-950004) (Ref. 11)

TABLE 4A

TRW TRIPLET PERFORMANCE DATA (REF. 12)

REPORT	INJECTOR TYPE	TEST NO.	P_c psia	TRIPLET MIXTURE RATIO[4,5] O/F	TRIPLET GO_2 FLOW[4,6] lb/sec	TRIPLET GH_2 FLOW[4,5,6] lb/sec	TOTAL GH_2 FLOW[1,2] lb/sec	TOTAL GO_2 FLOW[1] lb/sec	TOTAL MIXTURE RATIO[1] O/F	COMB. EFF. η	COMB. LENGTH INJ-TH in.	COMB. L* in.	$\sum A_{O_2}$ in.^{2}	$R_1(O_2)$ in.	$\sum A_{H_2}$ in.^{2}	COMMENTS
NASA CR-120869 Vol. I Table 21 Page 156 Thrust=15 lbf P_c=15 psia O/F = 2.5	Triplet 2 O_2/1 H_2 96 Elements 2 Rows - 48 ea. 20° Impingement Inner Row O_2 Dia.=0.0295" H_2 Dia.=0.0383" Outer Row O_2 Dia.=0.0419" H_2 Dia.=0.0564" 48 H_2 Film Coolent Orifices Dia.=0.0370	331A	14.35	2.091	0.0460	0.0220	0.0295	0.0468	1.584	93.1	3.728	18	0.1975	0.0256	0.2267	Mixture Ratio Series
		331B	14.73	2.107	0.0474	0.0225	0.0301	0.0482	1.600	93.1	3.728	18	0.1975	0.0256	0.2267	
		331C	14.86	3.577	0.0558	0.0156	0.0212	0.0566	2.662	93.5	3.728	18	0.1975	0.0256	0.2267	
		331D	14.78	4.425	0.0593	0.0134	0.0184	0.0601	3.254	93.5	3.728	18	0.1975	0.0256	0.2267	
		331E	14.61	5.440	0.0631	0.0116	0.0161	0.0639	3.963	92.6	3.728	18	0.1975	0.0256	0.2267	
		331F	15.05	5.624	0.0658	0.0117	0.0162	0.0666	4.136	93.4	3.728	18	0.1975	0.0256	0.2267	
		331G	15.15	4.343	0.0608	0.0150	0.0191	0.0616	3.226	93.1	3.728	18	0.1975	0.0256	0.2267	
		331H	15.09	3.566	0.0567	0.0159	0.0216	0.0575	2.655	93.6	3.728	18	0.1975	0.0256	0.2267	

Notes:

1. Includes $\dot{w}_{IGN}$ = 2% × $\dot{w}_T$ at r = 1.0; $\dot{w}_{O_2}$ = $\dot{w}_{H_2}$ = 0.0008 lb/sec.
2. Includes approx. 22.7% × $\dot{w}_{H_2\ TOTAL}$ for film cooling
3. Includes 0.0515 in^2 in 48- 0.0370 dia. film cooling orifices. $\sum A_{H_2}$ for 96 triplets = 0.1752 in.^{2} (Triplets Only)
4. Excludes $\dot{w}_{IGN}$ flow
5. Excludes $\dot{w}_{H_2}$ film coolant flow
6. Assume ambient propellants for all tests at 540°R

TABLE 4B

TRW TRIPLET PERFORMANCE DATA ANALYSIS*

INJECTOR TYPE	TEST NO.	P_c psia	U_{O_2} ft/sec	U_{H_2} ft/sec	V_R	COMB. EFF. η	R_1 in.	R_2 in.	F	$\frac{F \cdot L}{R_1}$
Triplet	331A	14.4	423	3621	8.56	93.1	.02559	.03515	.06572	9.5742
2 O_2/1 H_2	331B	14.7	425	3608	8.49	93.1	.02559	.03515	.06610	9.6296
96 Elements	331C	14.9	496	2480	5.00	93.5	.02559	.03515	.04107	5.9832
2 Rows - 48 ea.	331D	14.8	530	2142	4.04	93.5	.02559	.03515	.03225	4.6982
20° Impingement <	331E	14.6	570	1876	3.29	92.6	.02559	.03515	.02933	4.2728
Inner Row	331F	15.1	577	1836	3.18	93.4	.02559	.03515	.03025	4.4069
O_2 Dia. = 0.0295"	331G	15.2	530	2183	4.12	93.1	.02559	.03515	.03396	4.9474
H_2 Dia. = 0.0383"	331H	15.1	496	2489	5.02	93.6	.02559	.03515	.04149	6.0443
Outer Row										
O_2 Dia. = 0.0419"										
H_2 Dia. = 0.0564"										
48 H_2 Film										
Coolant Orifices Dia. = 0.0370										

*NASA CR-120869, Vol. I, Table 21, Page 156, Thrust = 15 lbf, P_c = 15 psia (Ref. 12)

TABLE 5A

BELL PERFORMANCE DATA - COAXIAL INJECTORS (REF.13)

REPORT	INJECTOR TYPE	TEST NO.	P_c psia	INJ. MIXTURE RATIO O/F	GO_2 FLOW lb/sec	GH_2 FLOW lb/sec	COMB. EFF. η	COMB. LENGTH INJ-TH in.	COMB L^* in.	T_{O_2} °R	T_{H_2} °R	$\sum A_{O_2}$ in^2	$\sum A_{H_2}$ in^2	$R_{1(O_2)}$	COMMENTS
R&D Model 8618 O_2/H_2 Coaxial Inj. 200LB-F,250 P_c	Coaxial, H_2 Annulus 19 Elements Nominal Conditions O/F=3.0 V_{O_2}=250 ft/sec V_{H_2}=750 ft/sec V_F/V_O=3.0 T=530°R	874	93.3	1.140	0.4894	0.4285	92.4	5.6	33	530	532	0.842	1.287	.119	Ratio Series in 33L* Chamber to Evaluate V_F/V_O
		875	93.6	1.290	0.5235	0.4054	90.7	5.6	33	530	532	0.842	1.287	.119	
		876	89.4	1.540	0.5459	0.3539	87.7	5.6	33	530	532	0.842	1.287	.119	
		877	92.7	1.820	0.6095	0.3346	86.0	5.6	33	530	530	0.842	1.287	.119	
		878	94.3	2.130	0.6682	0.3139	83.6	5.6	33	525	527	0.842	1.287	.119	
		879	90.1	2.700	0.7004	0.2597	81.6	5.6	33	528	527	0.842	1.287	.119	
		880	94.8	1.150	0.4863	0.4222	95.1	9.5	57	520	527	0.842	1.287	.119	Attempt to Increase Performance in 57L* Chamber
		881	92.3	1.471	0.5489	0.3725	89.0	9.5	57	519	520	0.842	1.287	.119	
		882	104.7	1.971	0.6682	0.3383	91.4	9.5	57	519	519	0.842	1.287	.119	
		883	102.4	2.460	0.7112	0.2886	89.2	9.5	57	519	515	0.842	1.287	.119	
		888	145.2	1.570	0.8635	0.5235	90.1	9.5	57	520	522	0.842	1.287	.119	To Evaluate Higher P_c
		889	127.8	2.690	0.8935	0.3090	90.6	9.5	57	518	520	0.842	1.287	.119	
		890	157.9	2.625	1.0922	0.3920	91.1	9.5	57	518	520	0.842	1.287	.119	
		891	259.0	2.155	1.6881	0.7834	91.6	9.5	57	514	524	0.842	1.287	.119	To Evaluate Higher P_c
		892	263.0	2.610	1.8235	0.6987	90.9	9.5	57	512	523	0.842	1.287	.119	
		894	257.5	3.430	1.9616	0.5716	89.0	9.5	57	500	513	0.842	1.287	.119	
		895	256.8	4.100	2.0780	0.5064	88.8	9.5	57	498	511	0.842	1.287	.119	
		896	255.1	4.460	2.1430	0.4803	87.9	9.5	57	497	510	0.842	1.287	.119	
R&D Model 8616 - Low Pressure Gaseous O_2/H_2 Engine	Coaxial, H_2 Annulus- 7 Elements Config. C $T_{O_2}=T_{H_2}$= Nominal 530°R	818	44.3	4.80	0.273	0.0568	86.0	4.24	7.74			0.327	0.960	.123	To Evaluate Lower L^*
		824	45.0	4.00	0.256	0.0640	86.6	4.24	7.74			0.327	0.960	.123	
		826	47.8	2.90	0.242	0.0835	88.7	4.24	7.74			0.327	0.960	.123	
		827	49.7	1.93	0.214	0.1110	92.8	4.24	7.74			0.327	0.960	.123	
		831	29.1	5.17	0.186	0.0358	85.7	4.24	7.74			0.327	0.960	.123	To Evaluate Lo P_c at Lo L^*
		832	29.4	3.86	0.168	0.0435	87.2	4.24	7.74			0.327	0.960	.123	
		833	28.6	2.90	0.146	0.0508	87.2	4.24	7.74			0.327	0.960	.123	
		834	29.7	2.03	0.132	0.0651	90.6	4.24	7.74			0.327	0.960	.123	

TABLE 5B

BELL PERFORMANCE DATA ANALYSIS*

INJECTOR TYPE	TEST NO.	P_c psia	U_{O_2} ft/sec	U_{H_2} ft/sec	V_R	COMB. EFF. η	R_1 in.	R_2 in.	F	$\frac{F \cdot L}{R_1}$
Coaxial,	874	93.3	159	1455	9.13	92.4	.11877	.18886	.24391	11.5003
H_2 Annulus	875	93.6	170	1372	8.07	90.7	.11877	.18886	.21285	10.0359
19 Elements	876	89.4	186	1254	6.76	87.7	.11877	.18886	.13510	6.3700
Nominal	877	92.7	200	1139	5.70	86.0	.11877	.18886	.10613	5.0040
Conditions	878	94.3	213	1045	4.90	83.6	.11877	.18886	.08762	4.1313
O/F = 3.0	879	90.1	235	905	3.84	81.6	.11877	.18886	.07065	3.3311
V_{O_2} = 250 ft/sec	880	94.8	153	1398	9.14	95.1	.11877	.18886	.14403	11.5205
V_{H_2} = 750 ft/sec	881	92.3	177	1250	7.06	89.0	.11877	.18886	.08545	6.8349
	882	104.7	190	999	5.26	91.4	.11877	.18886	.07091	5.6718
V_F/V_O = 3.0	883	102.4	207	864	4.18	89.2	.11877	.18886	.05312	4.2489
T = 530°F	888	145.0	177	1121	6.32	90.1	.11877	.18886	.07876	6.2997
	889	128.0	208	749	3.61	90.6	.11877	.18886	.05315	4.2513
	890	158.0	205	769	3.74	91.1	.11877	.18886	.05588	4.4696
	891	259.0	192	944	4.91	91.6	.11877	.18886	.06780	5.4231
	892	263.0	204	827	4.06	90.6	.11877	.18886	.05801	4.6400
	894	258.0	218	678	3.10	89.0	.11877	.18886	.04751	3.8082
	895	257.0	231	600	2.60	88.8	.11877	.18886	.04526	3.6202
	896	255.0	239	572	2.39	87.9	.11877	.18886	.04335	3.4674
Coaxial,	818	44.0	482	543	1.13	86.0	.12194	.24192	.09140	3.1781
H_2 Annulus-	824	45.0	445	602	1.35	85.6	.12194	.24192	.09210	3.2024
7 Elements	826	48.0	396	739	1.87	88.7	.12194	.24192	.10423	3.6242
Config. C	827	50.0	337	945	2.80	92.8	.12194	.24192	.14121	4.9100
$T_{O_2} = T_{H_2}$ =	831	29.0	500	521	1.04	85.7	.12194	.24192	.09490	3.2998
Nominal 530°R	832	29.0	447	626	1.40	87.2	.12194	.24192	.09377	3.2605
	833	29.0	399	752	1.88	87.2	.12194	.24192	.09965	3.4649
	834	30.0	348	927	2.67	90.6	.12194	.24192	.12234	4.2539

*Bell IR&D Model 8618 - High Pressure Gaseous H_2/O_2 and Bell IR&D Model 8616 - Low Pressure Gaseous H_2/O_2 (Ref. 13)

FIGURE 1. CORRELATION FUNCTION FOR GASEOUS H_2/O_2 ROCKET ENGINE PERFORMANCE

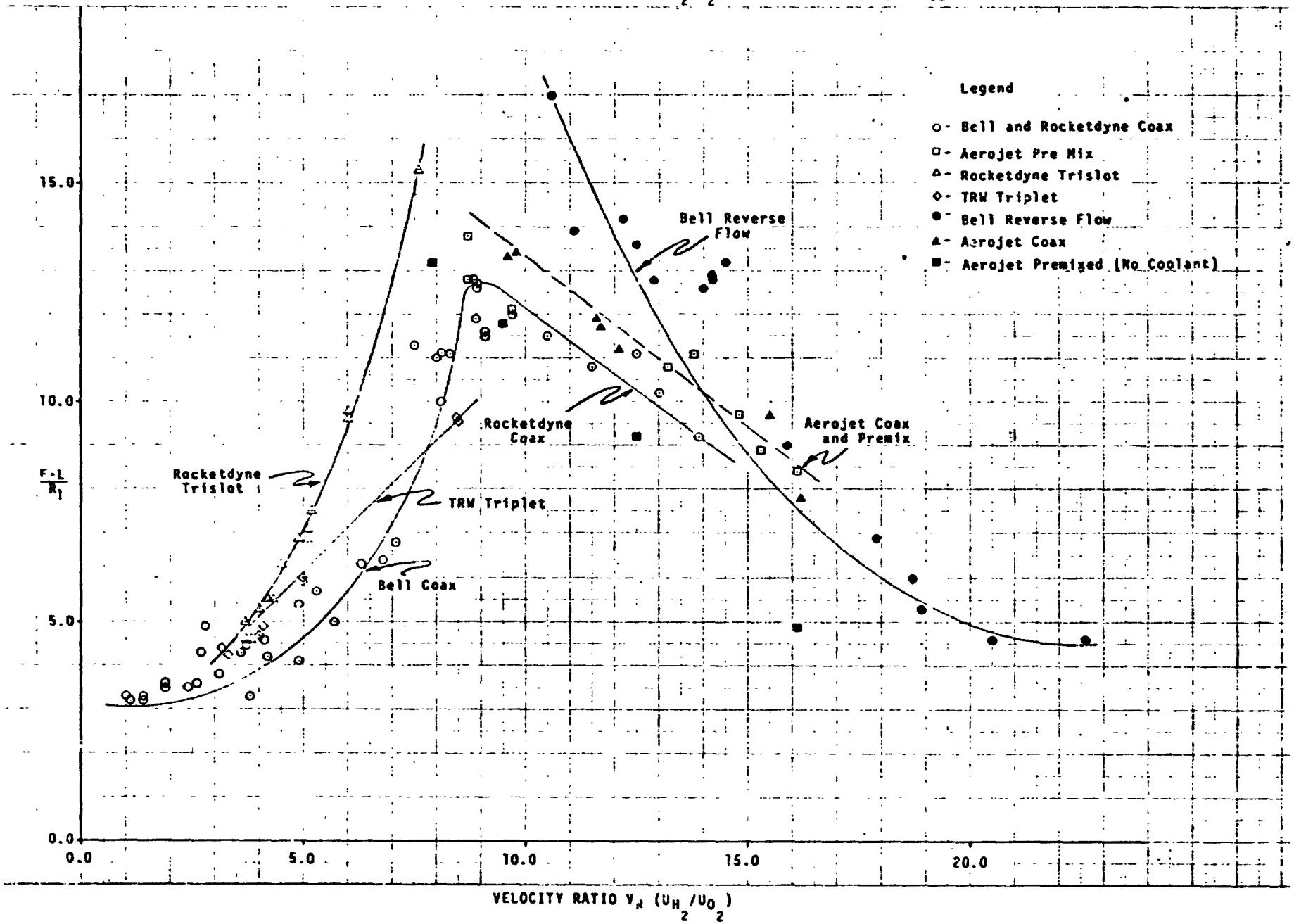

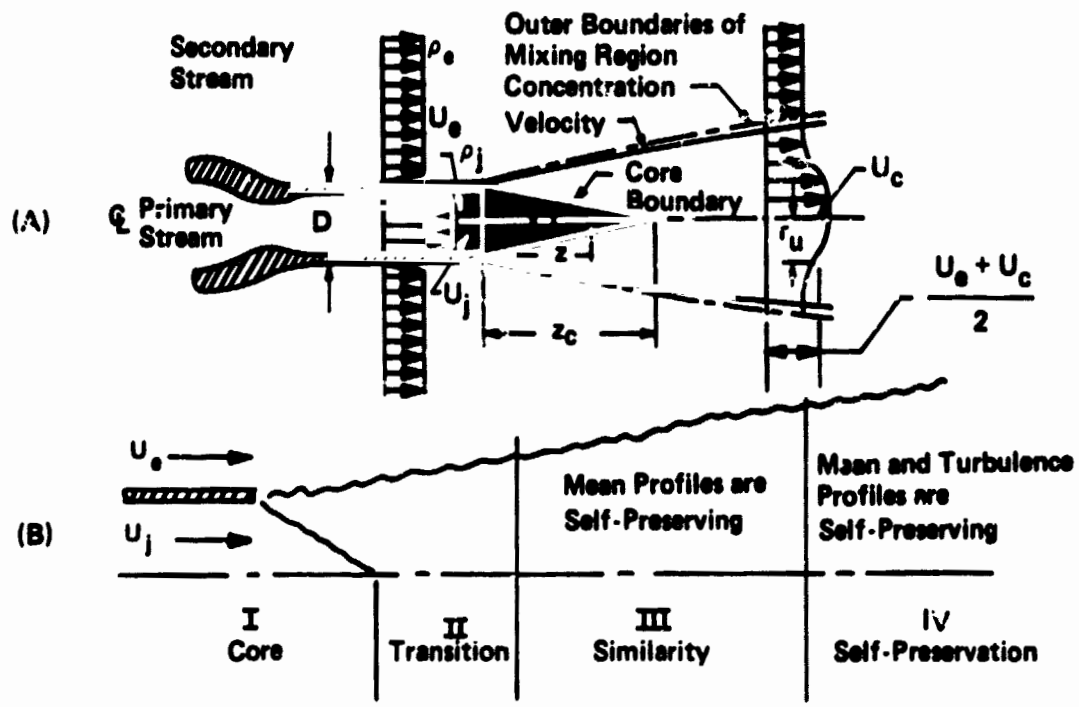

FIGURE 2. Schematic of Coaxial Turbulent Jet and Definition of Mixing Regions

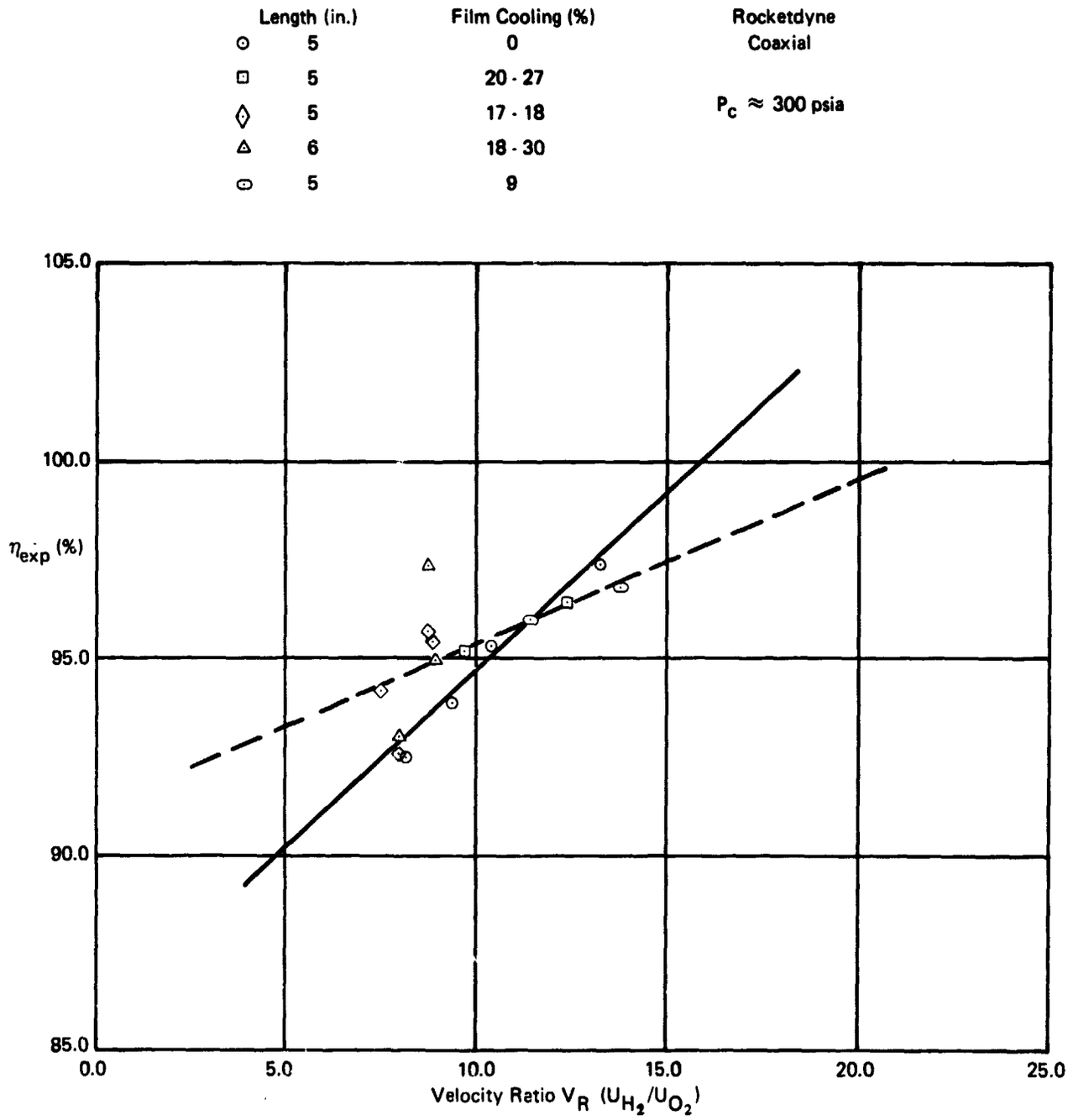

Figure 3A. Rocketdyne Coaxial Injector Performance Data
Reference 9

FIGURE 3B. CORRELATION OF ROCKETDYNE COAXIAL INJECTOR PERFORMANCE DATA

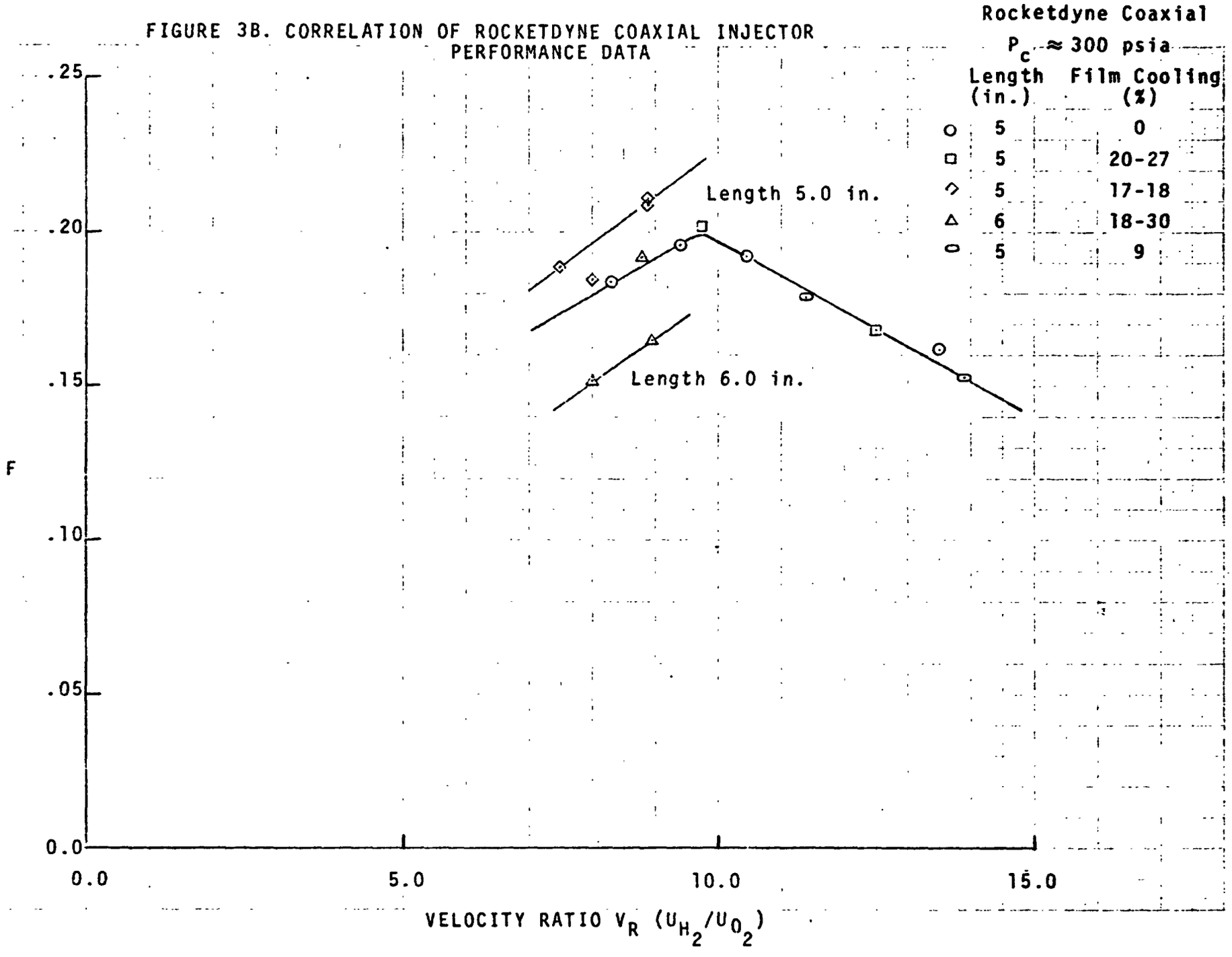

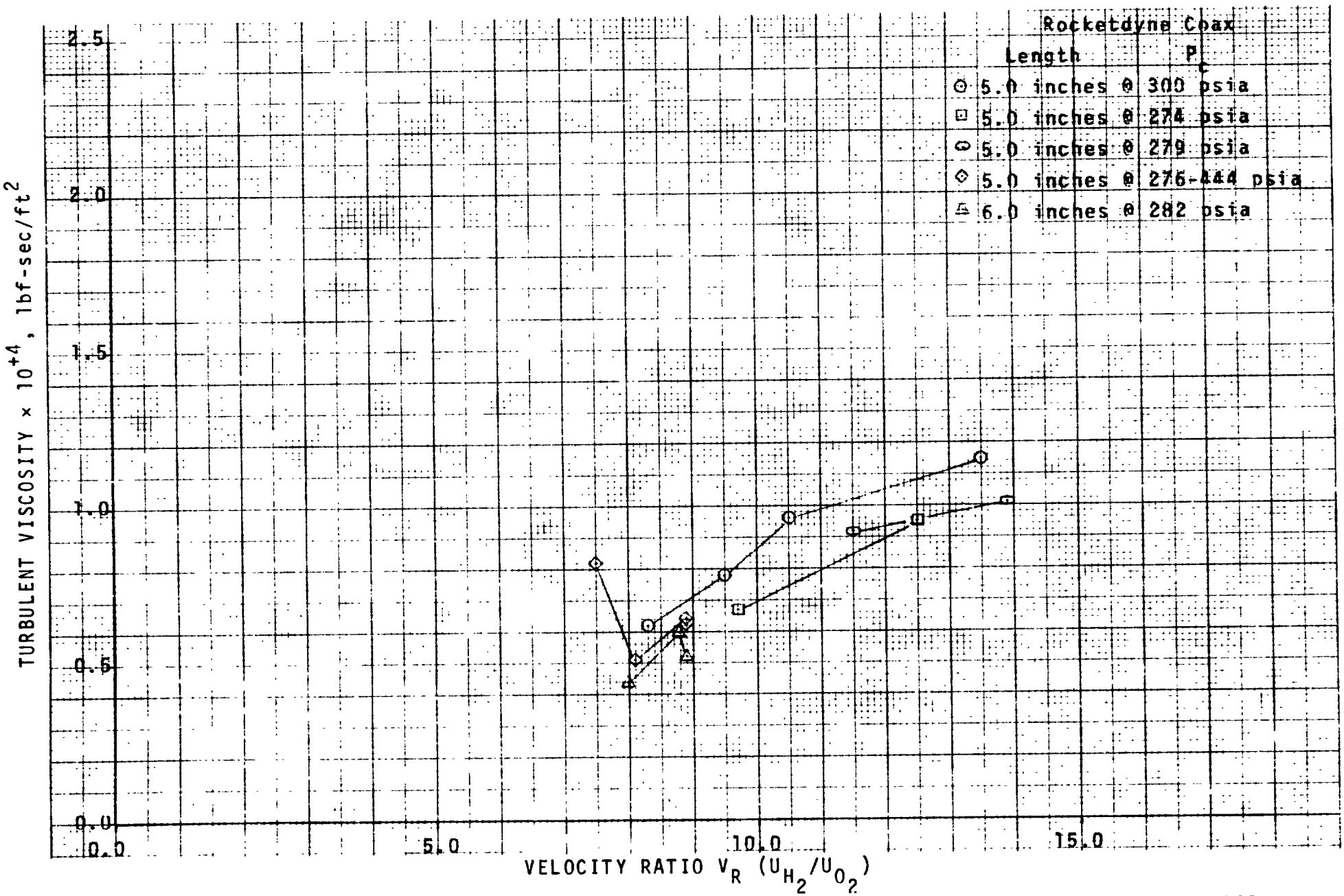

FIGURE 3C. FINAL VALUE OF TURBULENT (EDDY) VISCOSITY, ε_η. ROCKETDYNE COAXIAL INJECTOR

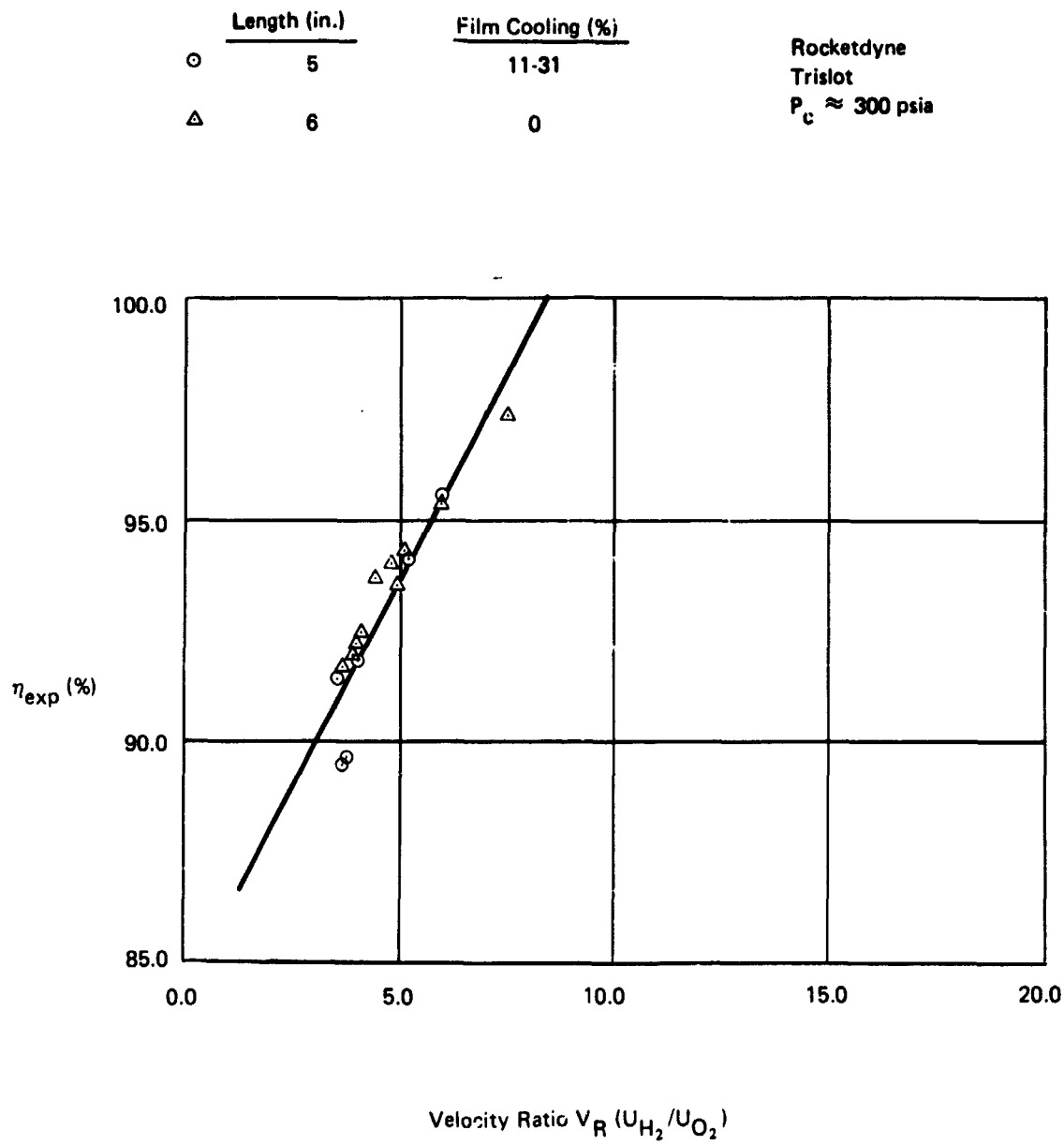

Figure 4A. Rocketdyne Trislot Injector Performance Data
Reference 9

PRECEDING PAGE BLANK NOT FILMED

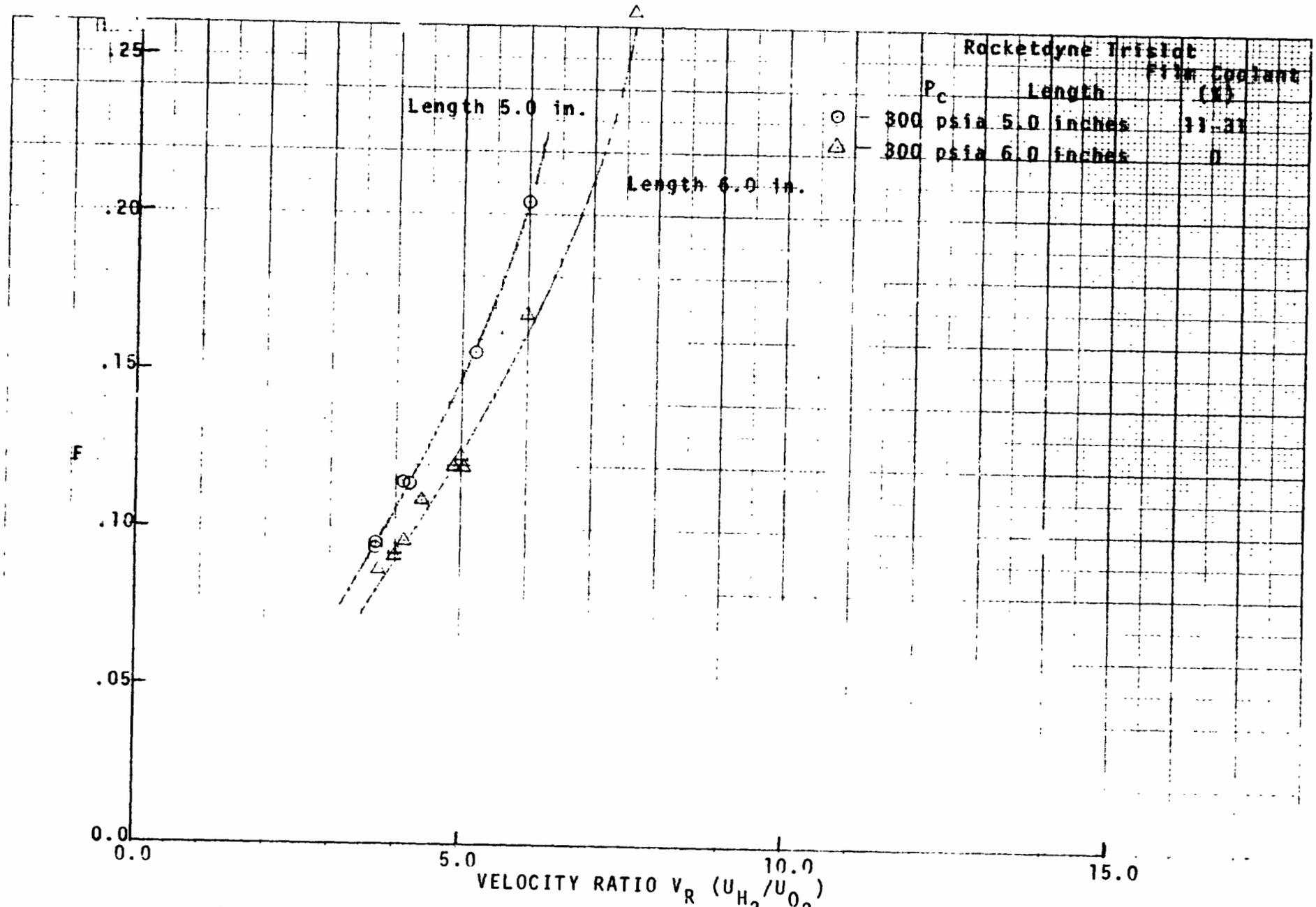

FIGURE 4B. CORRELATION OF ROCKETDYNE TRISLOT INJECTOR PERFORMANCE DATA

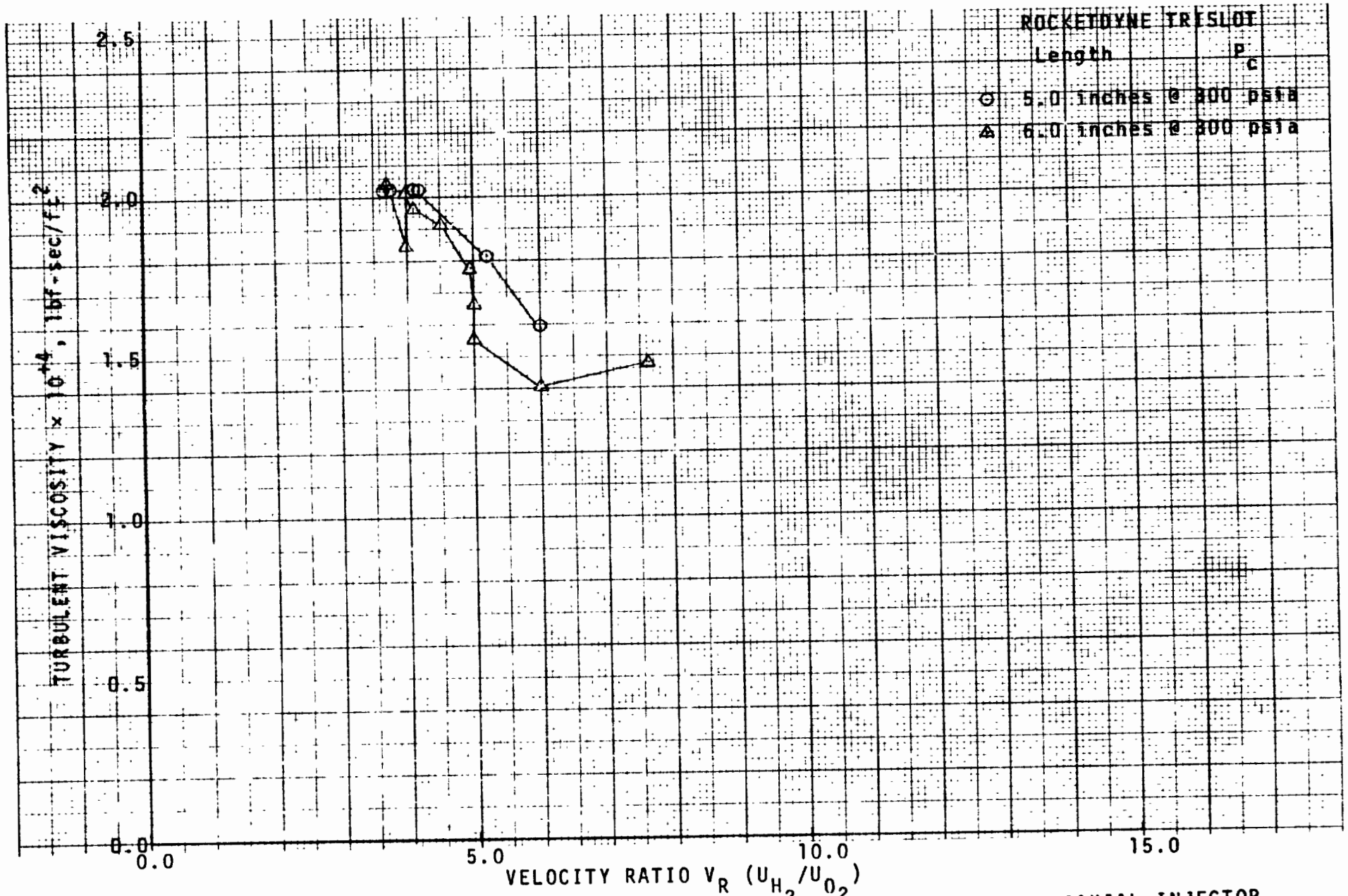

FIGURE 4C. FINAL VALUE OF TURBULENT (EDDY) VISCOSITY, ε_η. ROCKETDYNE COAXIAL INJECTOR

	Length (In.)	Film Cooling (%)
⊙	8.3	0
⊡	8.3	20 - 30
△	5.5	0

Aerojet
Coaxial

$P_c \approx 320$ psia

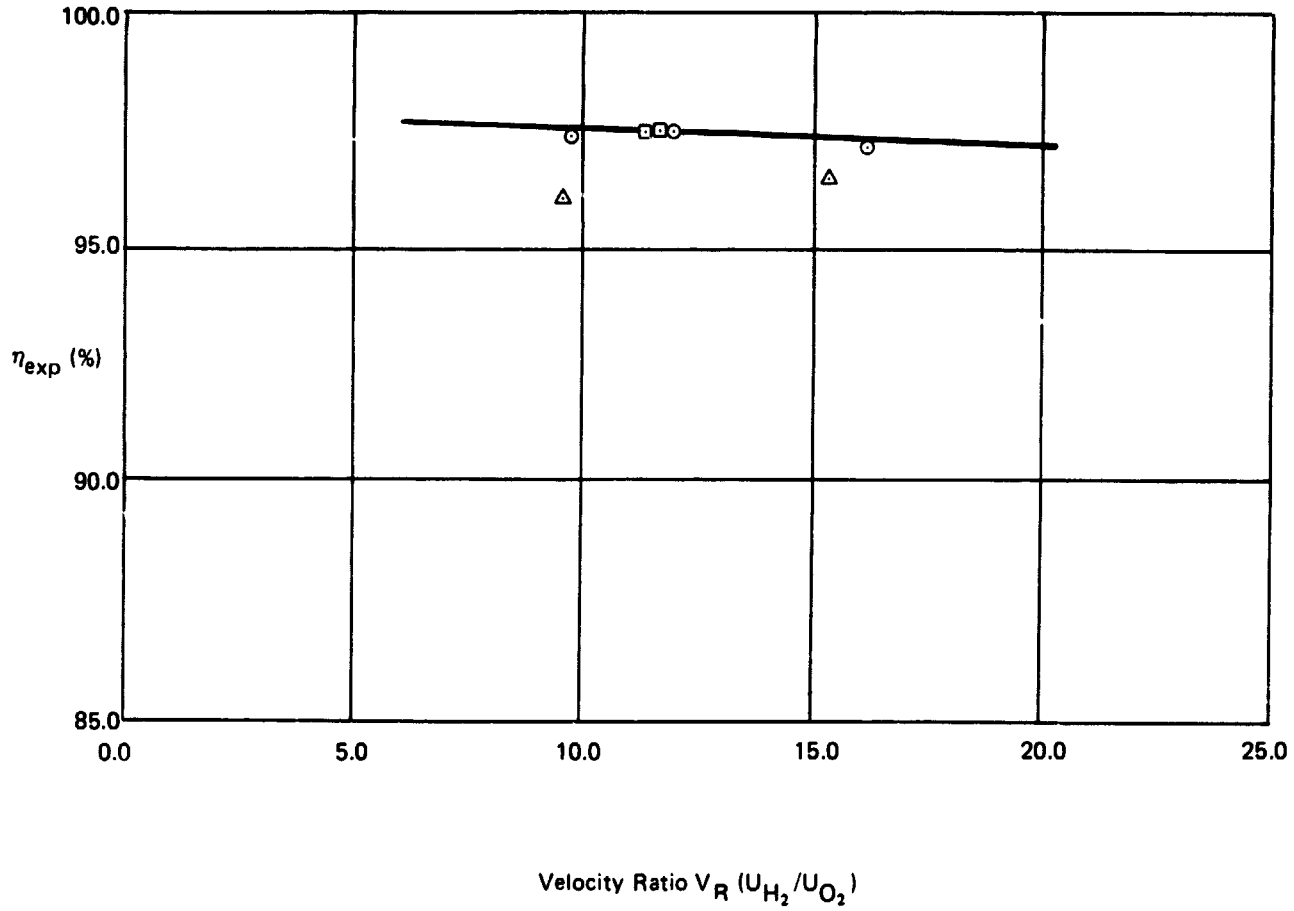

Figure 5A. Aerojet Coaxial Injector Performance Data
Reference 10

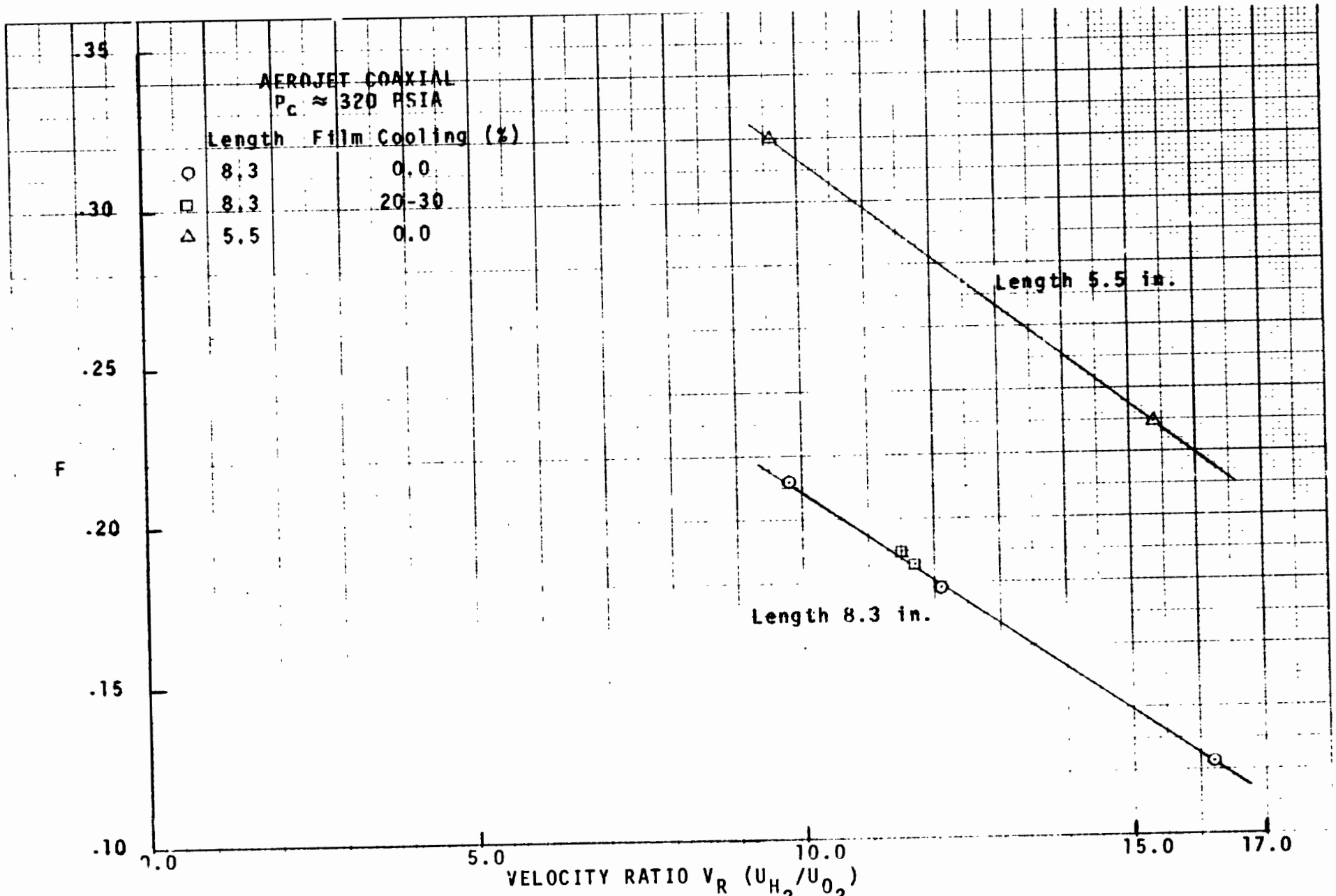

FIGURE 5B. CORRELATION OF AEROJET COAXIAL INJECTOR PERFORMANCE DATA

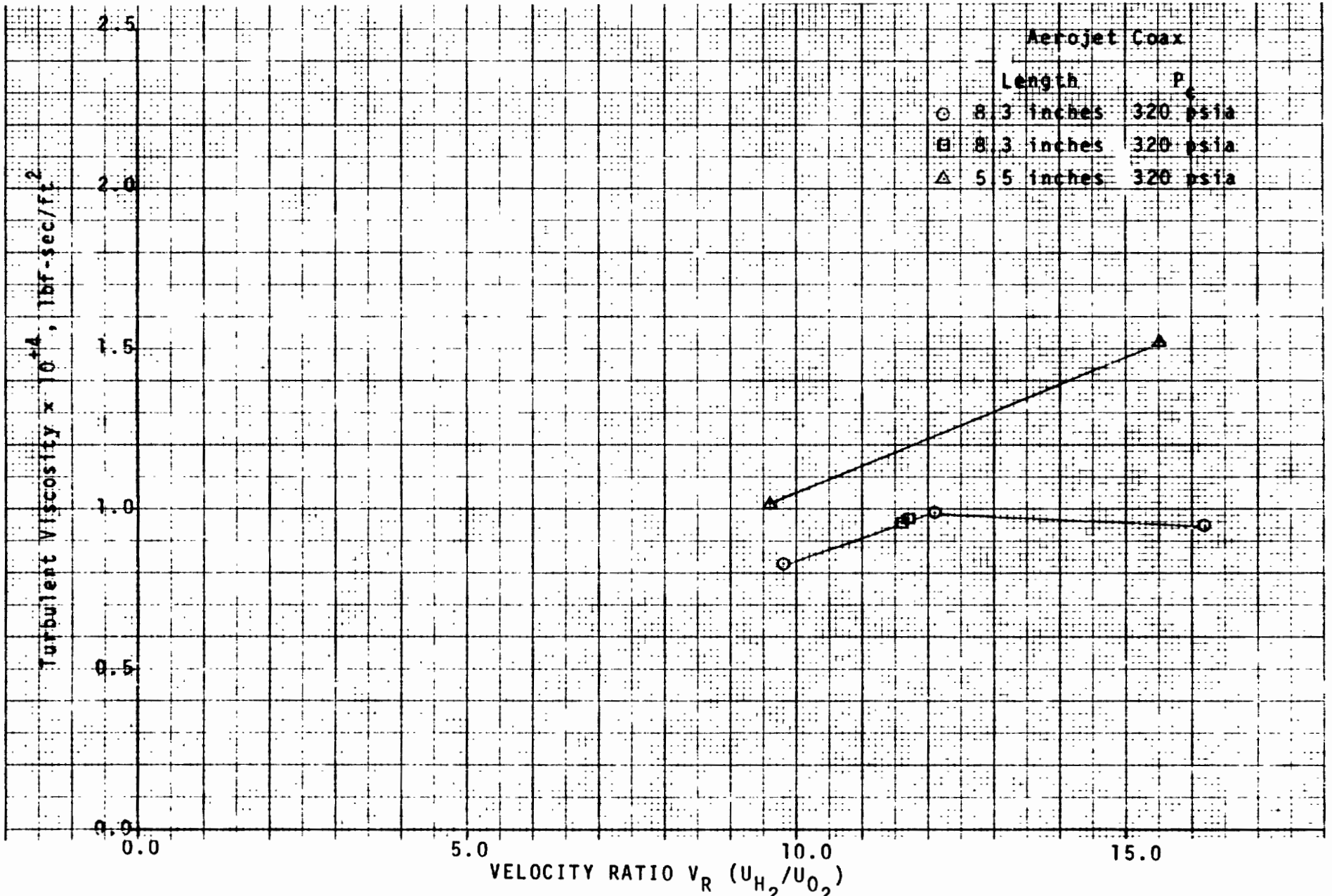

FIGURE 5C. FINAL VALUE OF TURBULENT (EDDY) VISCOSITY, ε_η. AEROJET COAXIAL INJECTOR

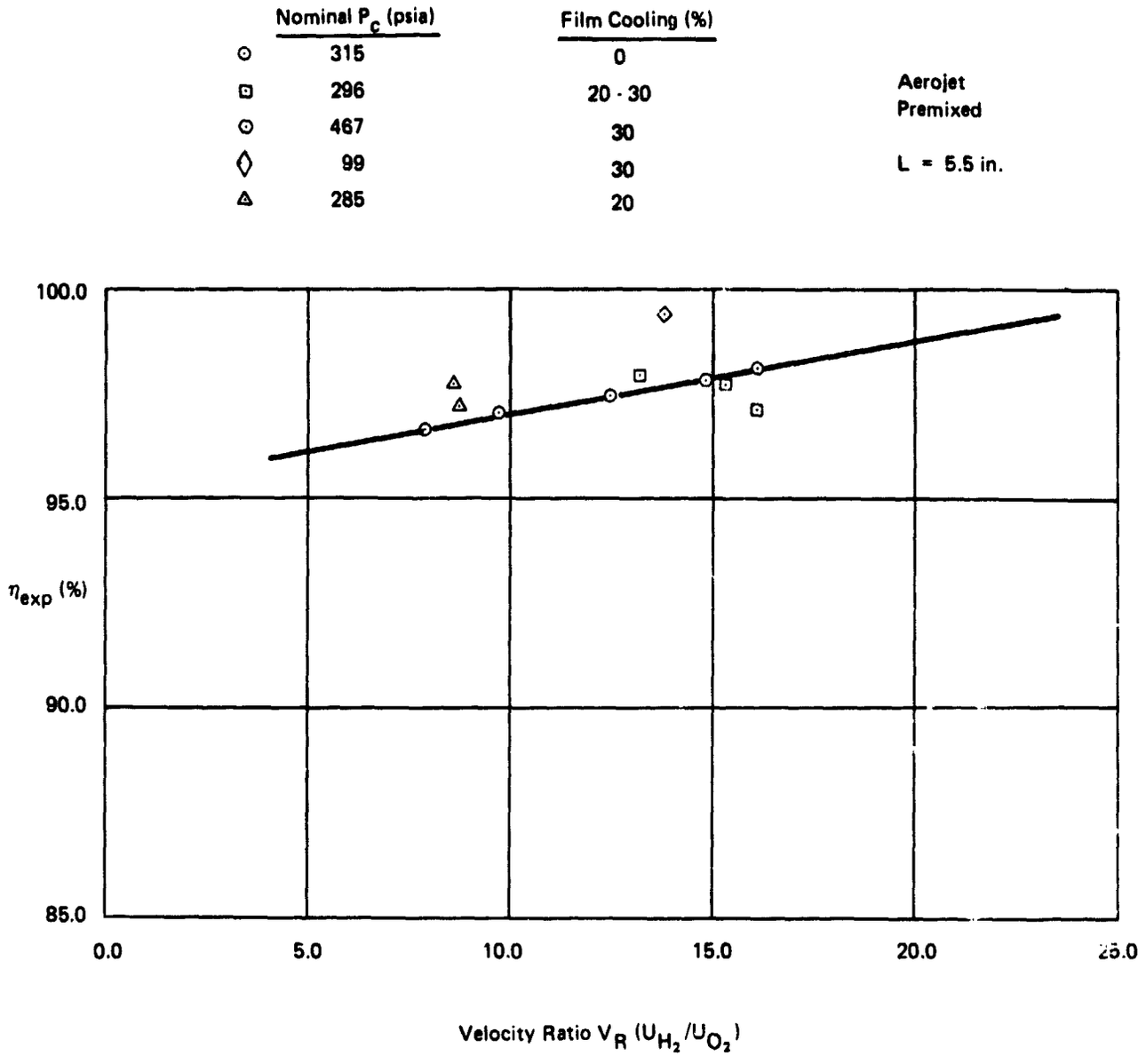

Figure 6A. Aerojet Premixed Injector Performance Data
Reference 10

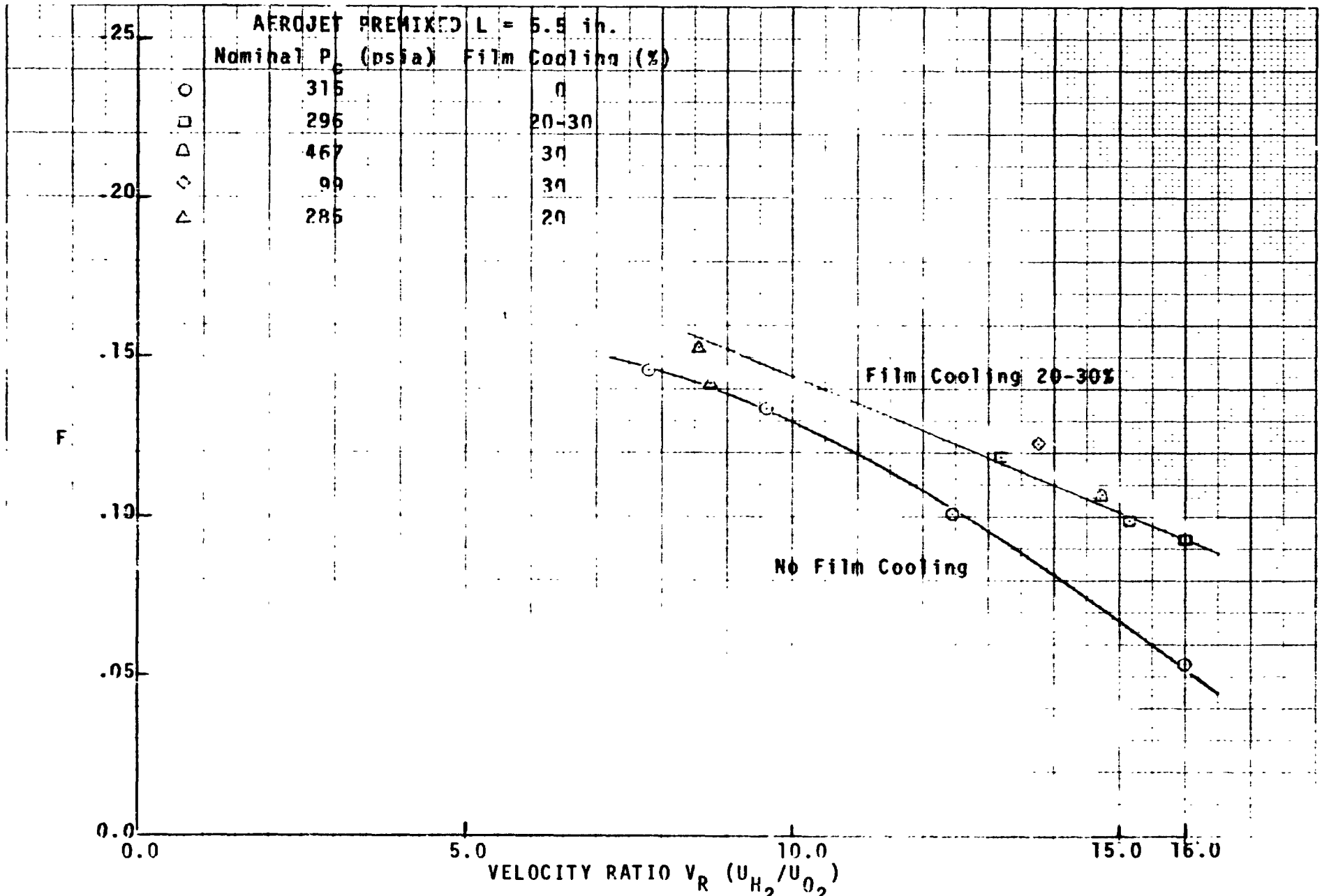

FIGURE 6B. CORRELATION OF AEROJET PREMIX INJECTOR PERFORMANCE DATA

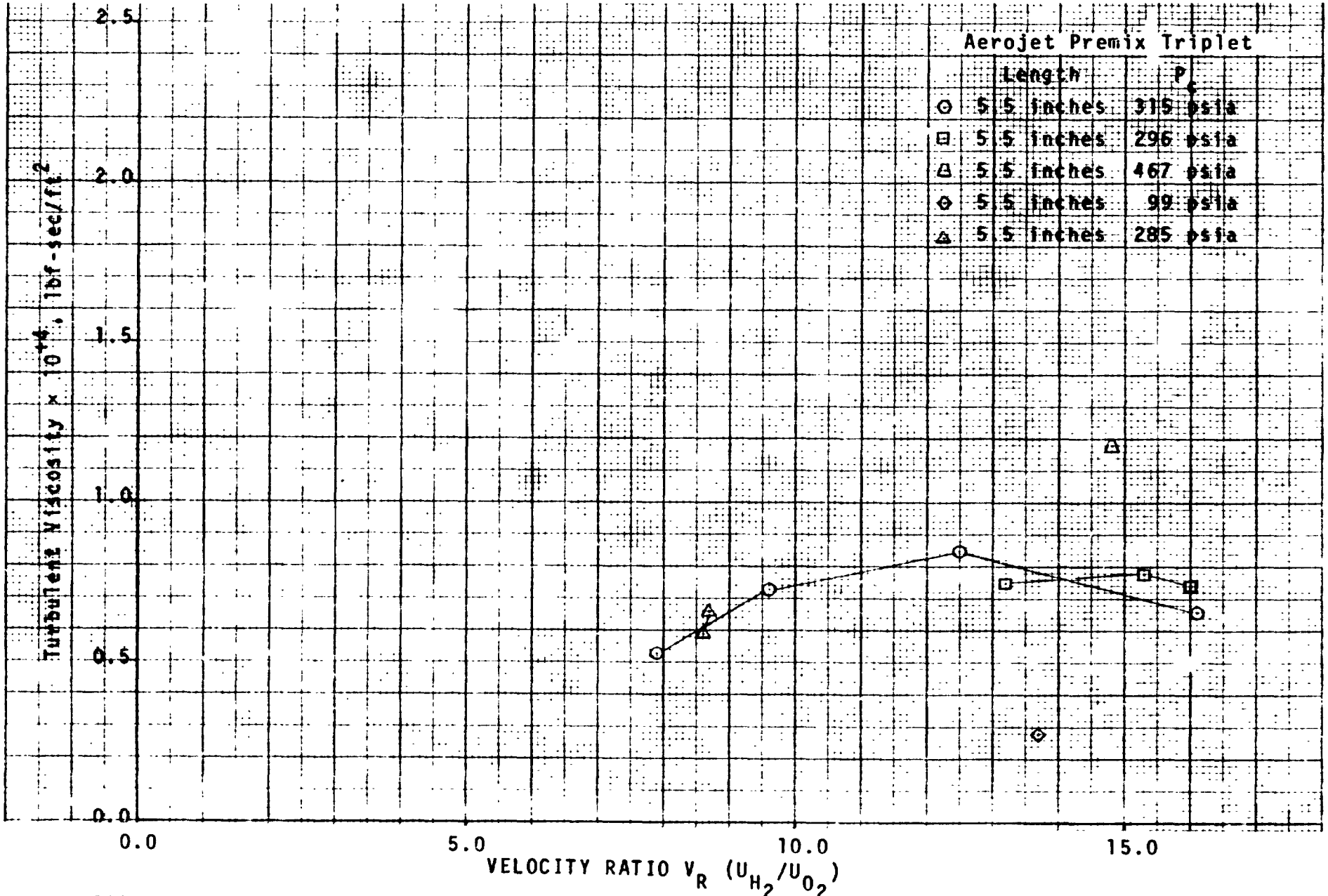

FIGURE 6C. FINAL VALUE OF TURBULENT (EDDY) VISCOSITY, ε_η. ROCKETDYNE COAXIAL INJECTOR

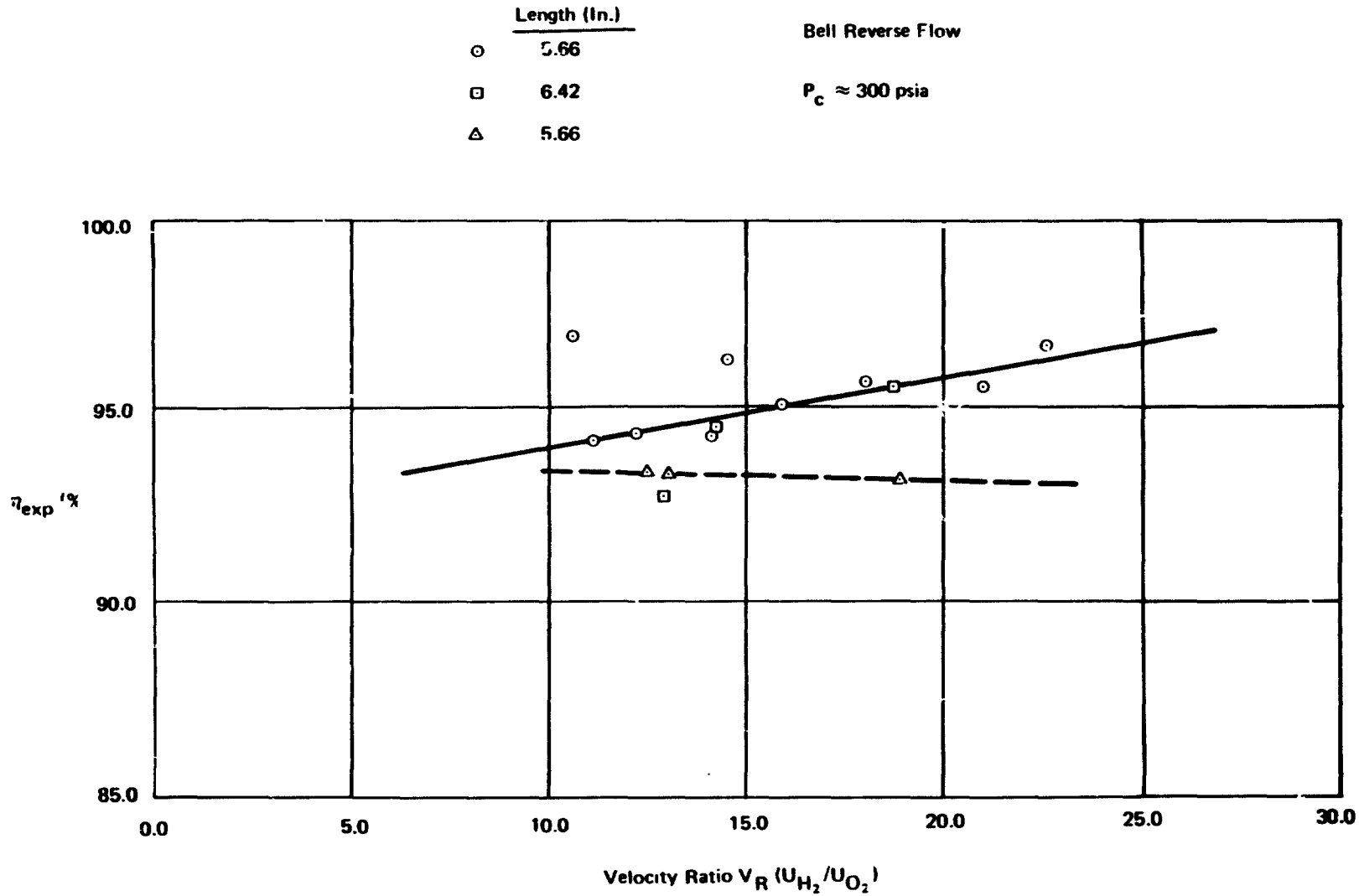

Figure 7A Bell Reverse Flow Injector Performance Data Reference 11

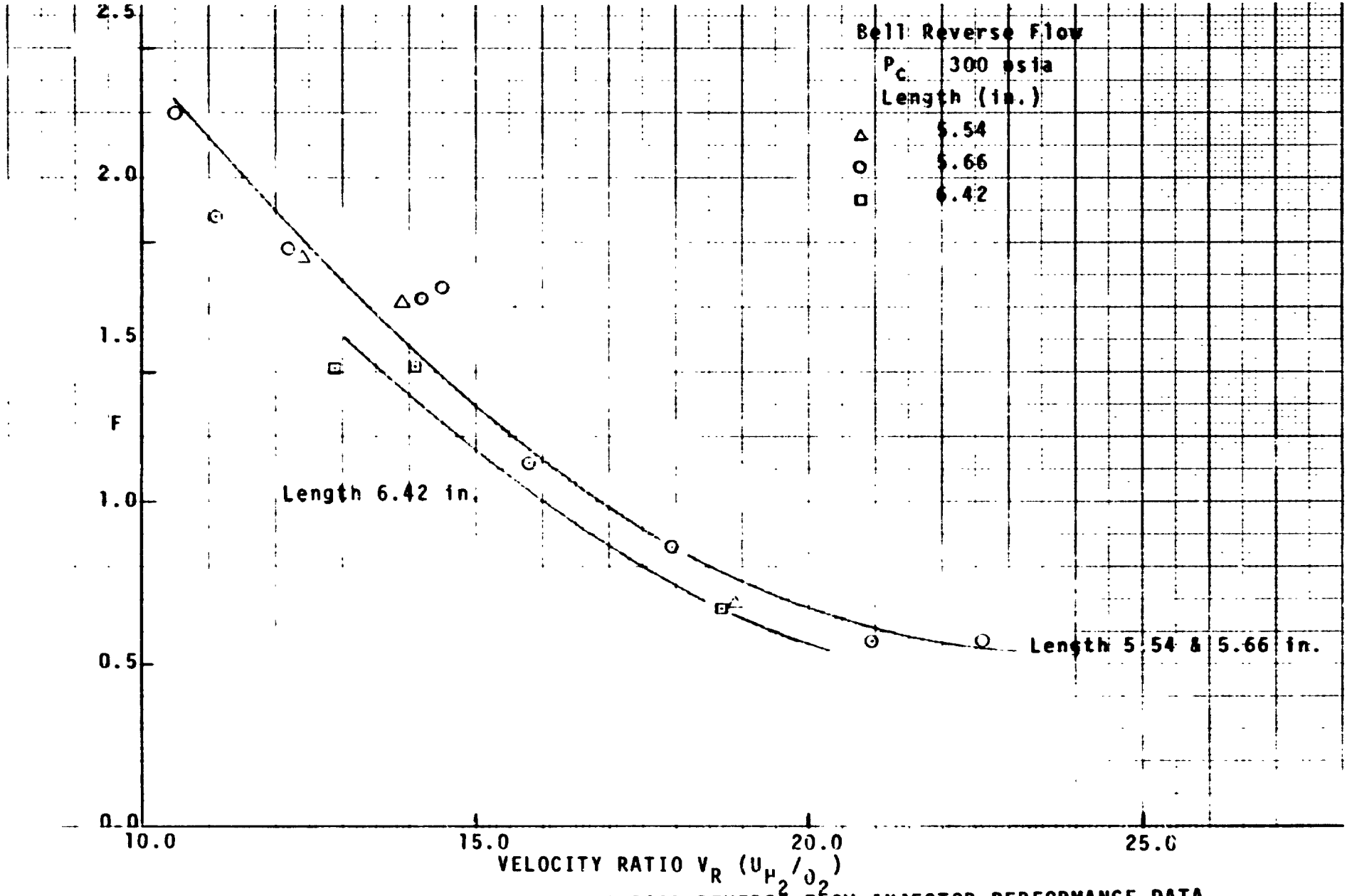

FIGURE 7B. CORRELATION OF BELL AEROSPACE REVERSE FLOW INJECTOR PERFORMANCE DATA

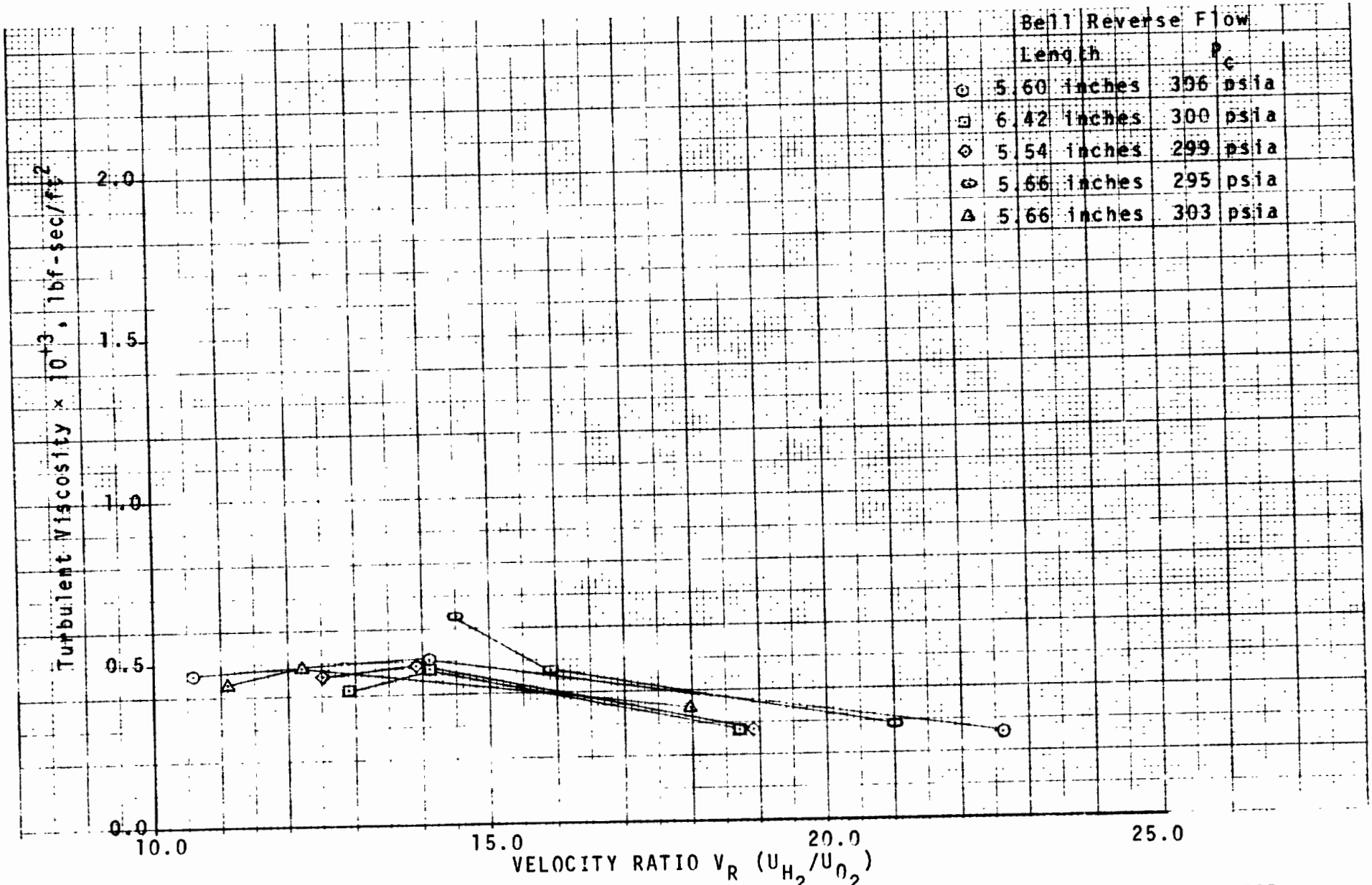

FIGURE 7C. FINAL VALUE OF TURBULENT (EDDY) VISCOSITY, ε_η. ROCKETDYNE COAXIAL INJECTOR

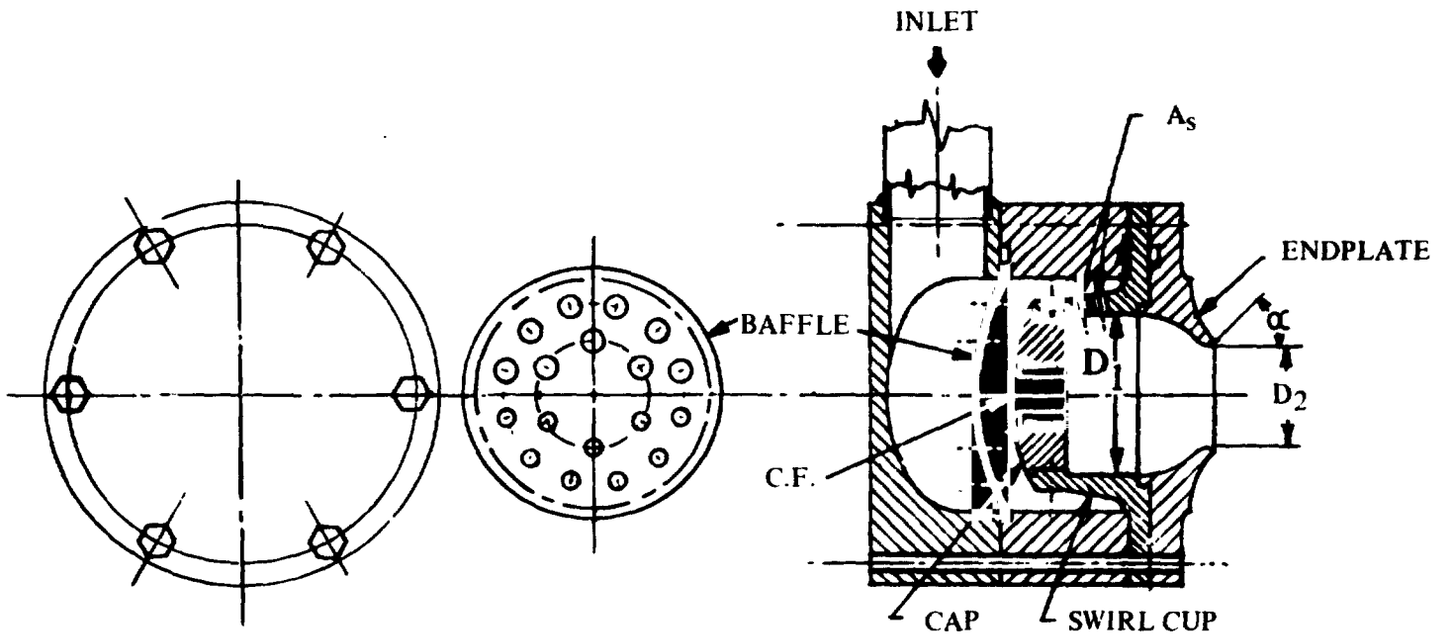

Figure 7D. Oxidizer Injector Cold Flow Model

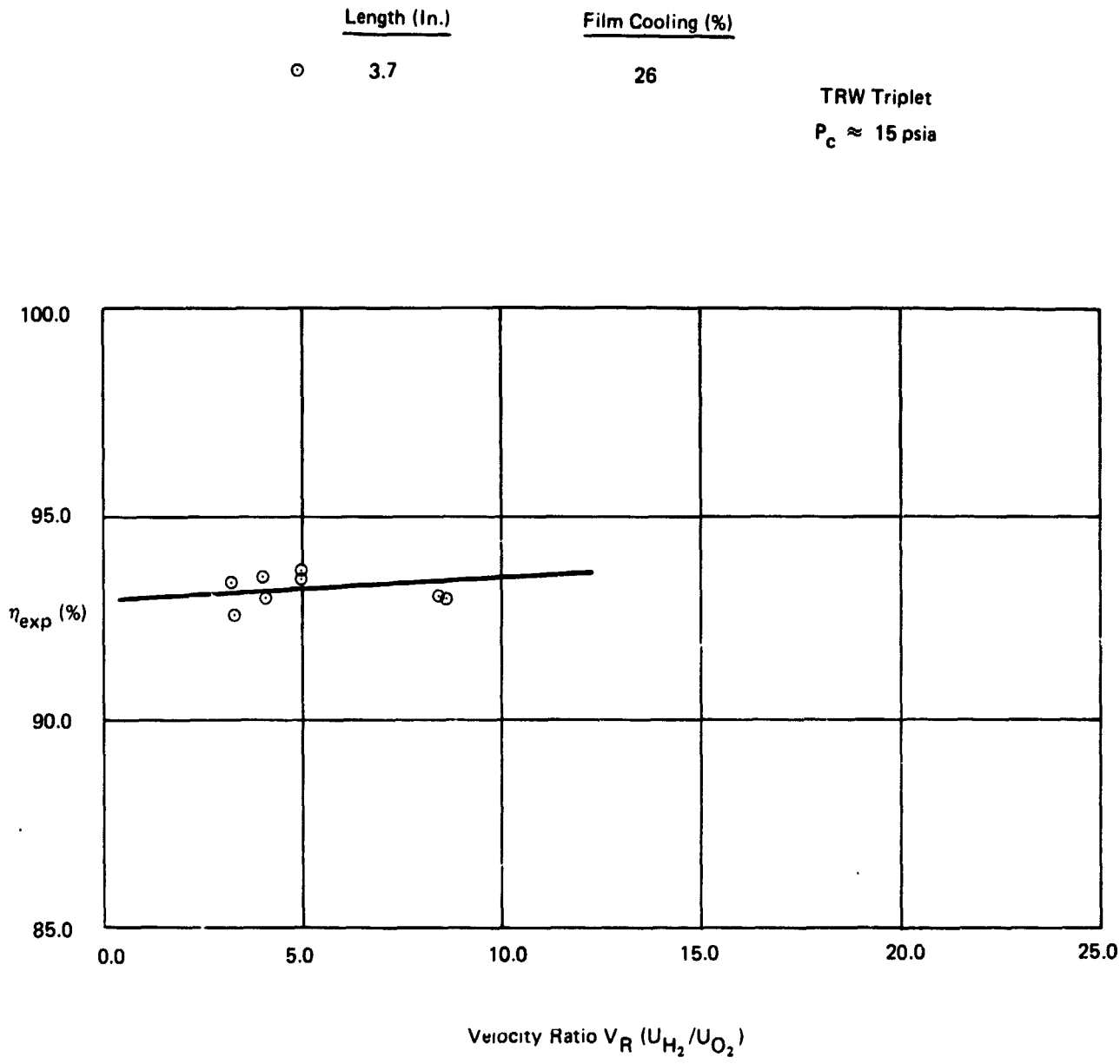

FIGURE 8A. TRW Triplet Injector Performance Data
Reference 12

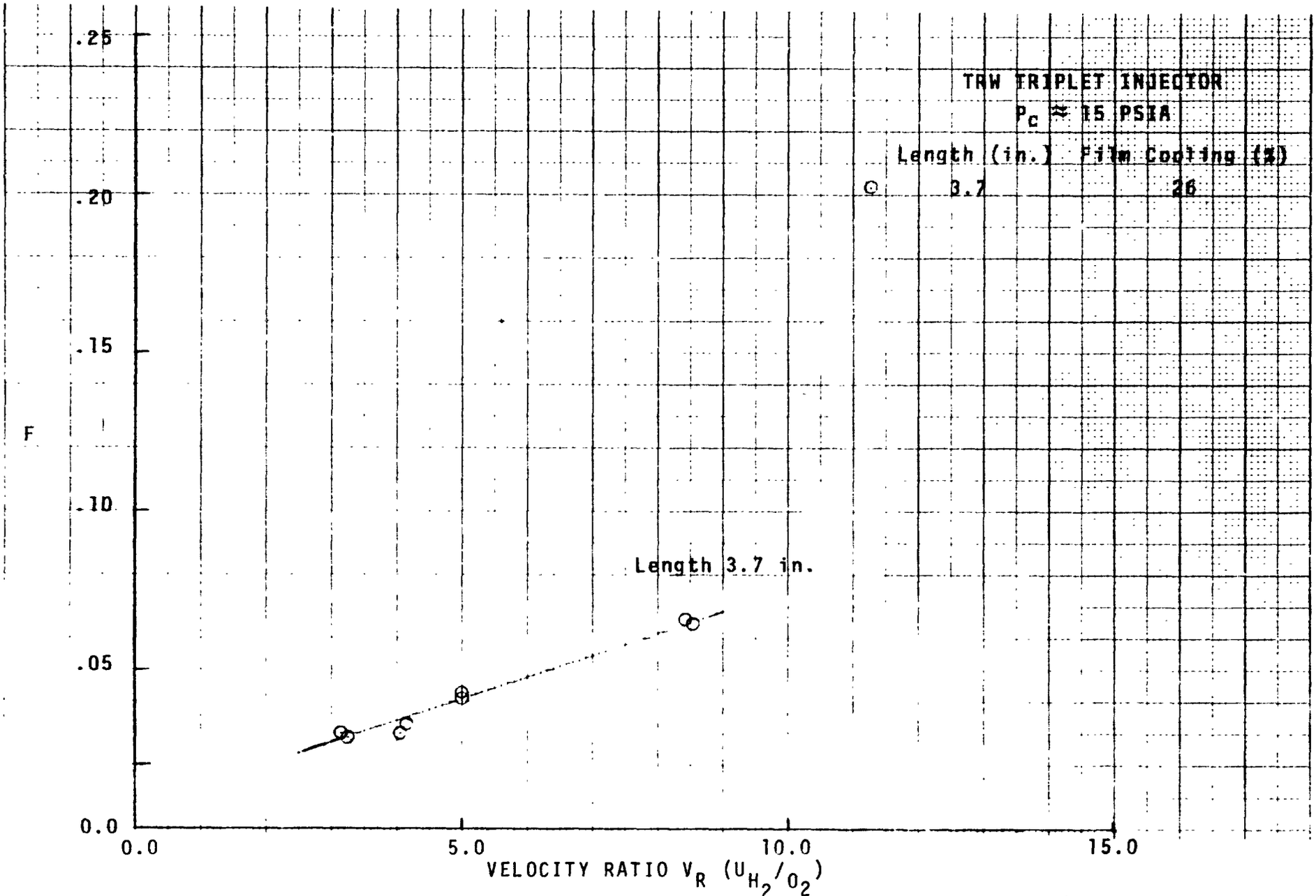

FIGURE 8B. CORRELATION OF TRW TRIPLET INJECTOR PERFORMANCE DATA

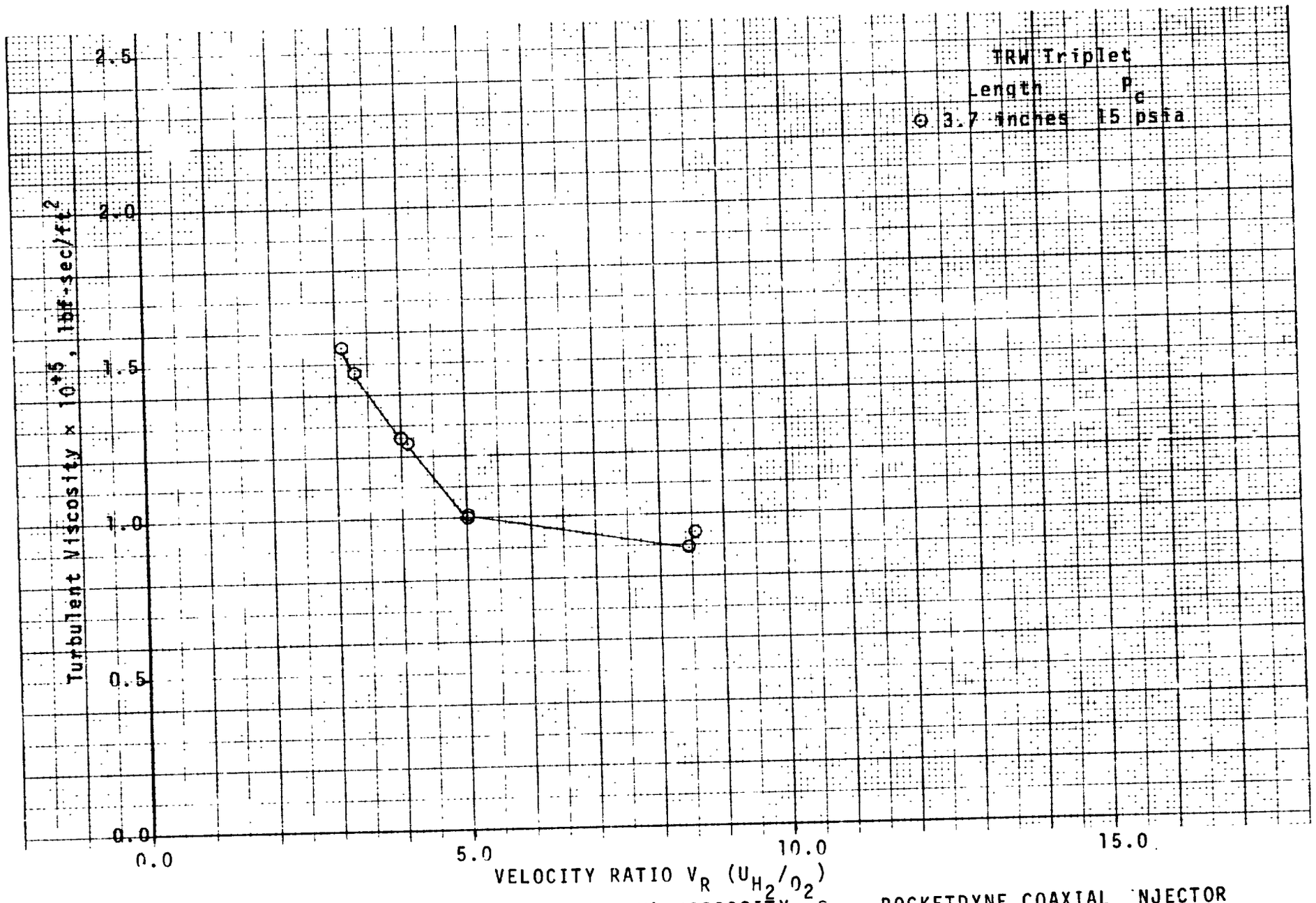

FIGURE 8C. FINAL VALUE OF TURBULENT (EDDY) VISCOSITY, ε_η. ROCKETDYNE COAXIAL INJECTOR

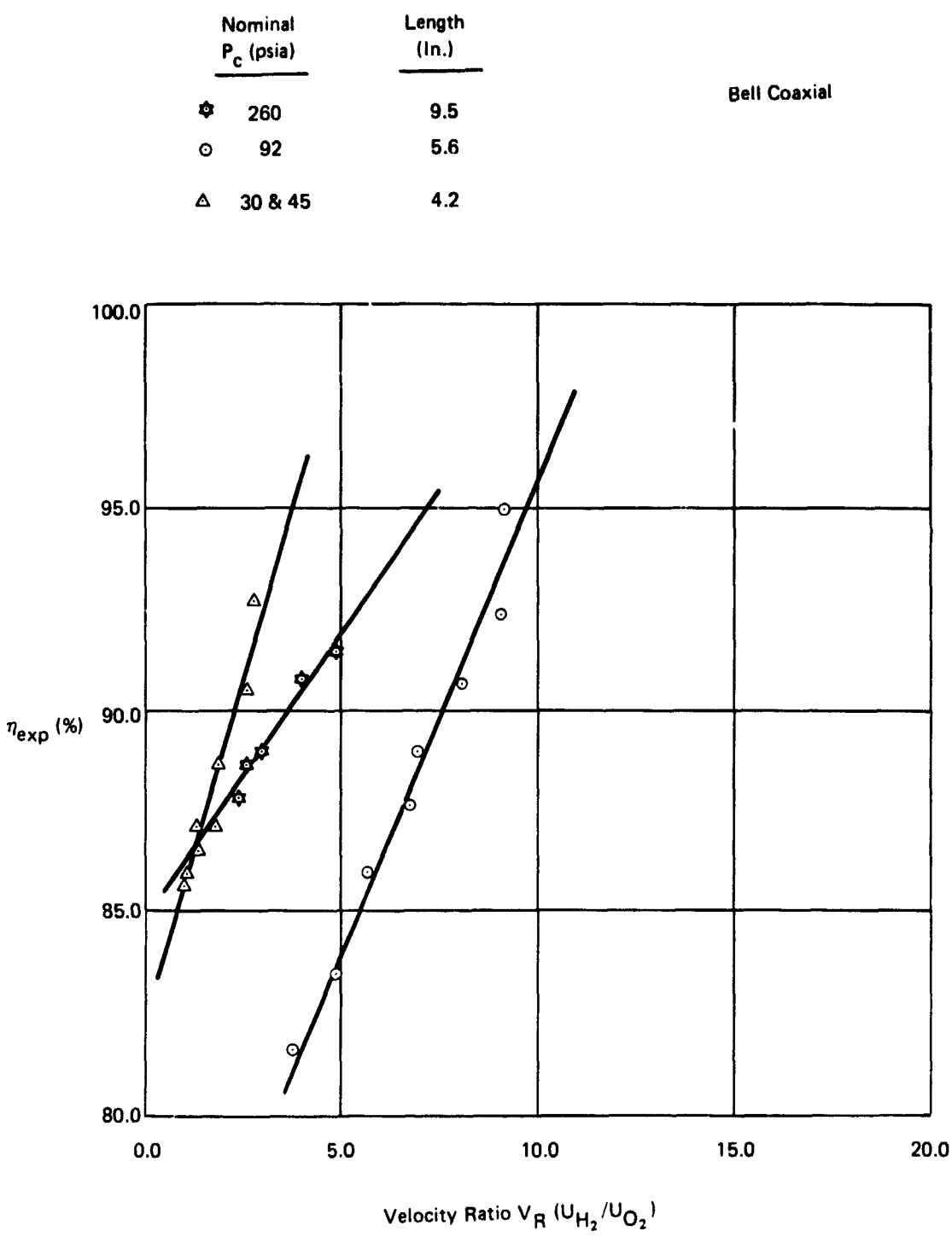

FIGURE 9A. Bell Coaxial Injector Performance Data
Reference 13

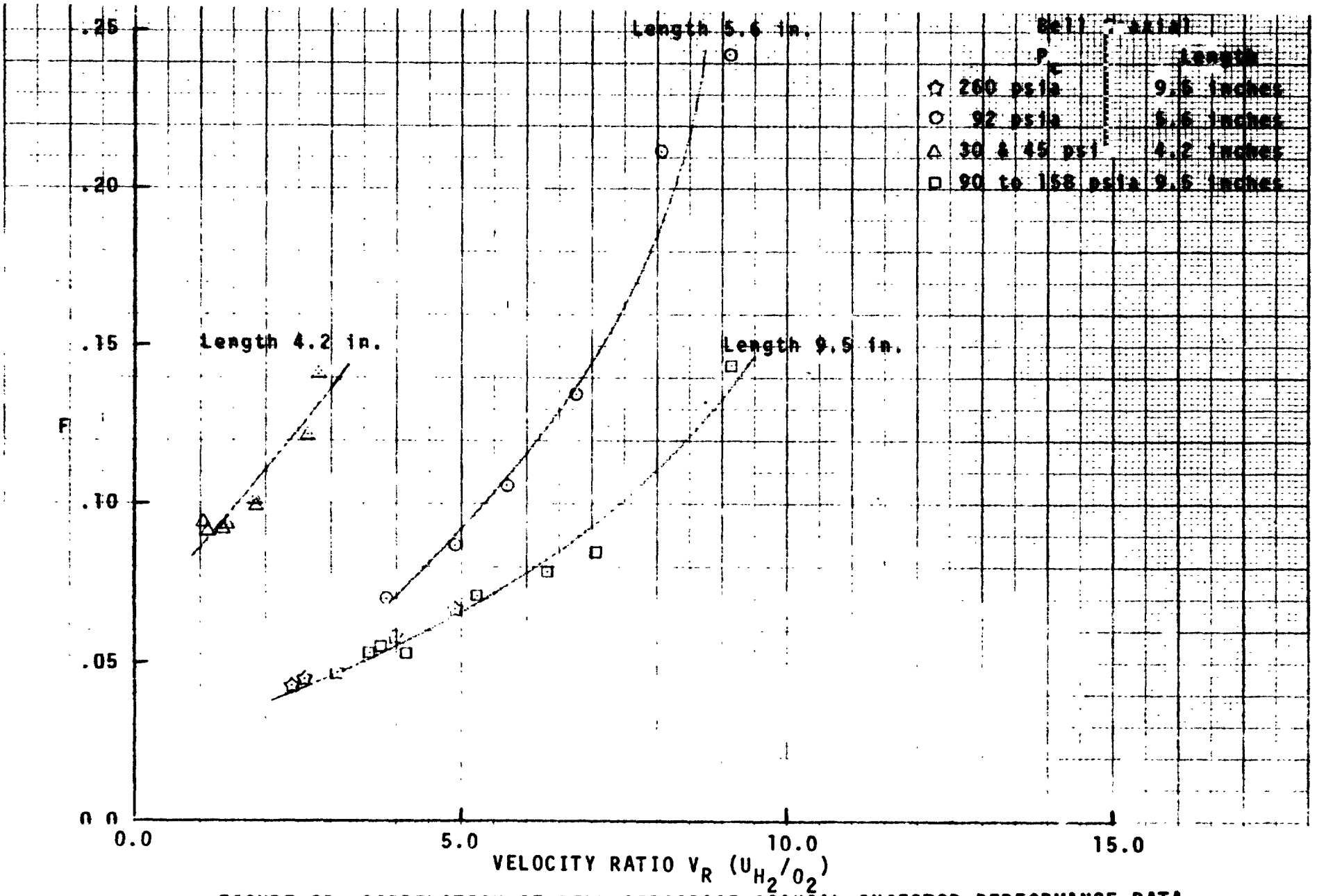

FIGURE 9B. CORRELATION OF BELL AEROSPACE COAXIAL INJECTOR PERFORMANCE DATA

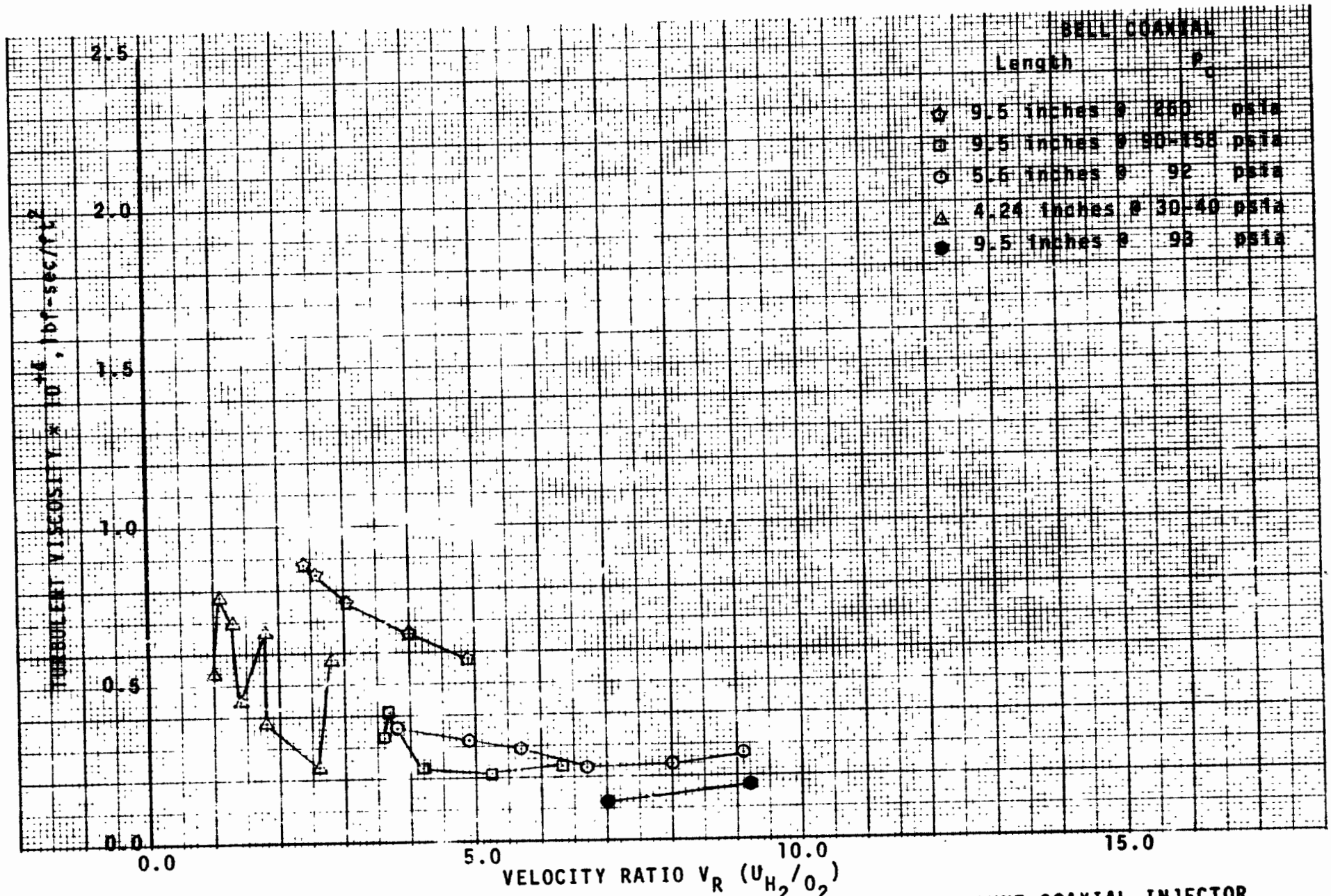

FIGURE 9C. FINAL VALUE OF TURBULENT (EDDY) VISCOSITY, ε_η. ROCKETDYNE COAXIAL INJECTOR

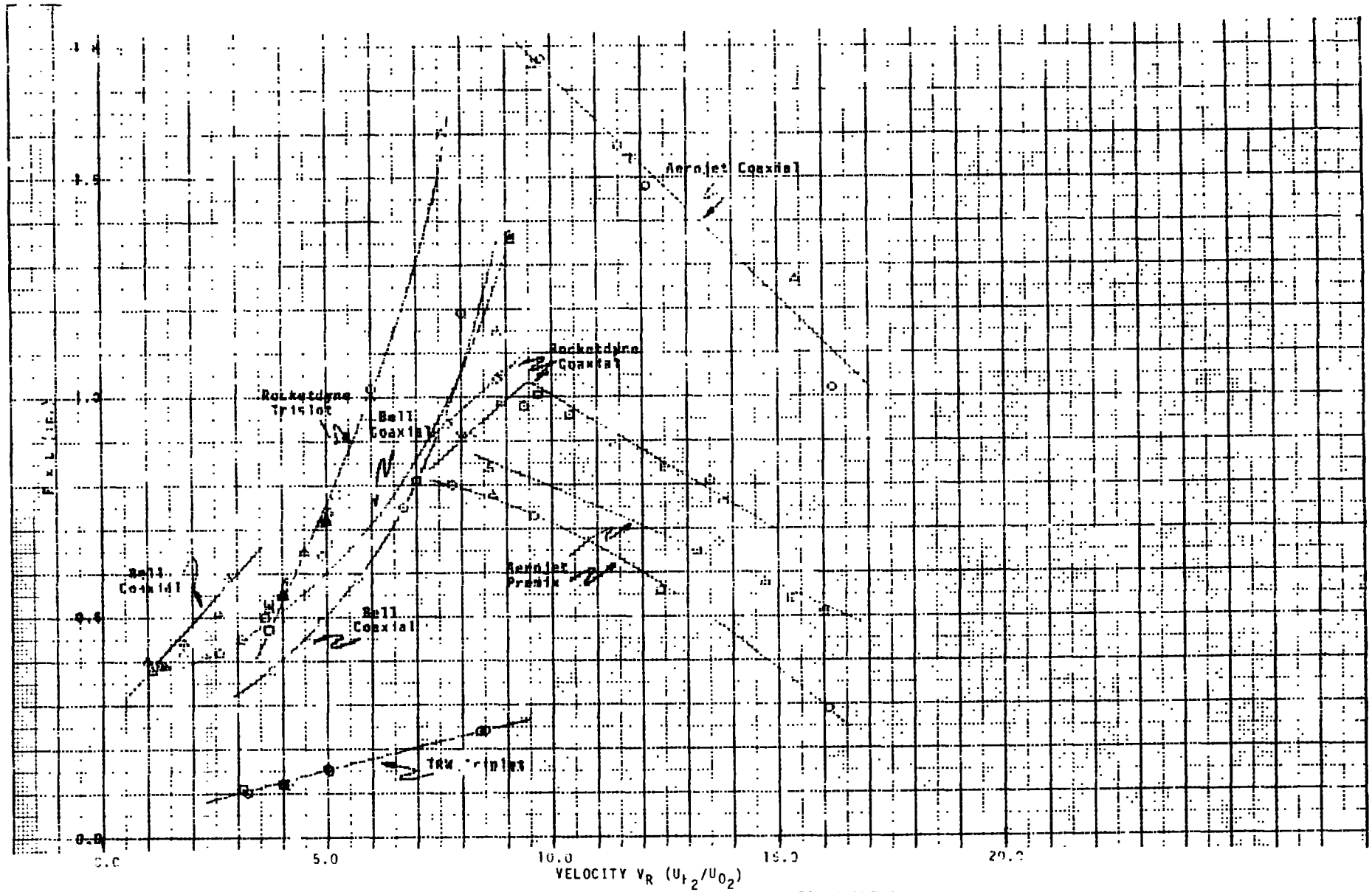

FIGURE 10A. CORRELATION FOR VARIOUS INJECTOR ELEMENTS.

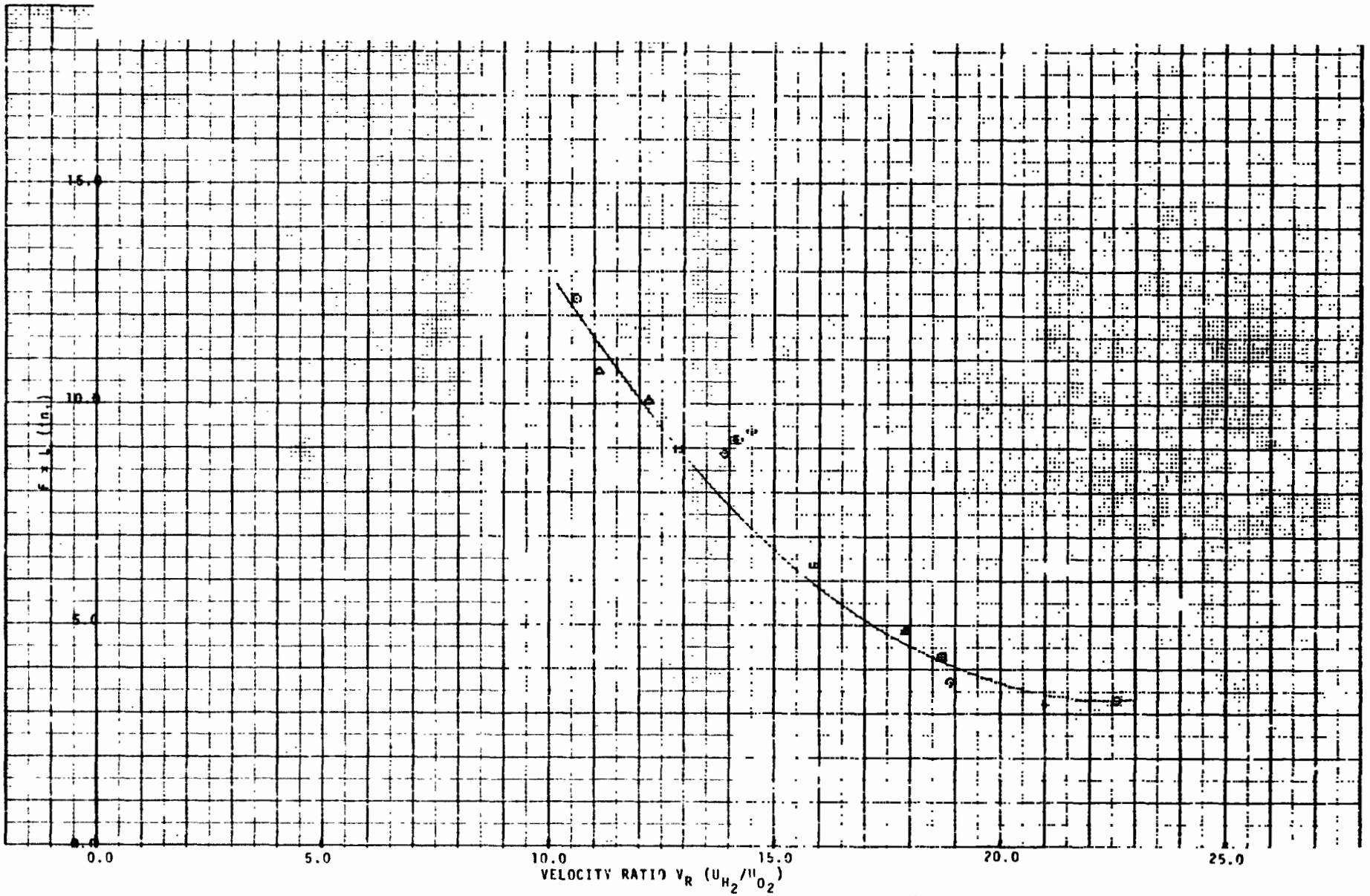

FIGURE 10B. COMBUSTION FOR BELL REVERSE FLOW INJECTOR ELEMENT

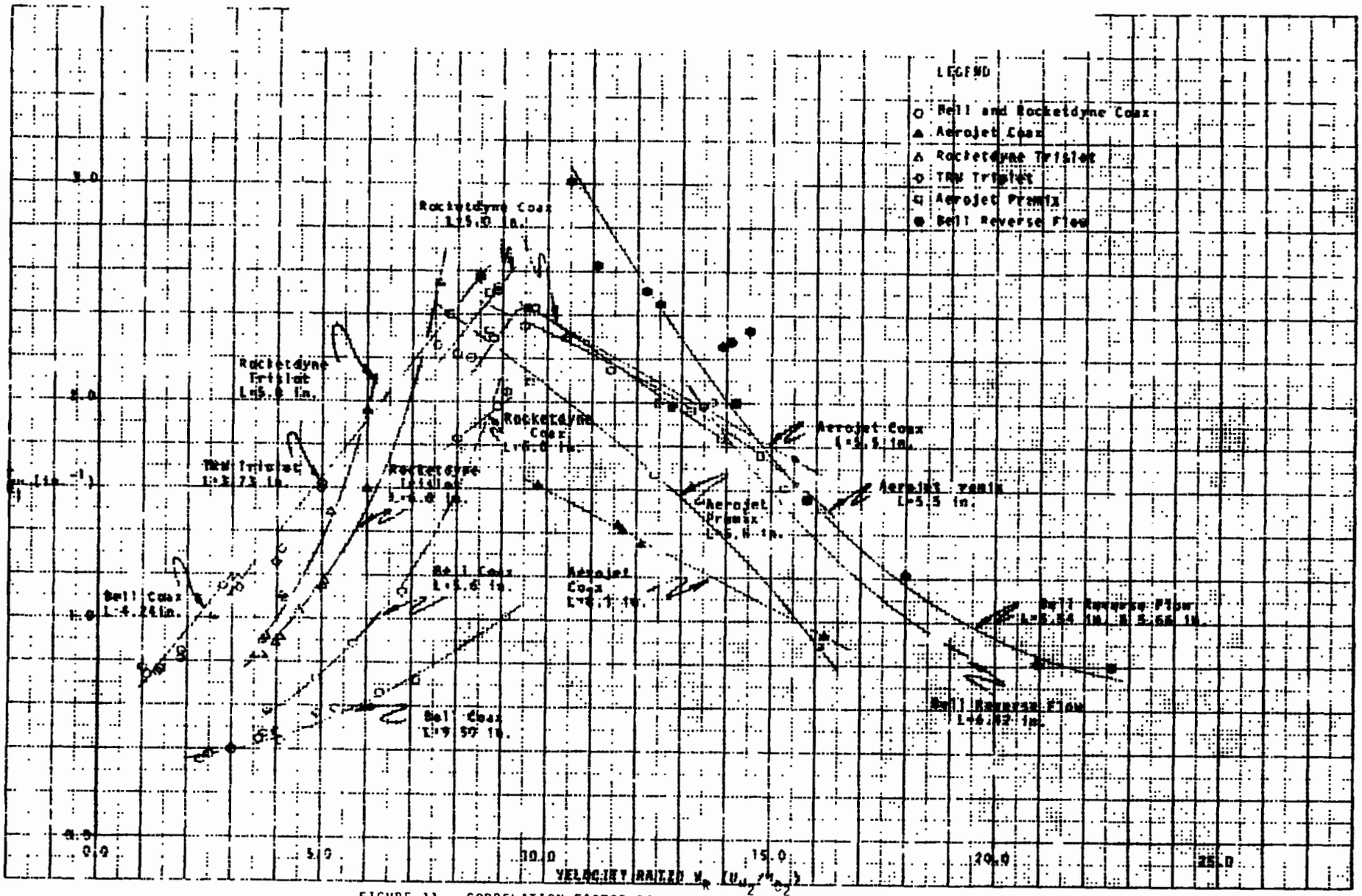

FIGURE 11. CORRELATION FACTOR DIVIDED BY CENTRAL OXYGEN JET RADIUS

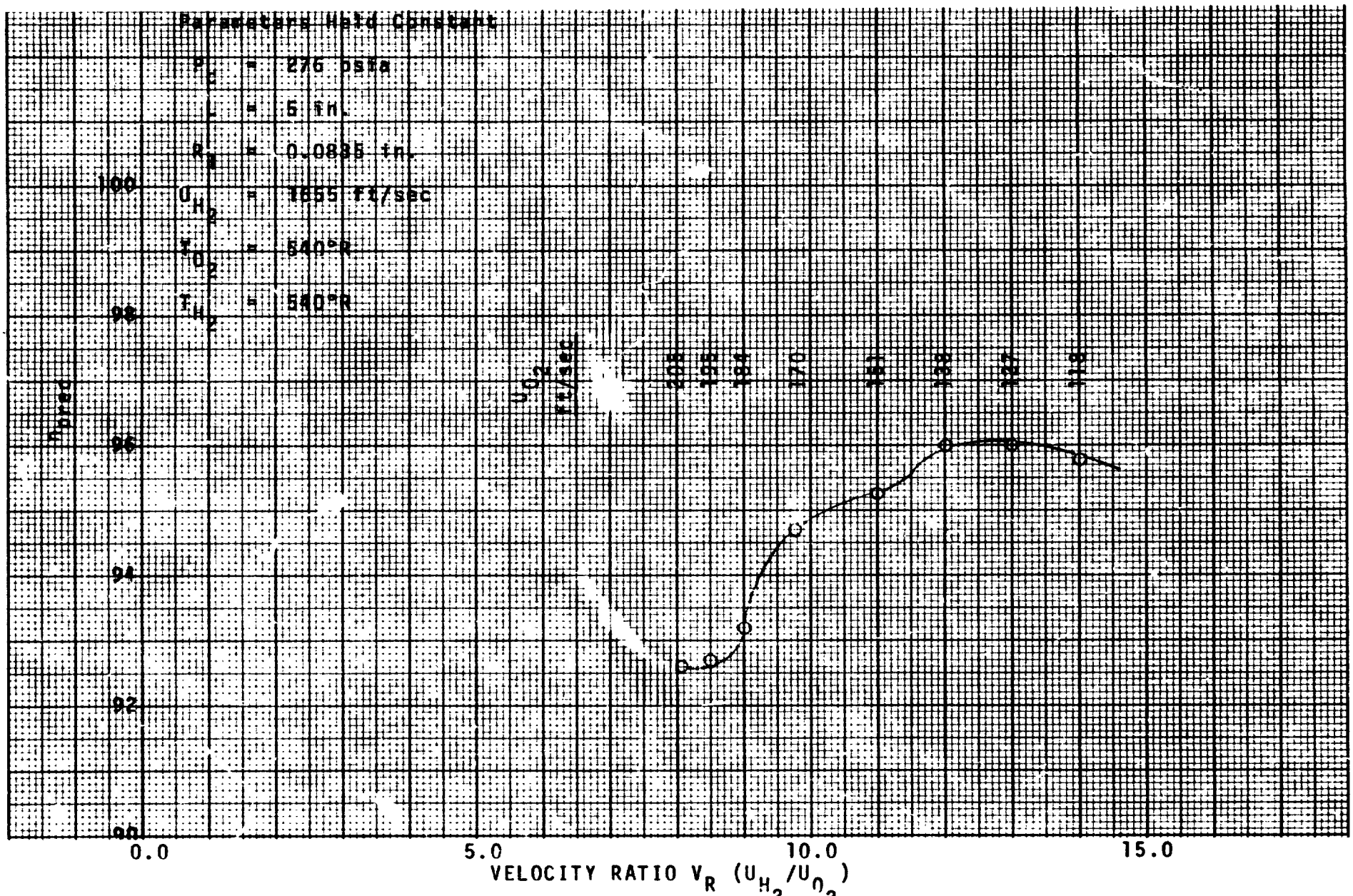

FIGURE 12. PREDICTION OF COMBUSTION EFFICIENCY VARIATION WITH U_{O_2}.

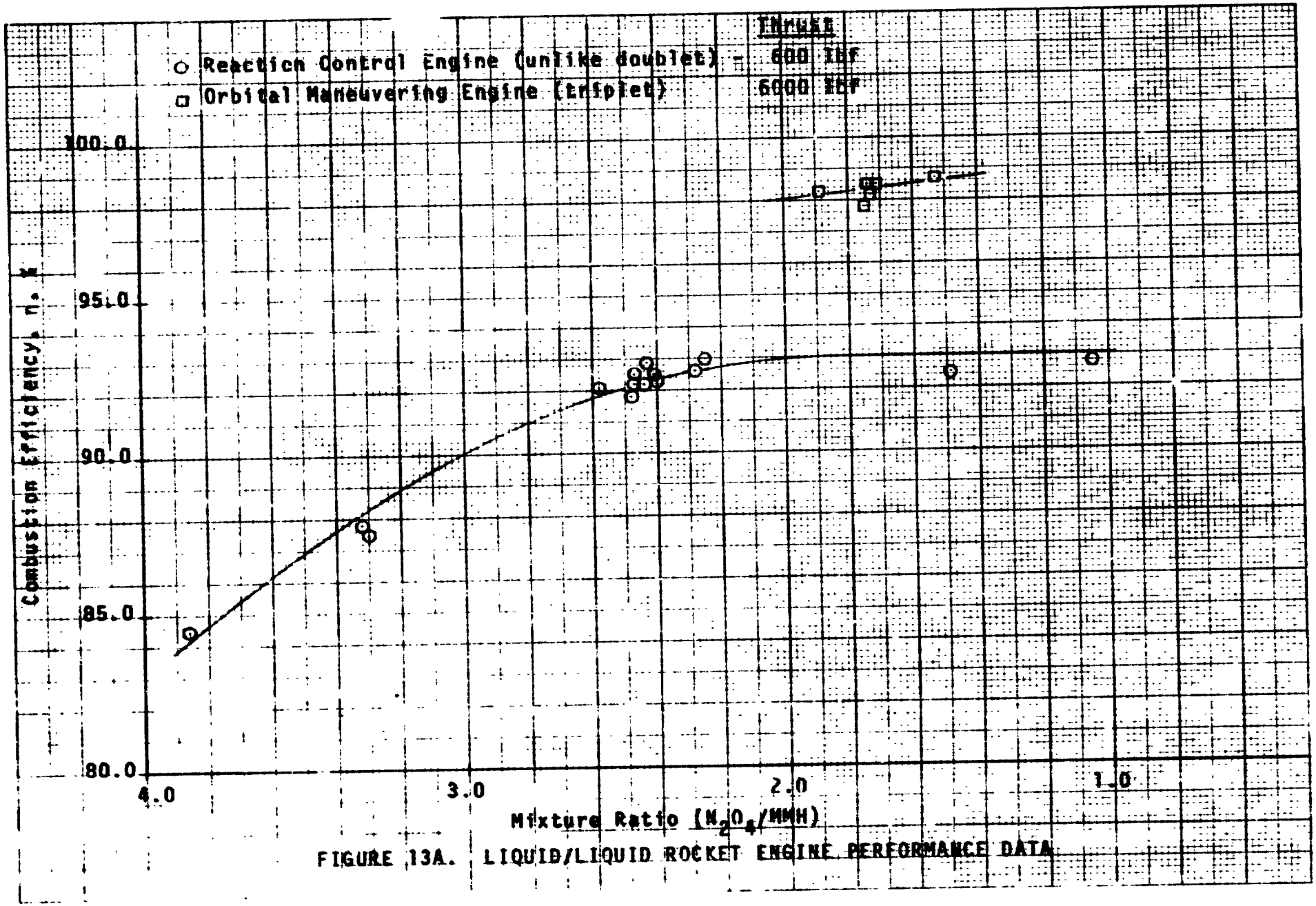

FIGURE 13A. LIQUID/LIQUID ROCKET ENGINE PERFORMANCE DATA

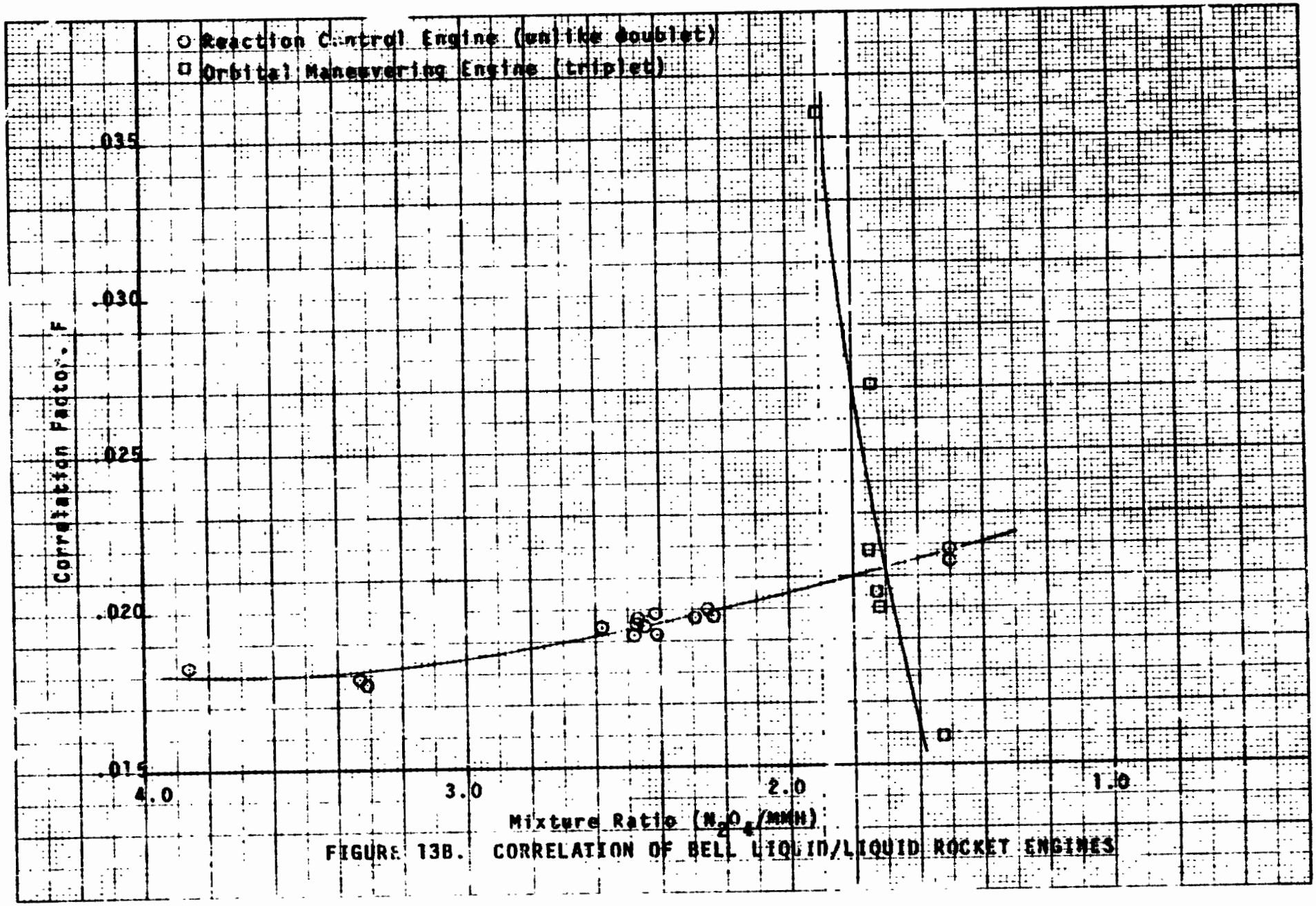

FIGURE 13B. CORRELATION OF BELL LIQUID/LIQUID ROCKET ENGINES

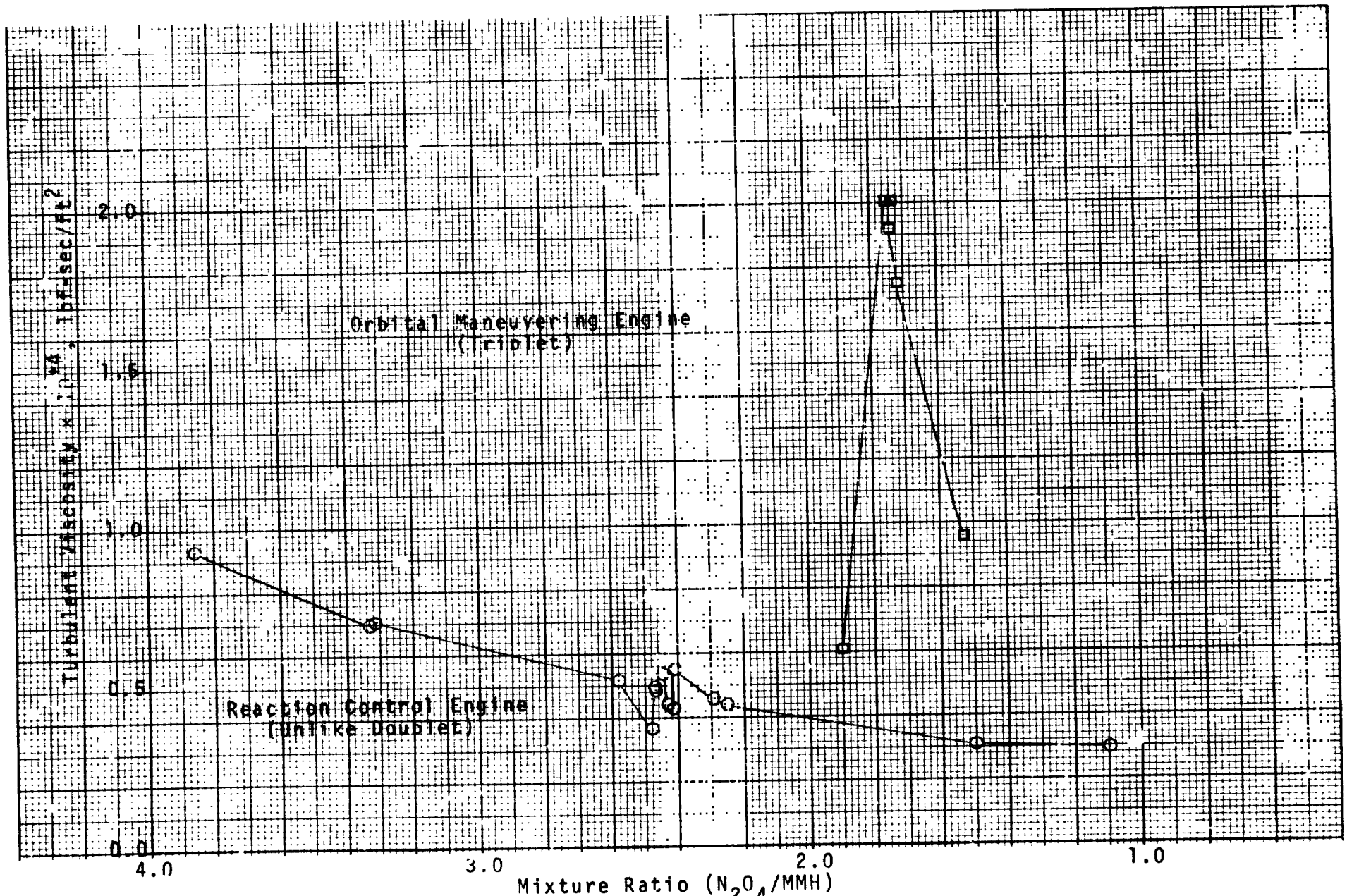

FIGURE 14. FINAL VALUE ε_η, BELL LIQUID/LIQUID ROCKET DATA

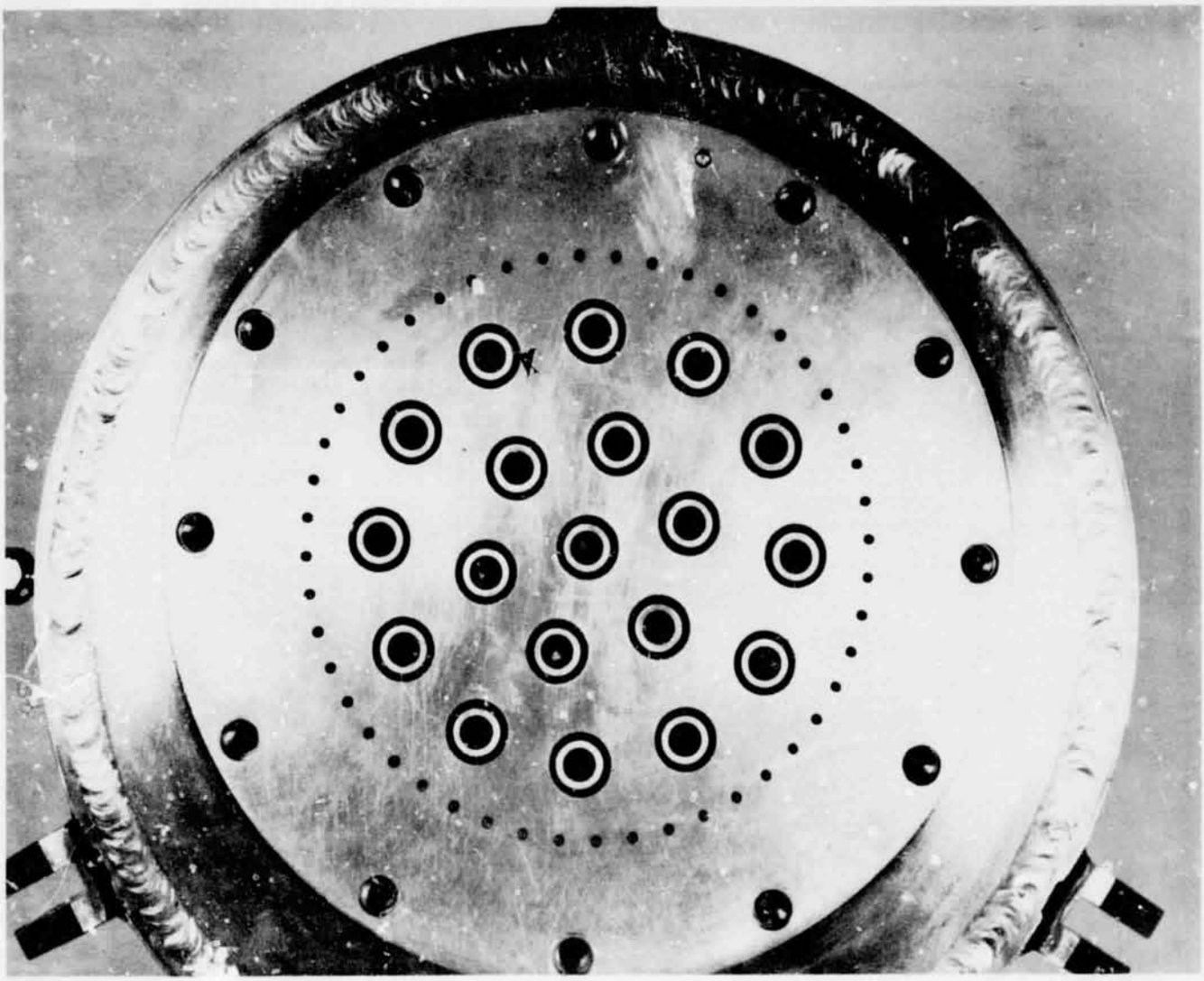

FIGURE 15

PHOTOGRAPH OF THE 19 ELEMENT INJECTOR USED FOR GASEOUS HYDROGEN-OXYGEN ROCKET ENGINE TESTS

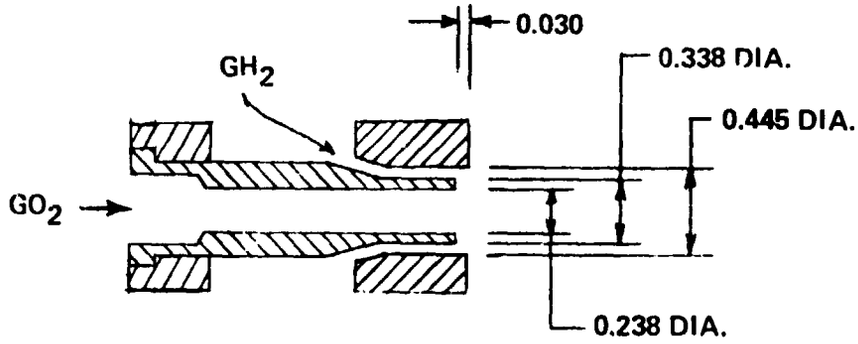

Figure 16. Bell Hydrogen/Oxygen Injector Element

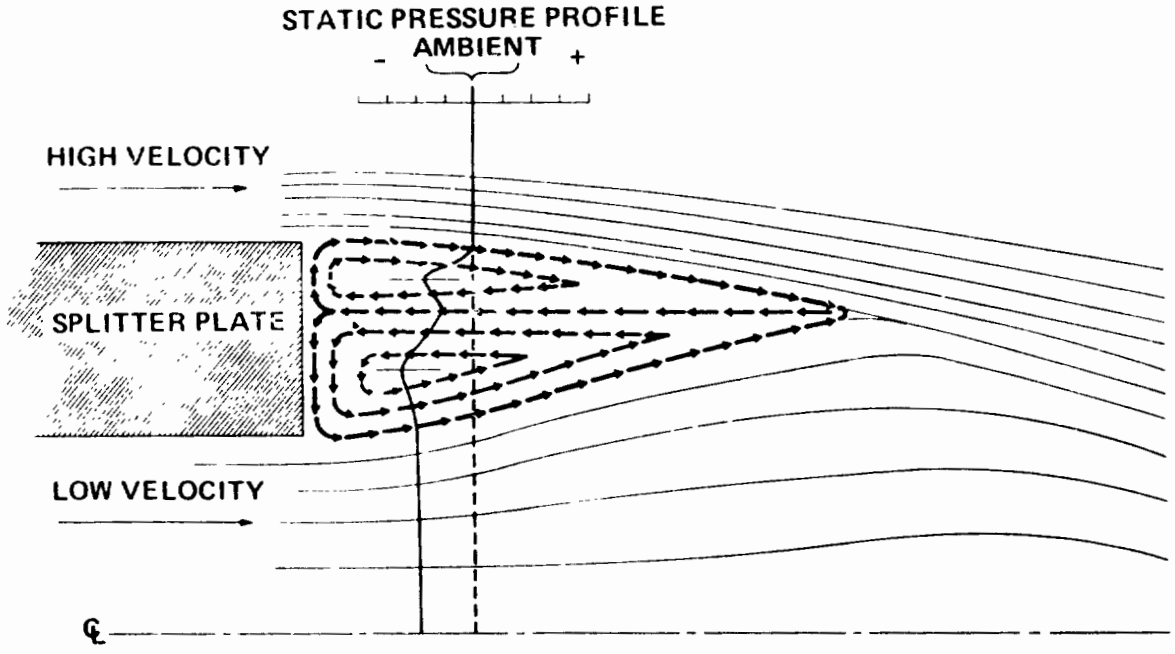

Figure 17. Sketch of Flow Around Splitter Plate for High Velocity Outer and Low Velocity Inner Jets

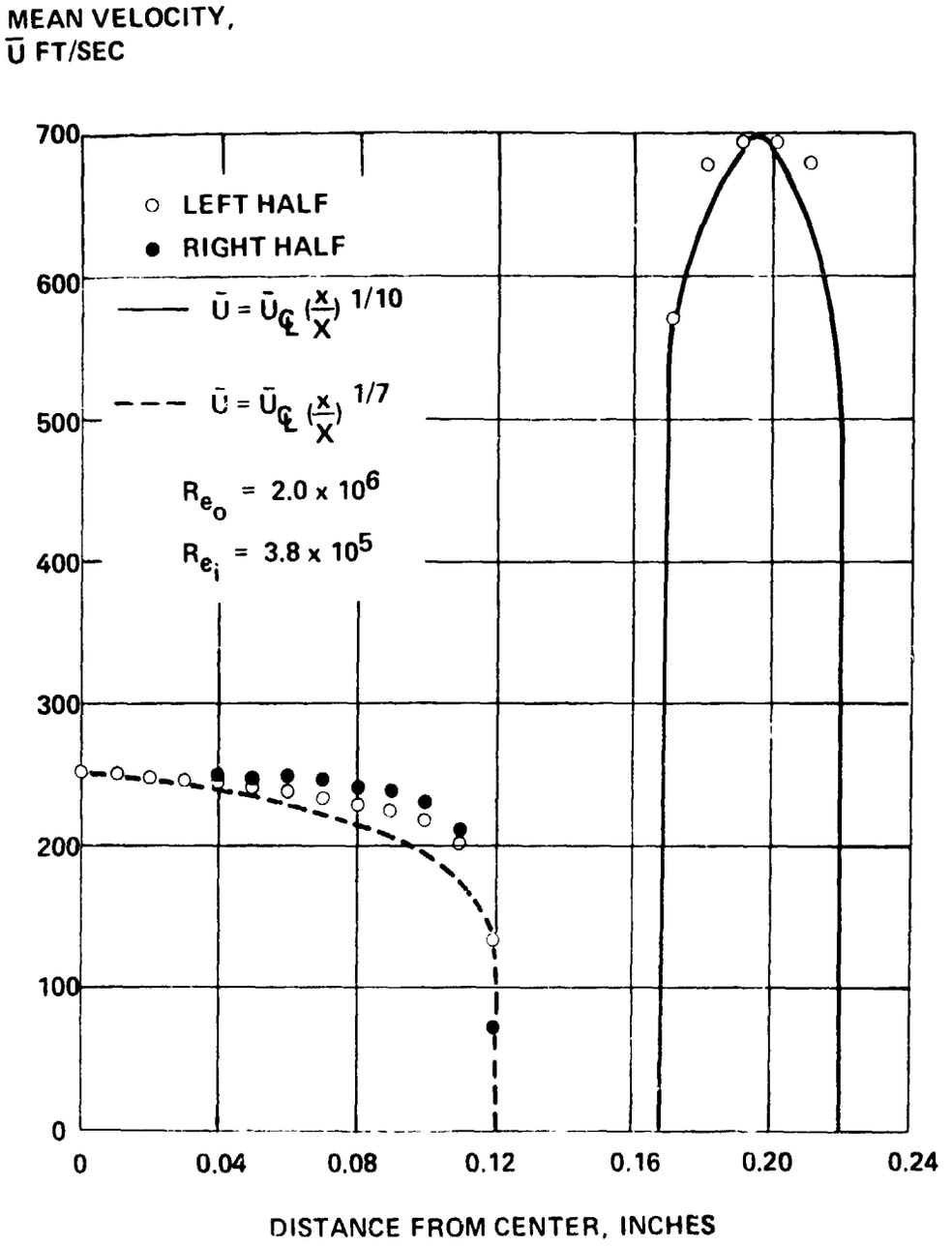

Figure 18. Comparison of Initial Velocity Profiles with 1/7 and 1/10 Power Laws

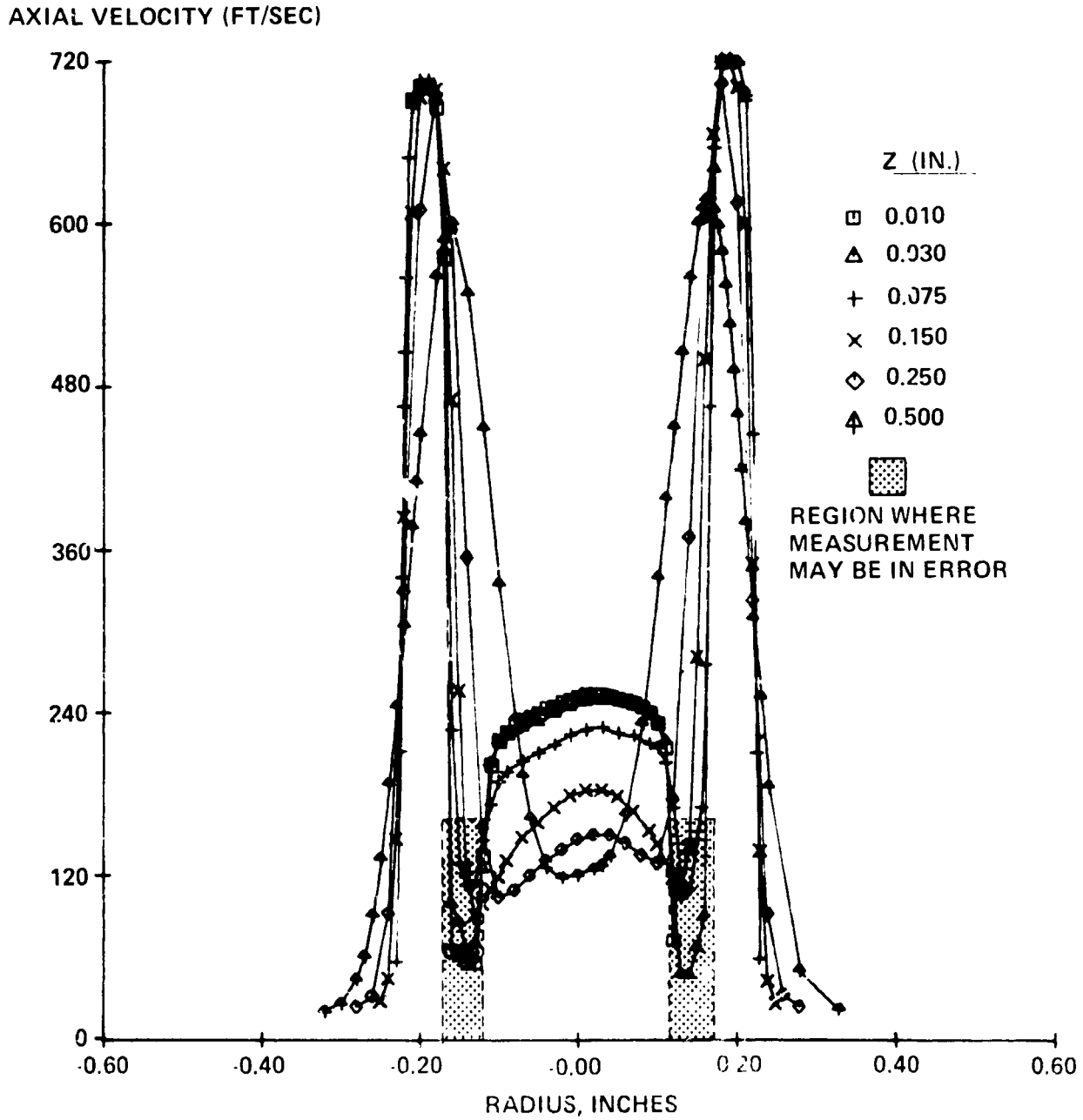

Figure 19a. Comparison of Mean Velocity Profiles for $0.01 \leq Z \leq 0.5$

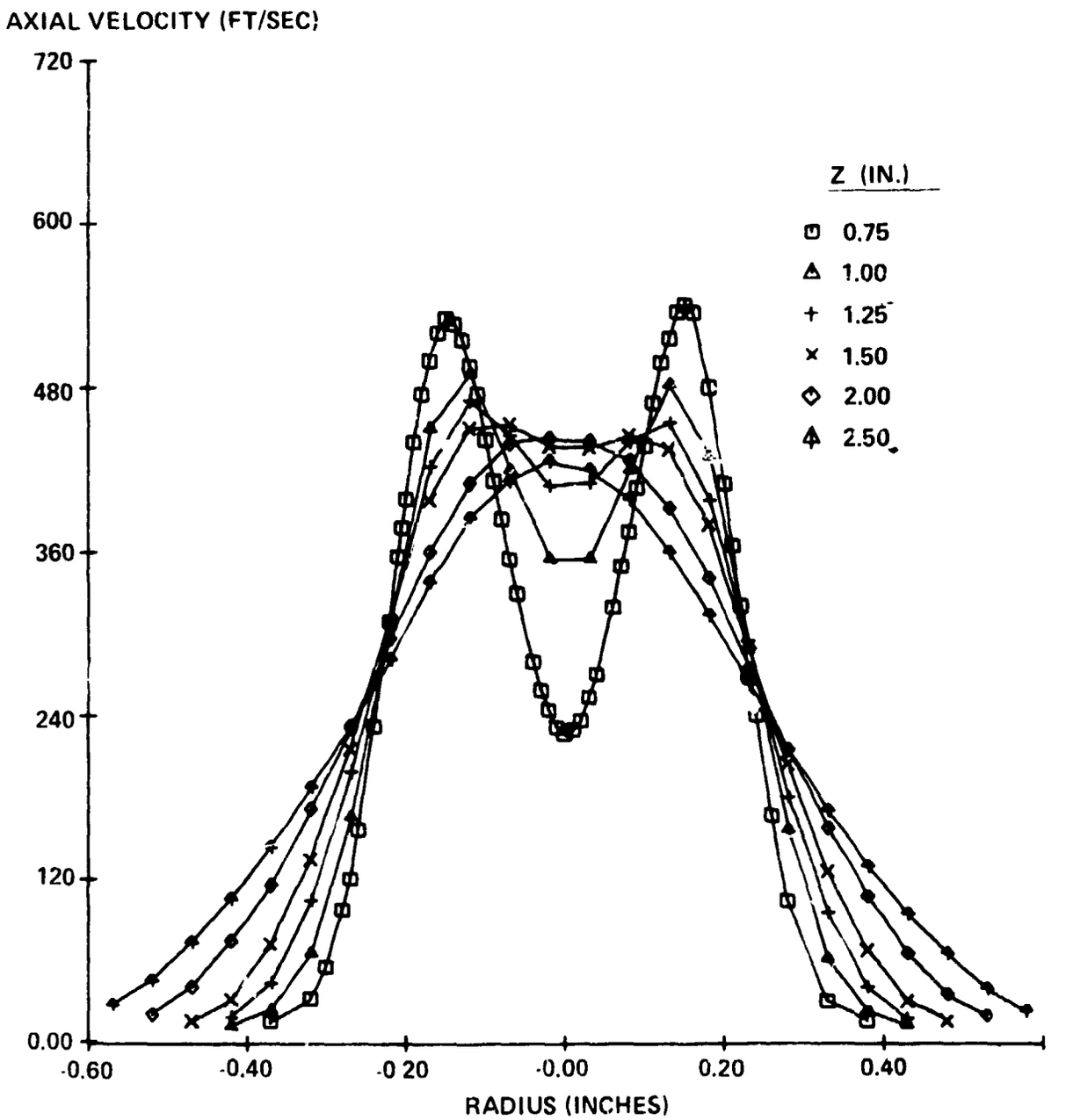

Figure 19b. Comparison of Mean Velocity Profiles for $0.75 \leq Z \leq 2.5$

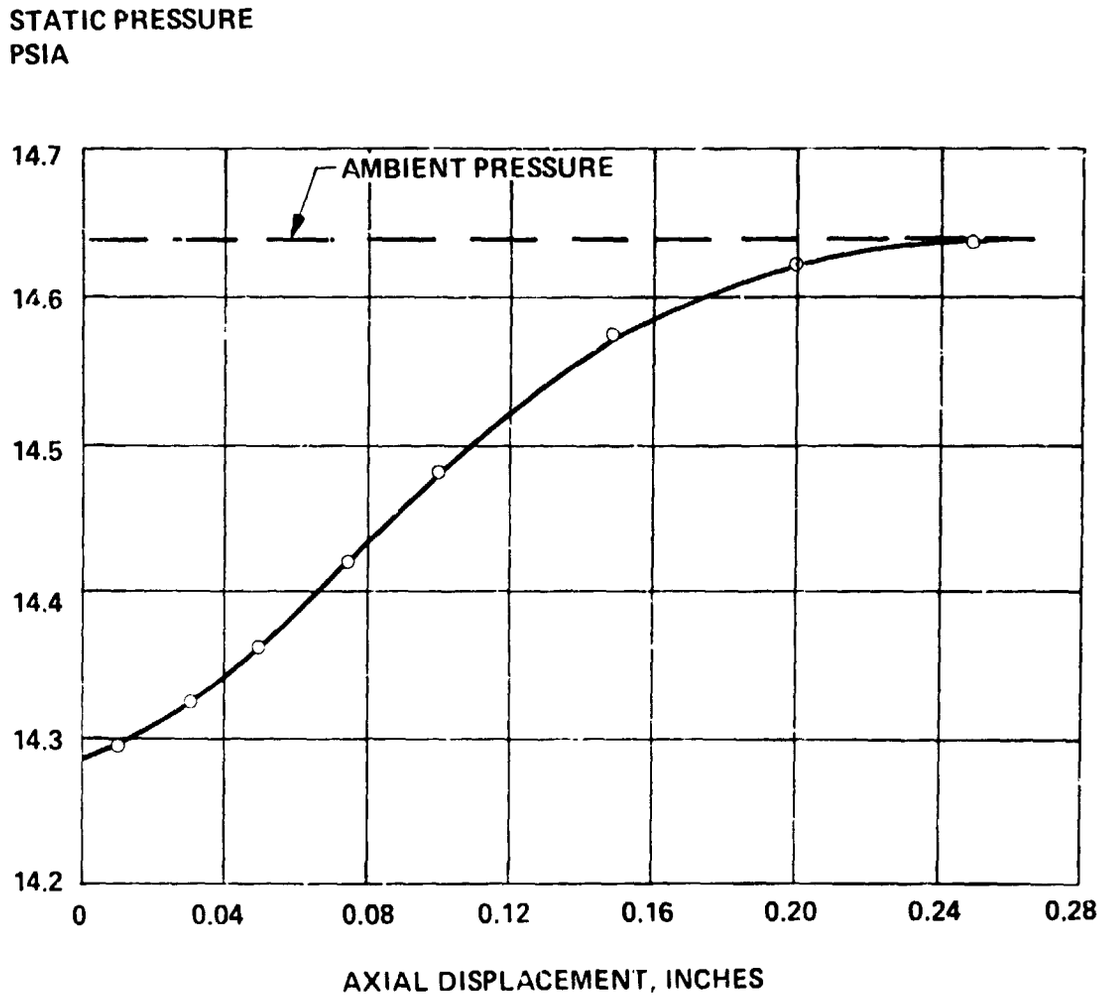

Figure 20. Centerline Static Pressure Versus Axial Displacement

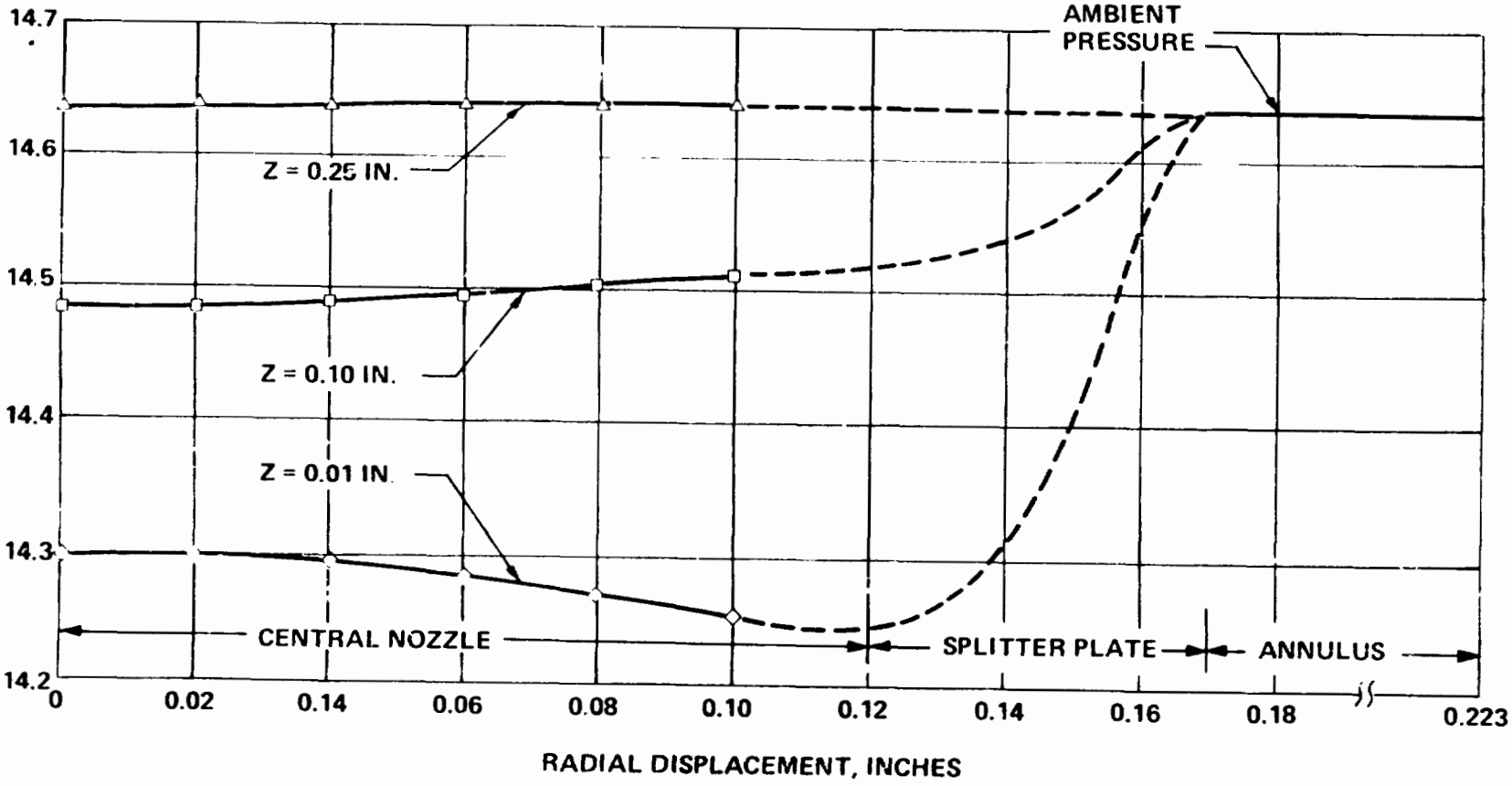

Figure 21. Radial Static Pressure Profiles

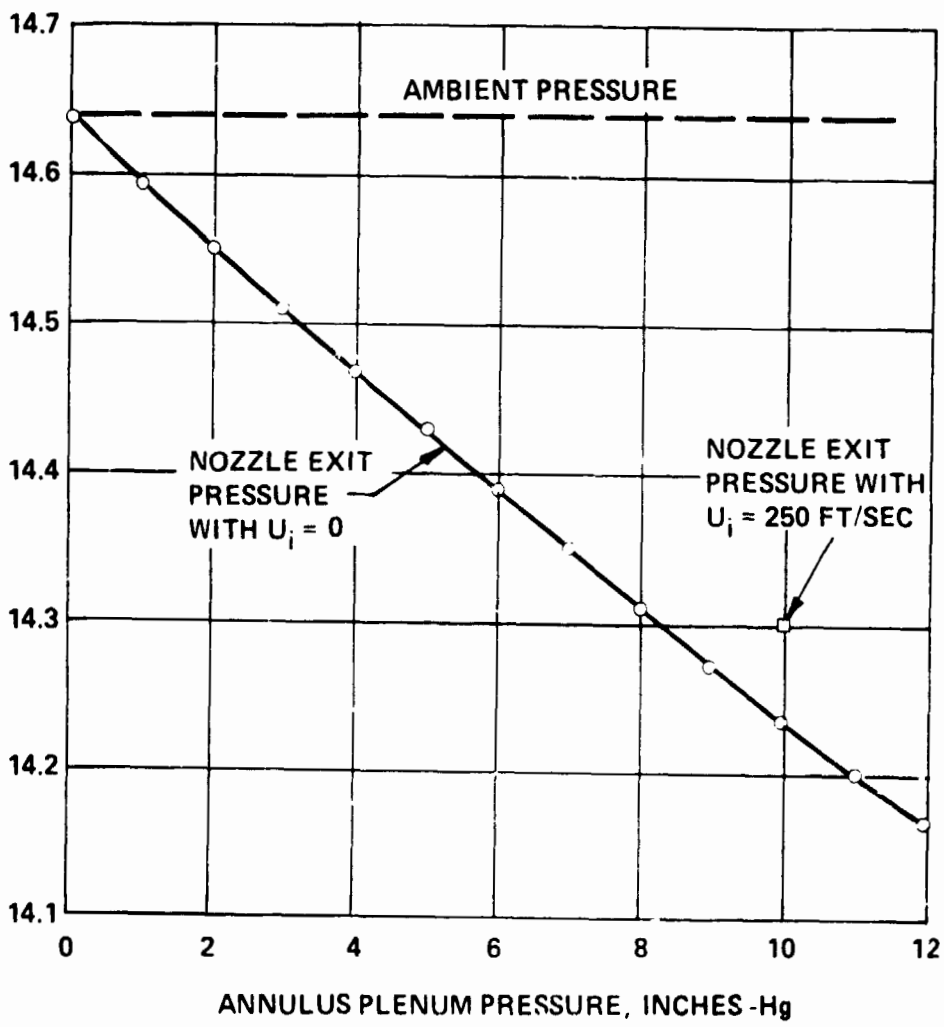

Figure 22. Pressure at Injector Exit Versus Annulus Plenum Pressure

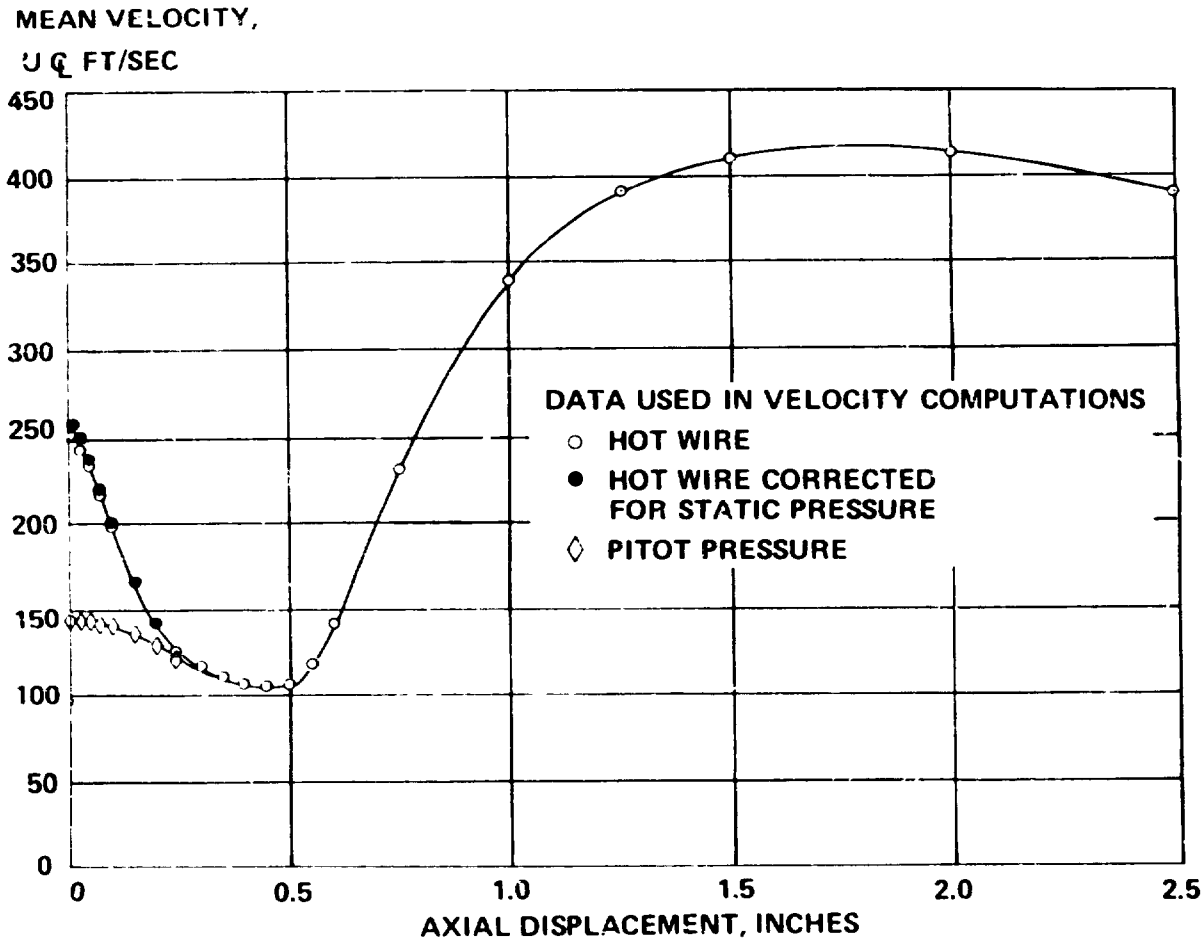

Figure 23. Centerline Velocity versus Axial Displacement

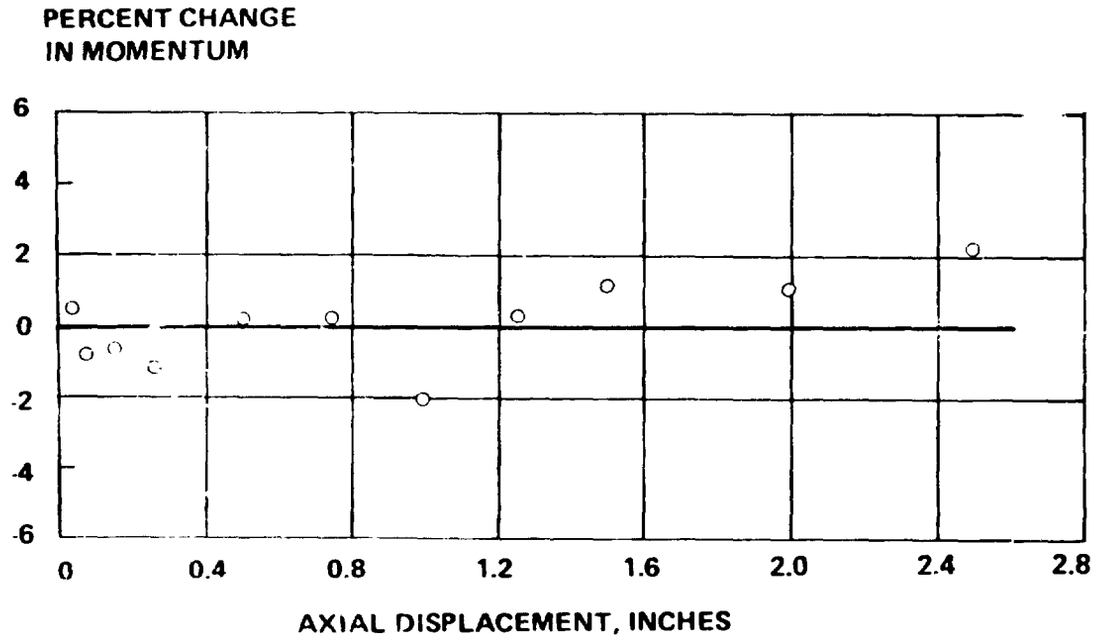

Figure 24. Percent Change in Momentum with Axial Displacement

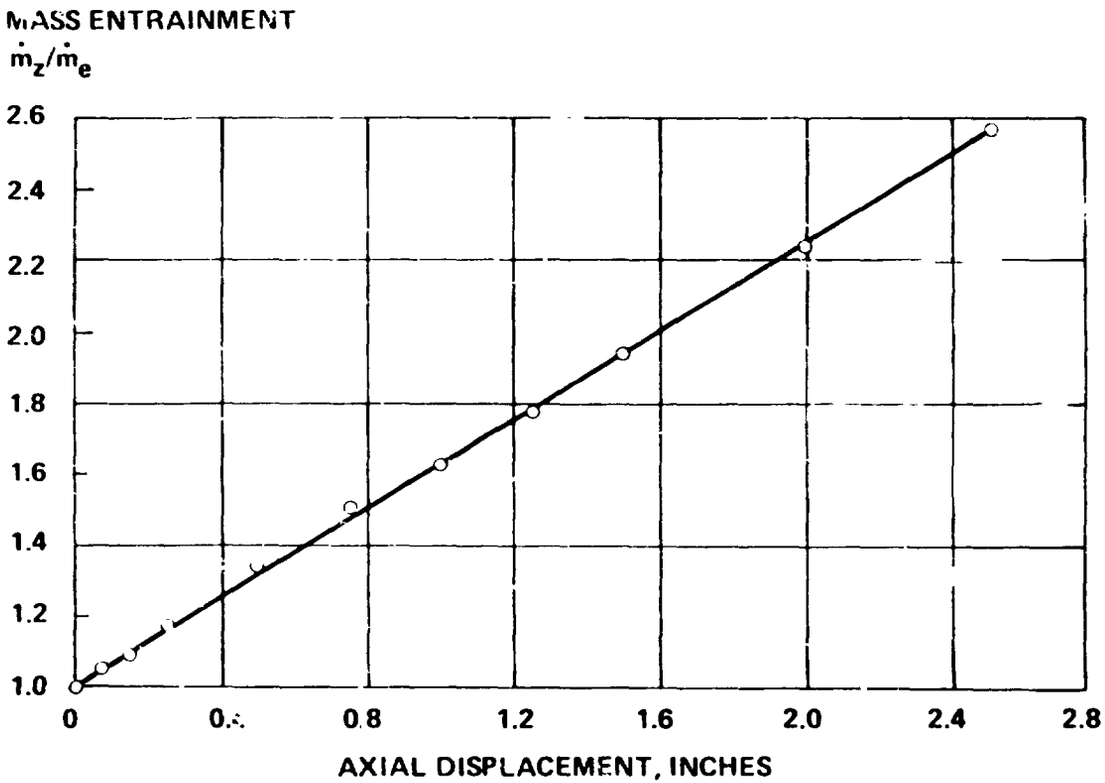

Figure 25. Variation of Mass Entrainment with Axial Displacement

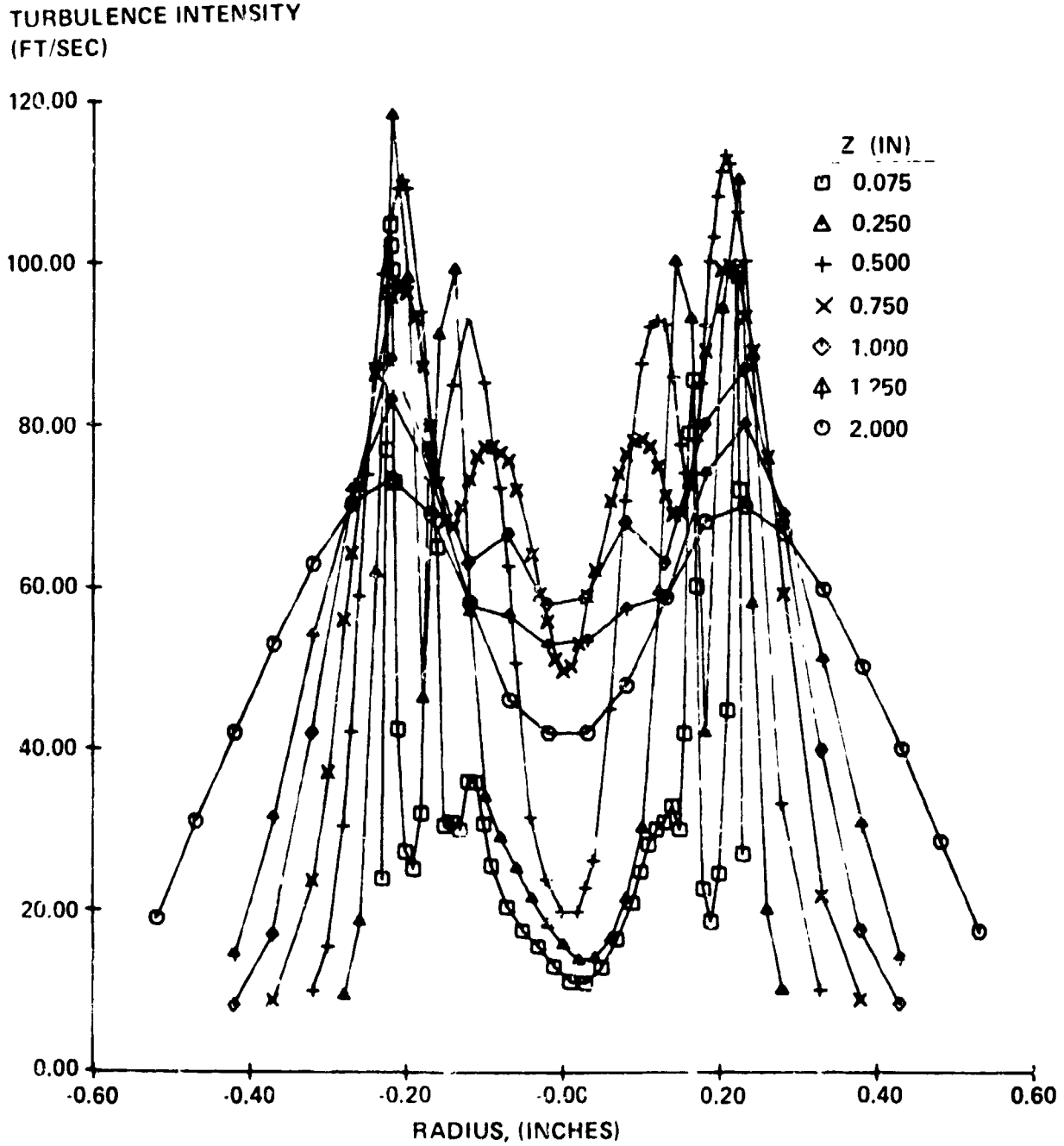

Figure 26. Comparison of Turbulence Intensity Profile for $0.075 \leq Z \leq 2.0$

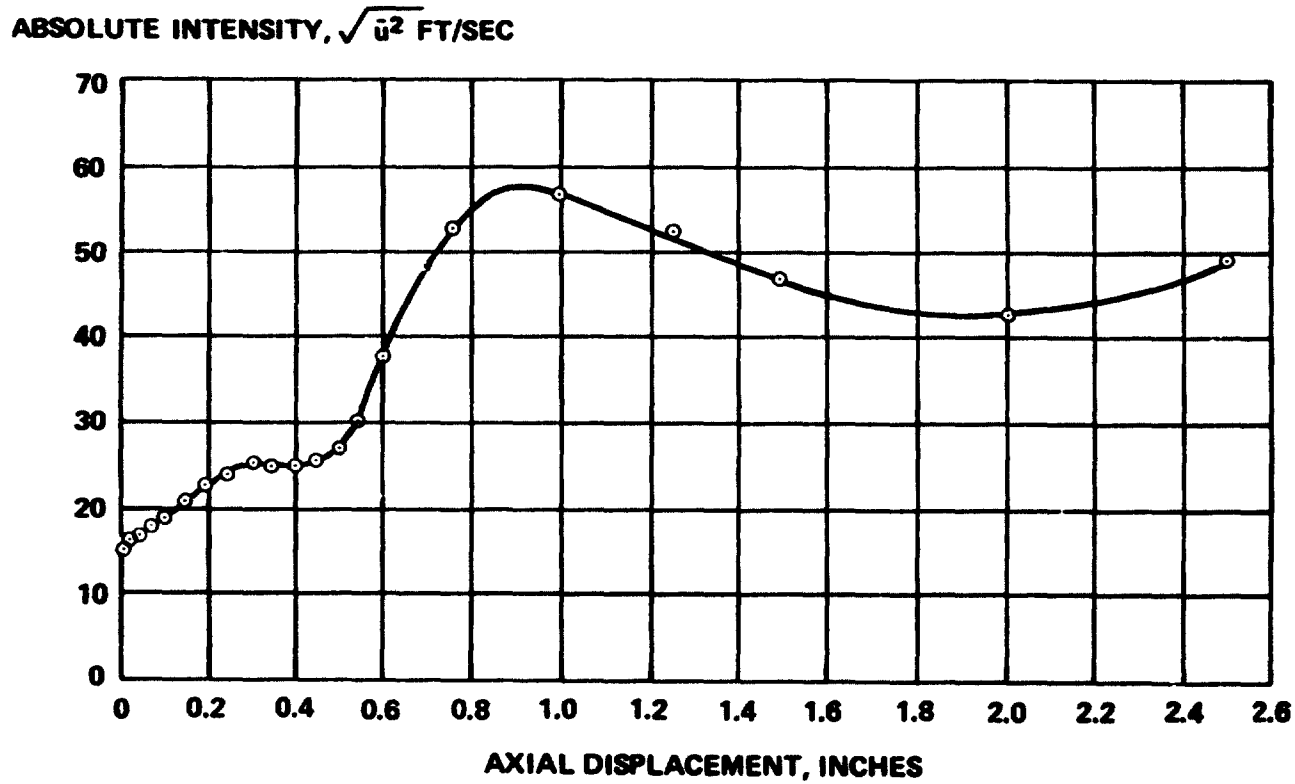

Figure 27. Centerline Turbulence Intensity versus Axial Displacement

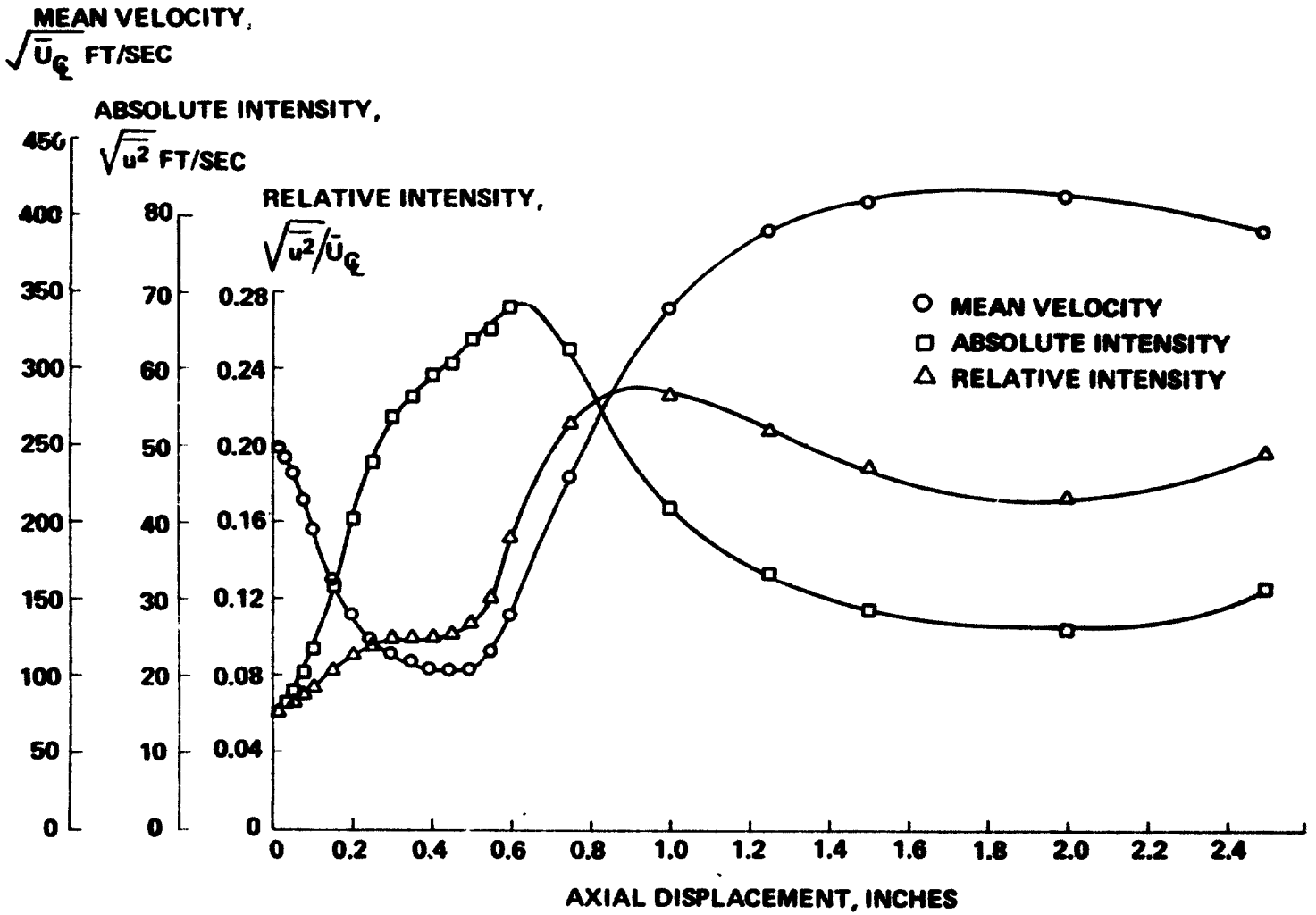

Figure 28. Comparison of Mean Velocity and Turbulence Intensity as Function of Axial Displacement

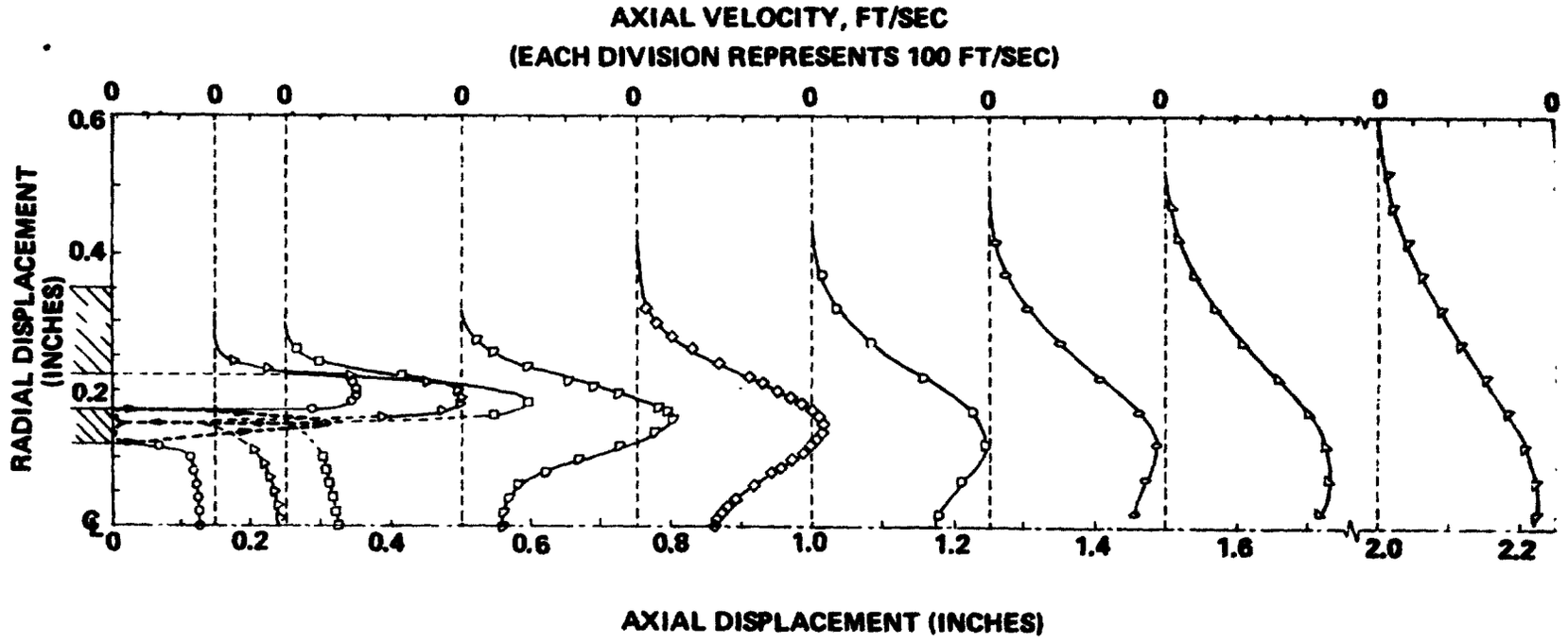

Figure 29. Coaxial Injector Flow Field Development for $U_o/U_i = 2.5$

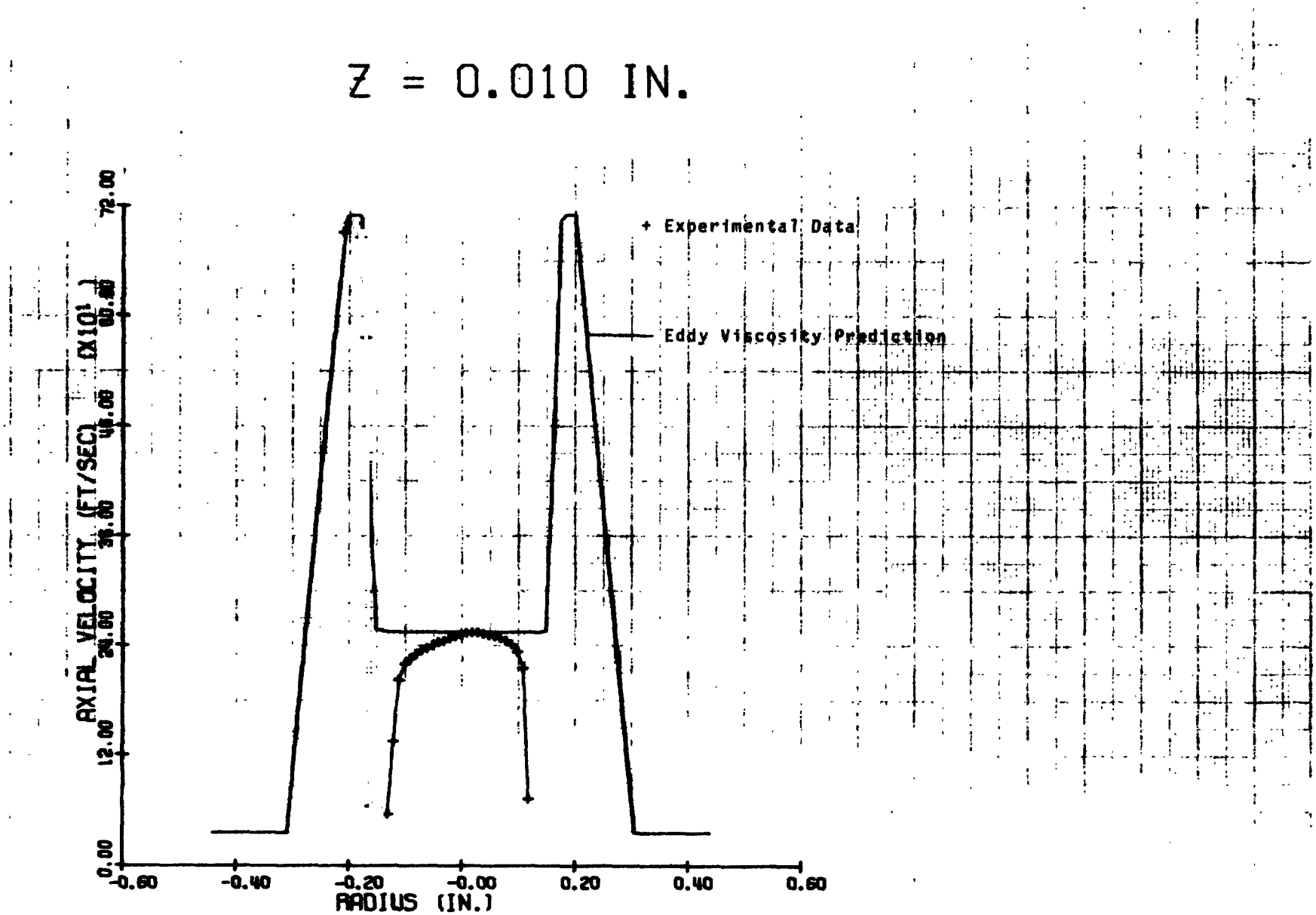

FIGURE 30. COMPARISON OF EXPERIMENTAL AND PREDICTED MEAN AXIAL VELOCITY PROFILES, z = 0.010 in.

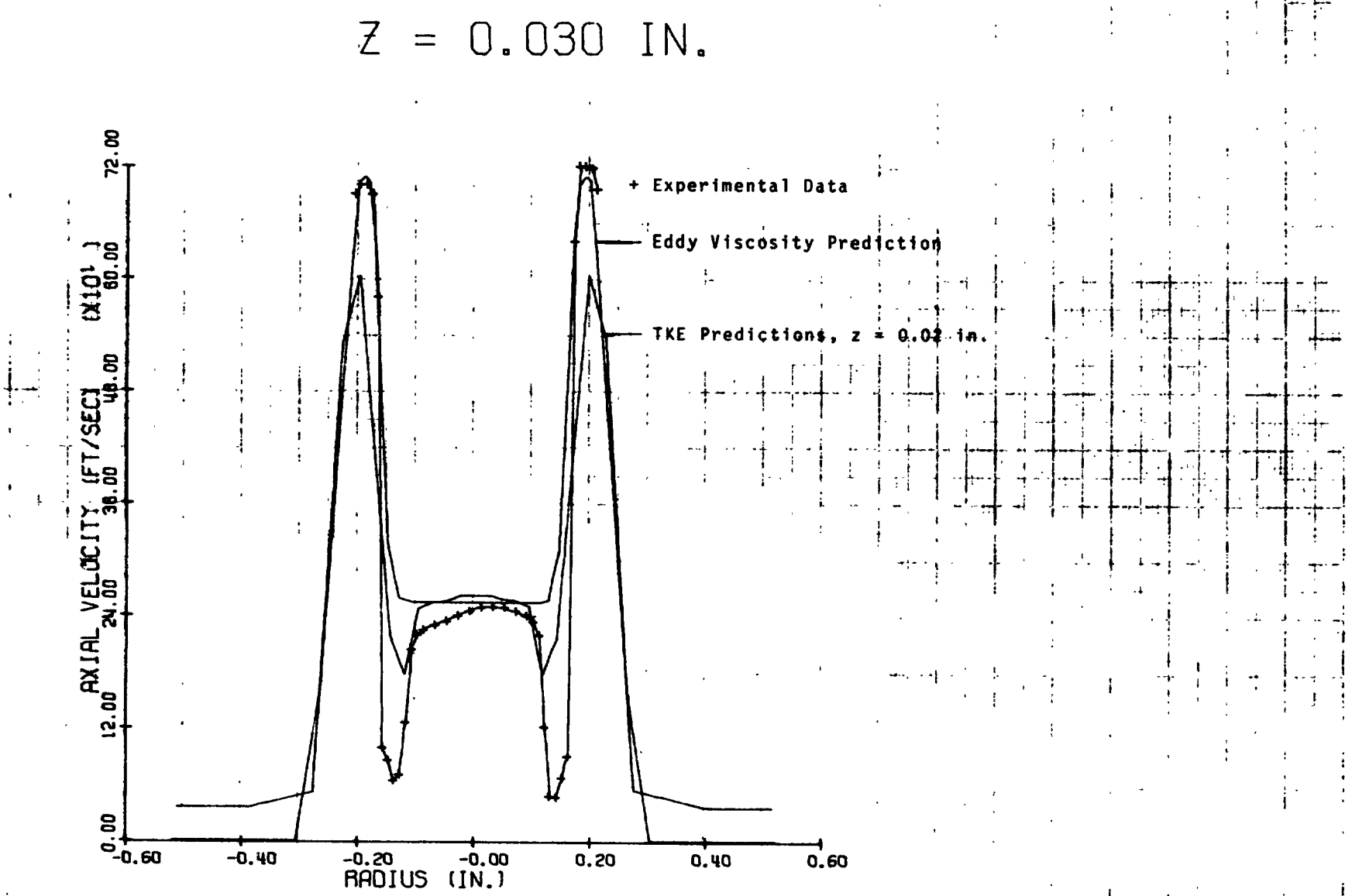

FIGURE 31. COMPARISON OF EXPERIMENTAL AND PREDICTED MEAN AXIAL VELOCITY PROFILES, z = 0.030 in.

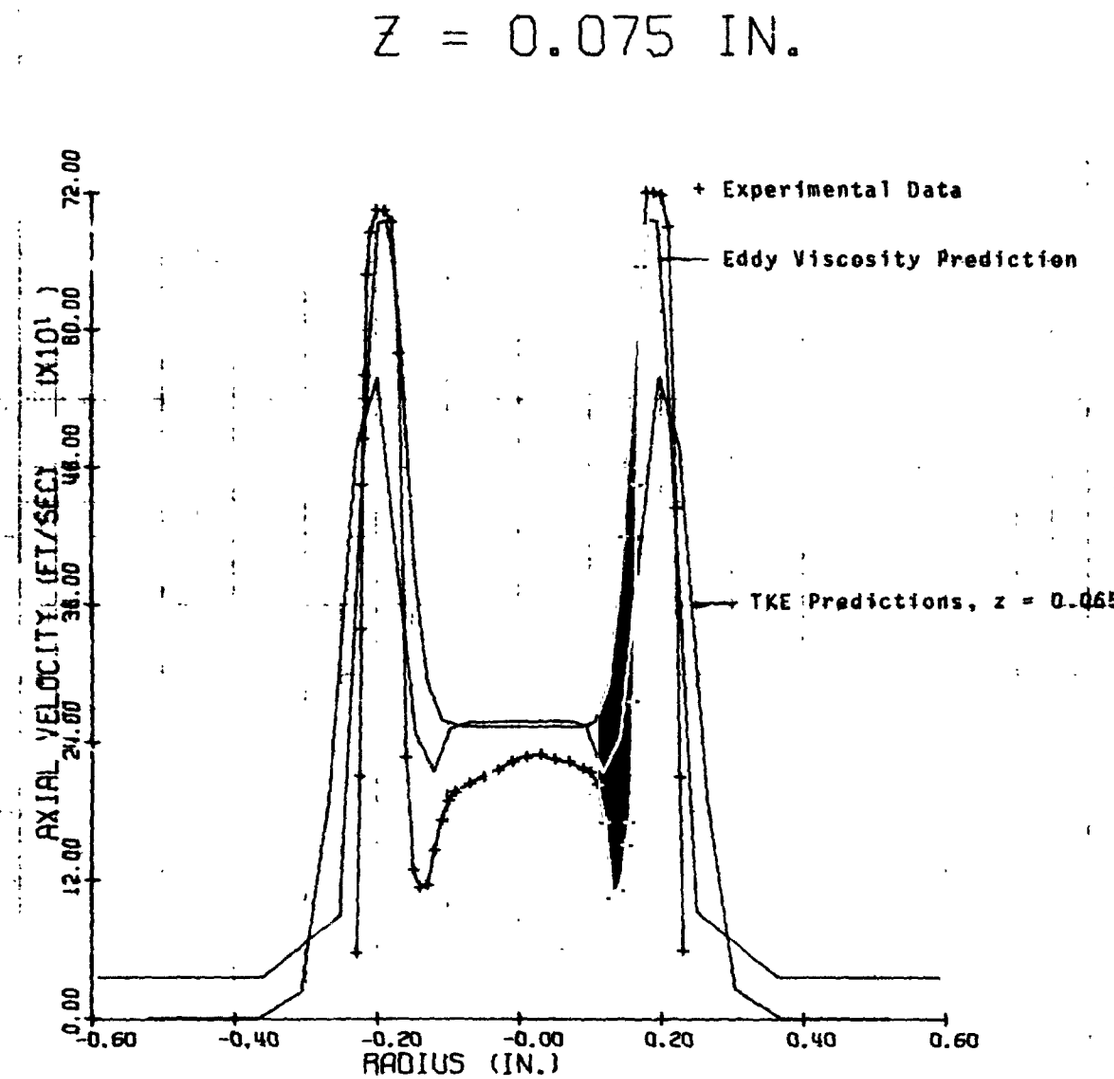

FIGURE 32. COMPARISON OF EXPERIMENTAL AND PREDICTED MEAN AXIAL VELOCITY PROFILES, z = 0.075 in.

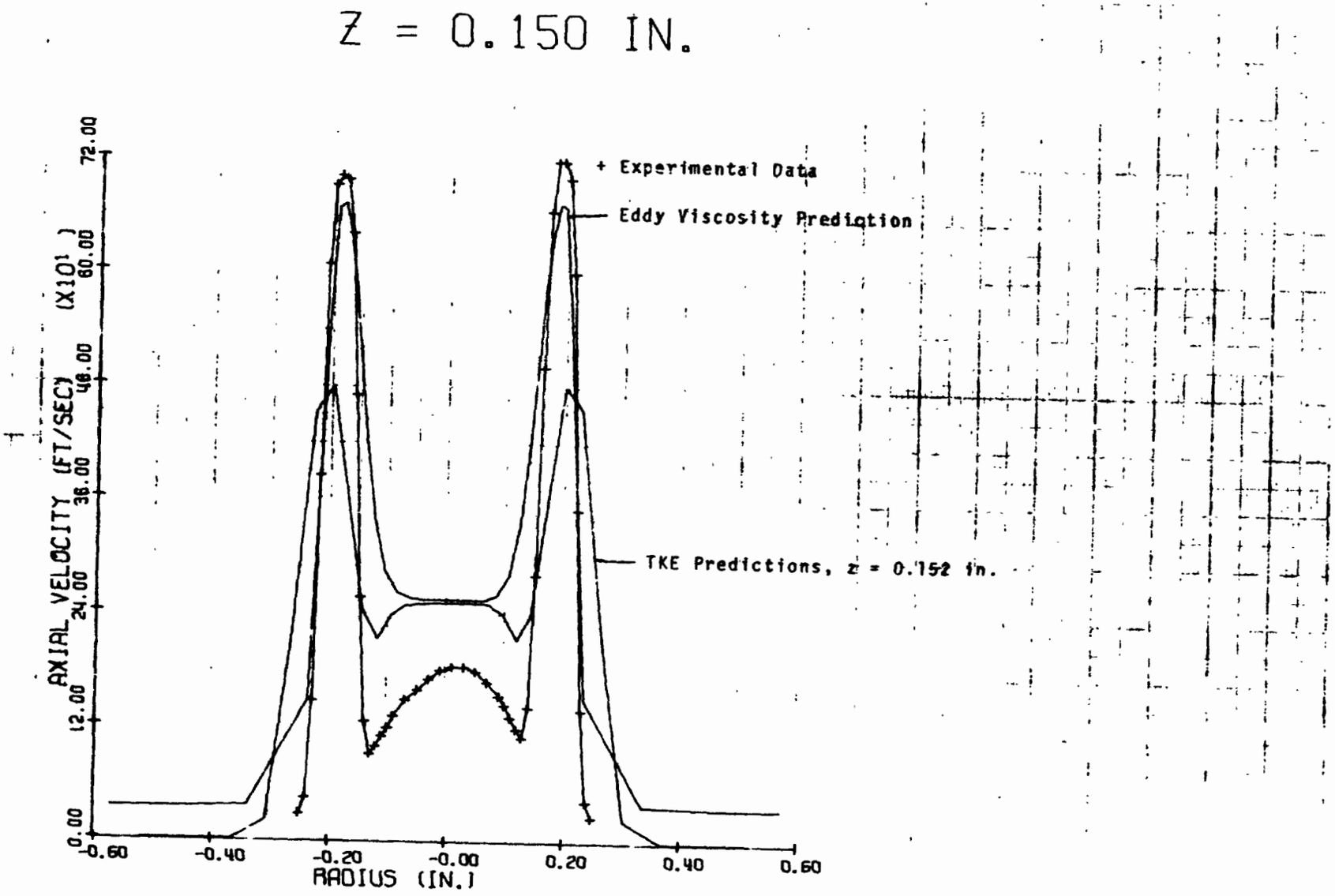

FIGURE 33. COMPARISON OF EXPERIMENTAL AND PREDICTED MEAN AXIAL VELOCITY PROFILES, z = 0.150 in.

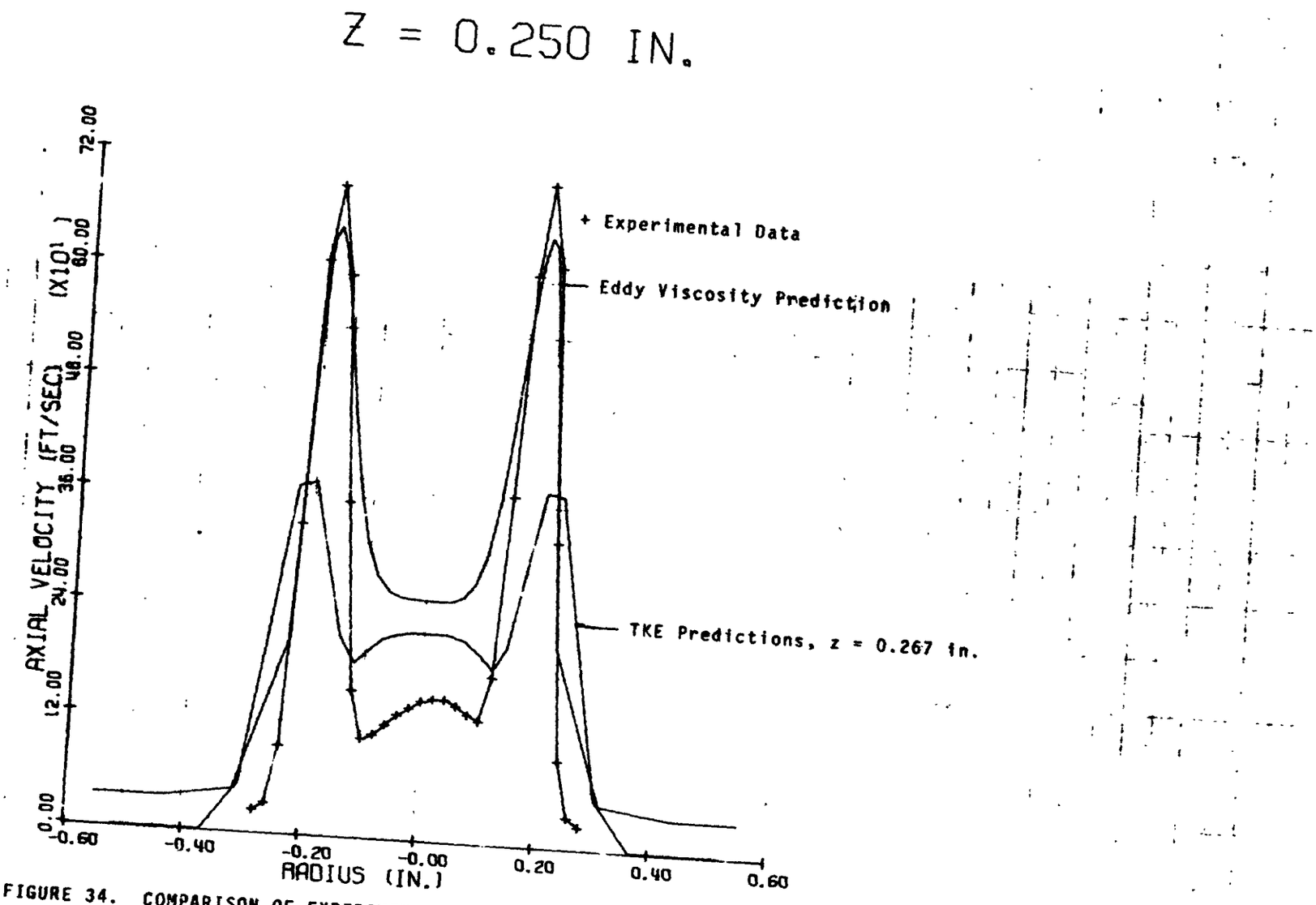

FIGURE 34. COMPARISON OF EXPERIMENTAL AND PREDICTED MEAN AXIAL VELOCITY PROFILES, z = 0.250 in.

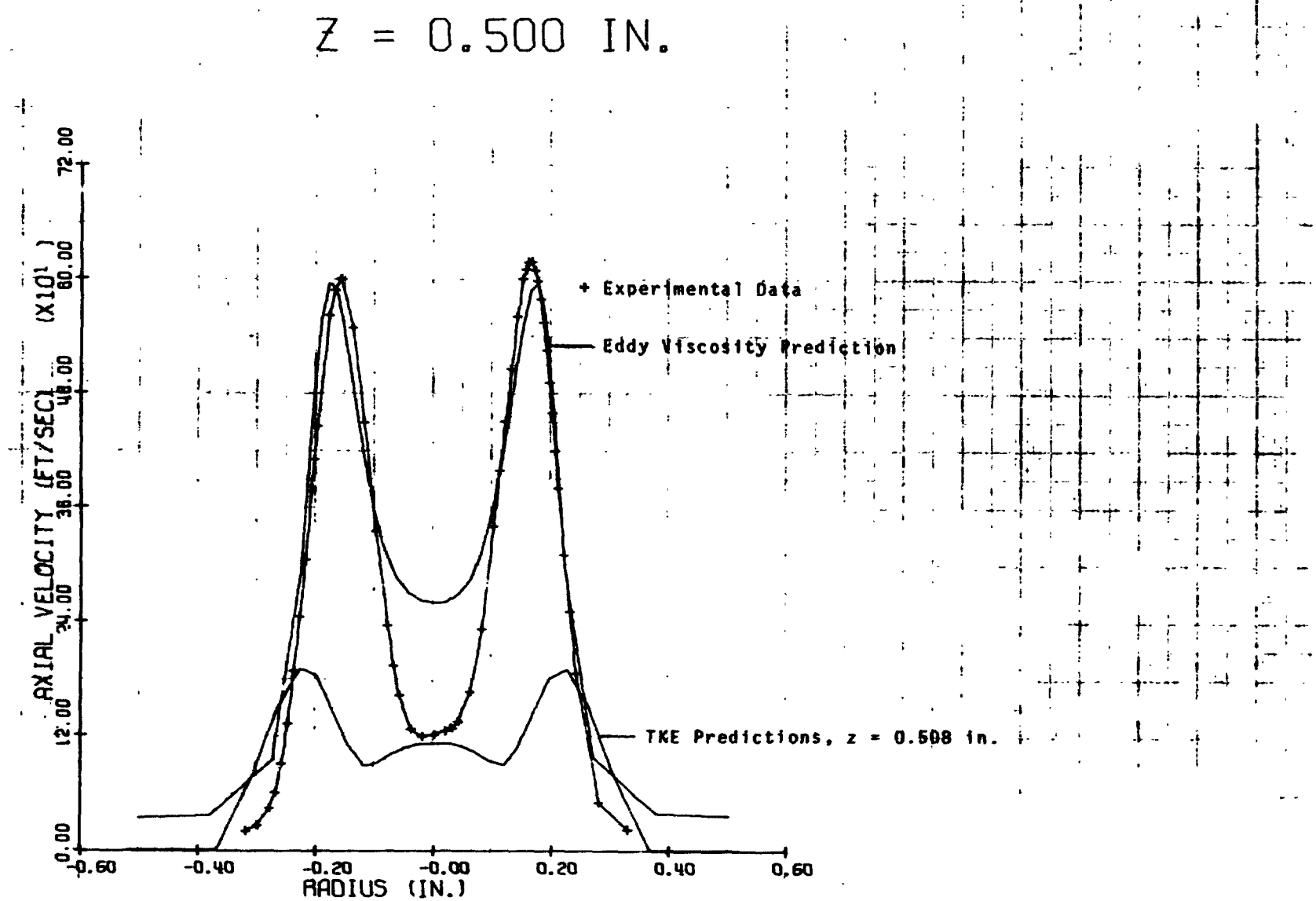

FIGURE 35. COMPARISON OF EXPERIMENTAL AND PREDICTED MEAN AXIAL VELOCITY PROFILES, z = 0.500 in.

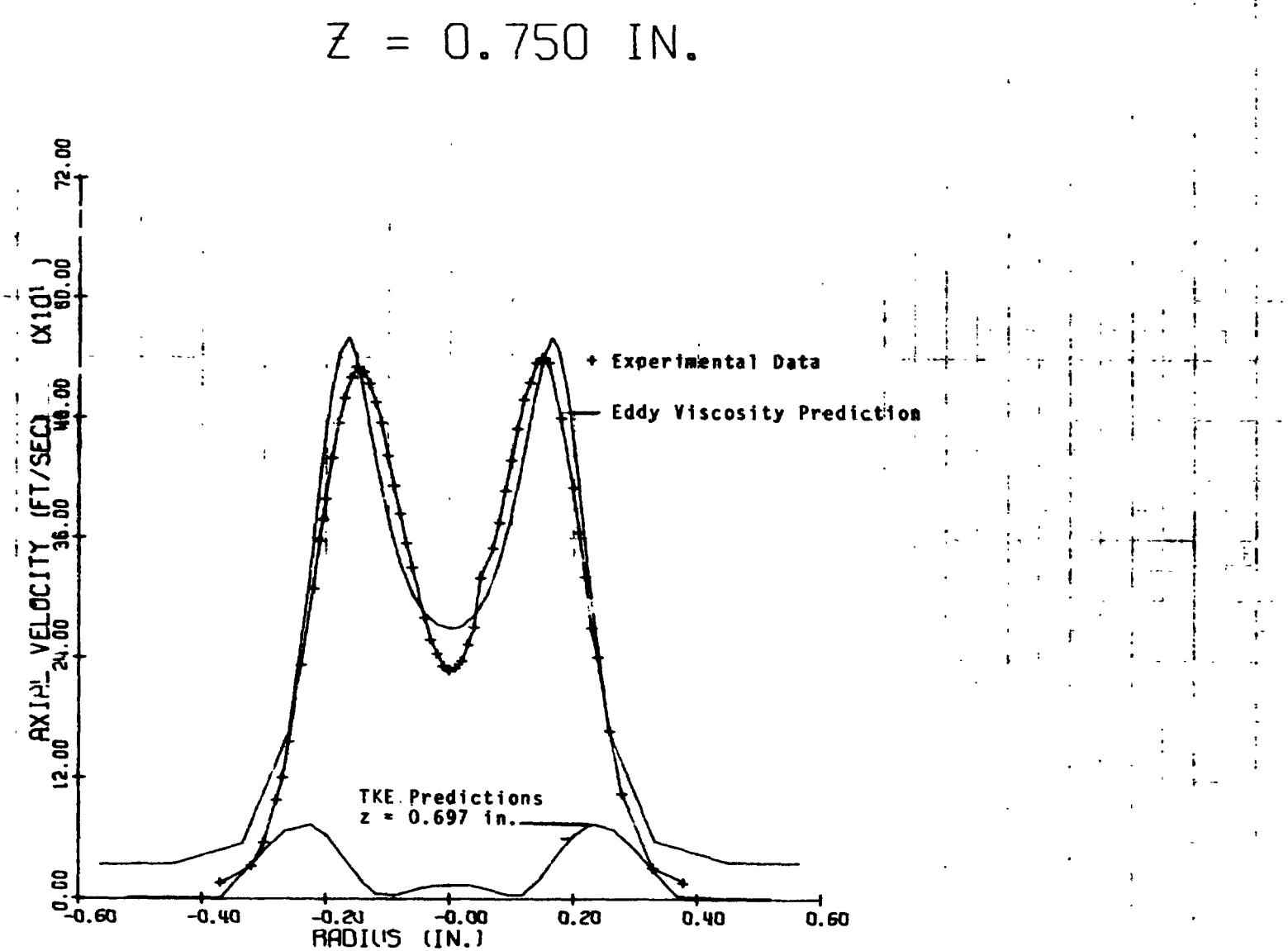

FIGURE 36. COMPARISON OF EXPERIMENTAL AND PREDICTED MEAN AXIAL VELOCITY PROFILES, z = 0.750 in.

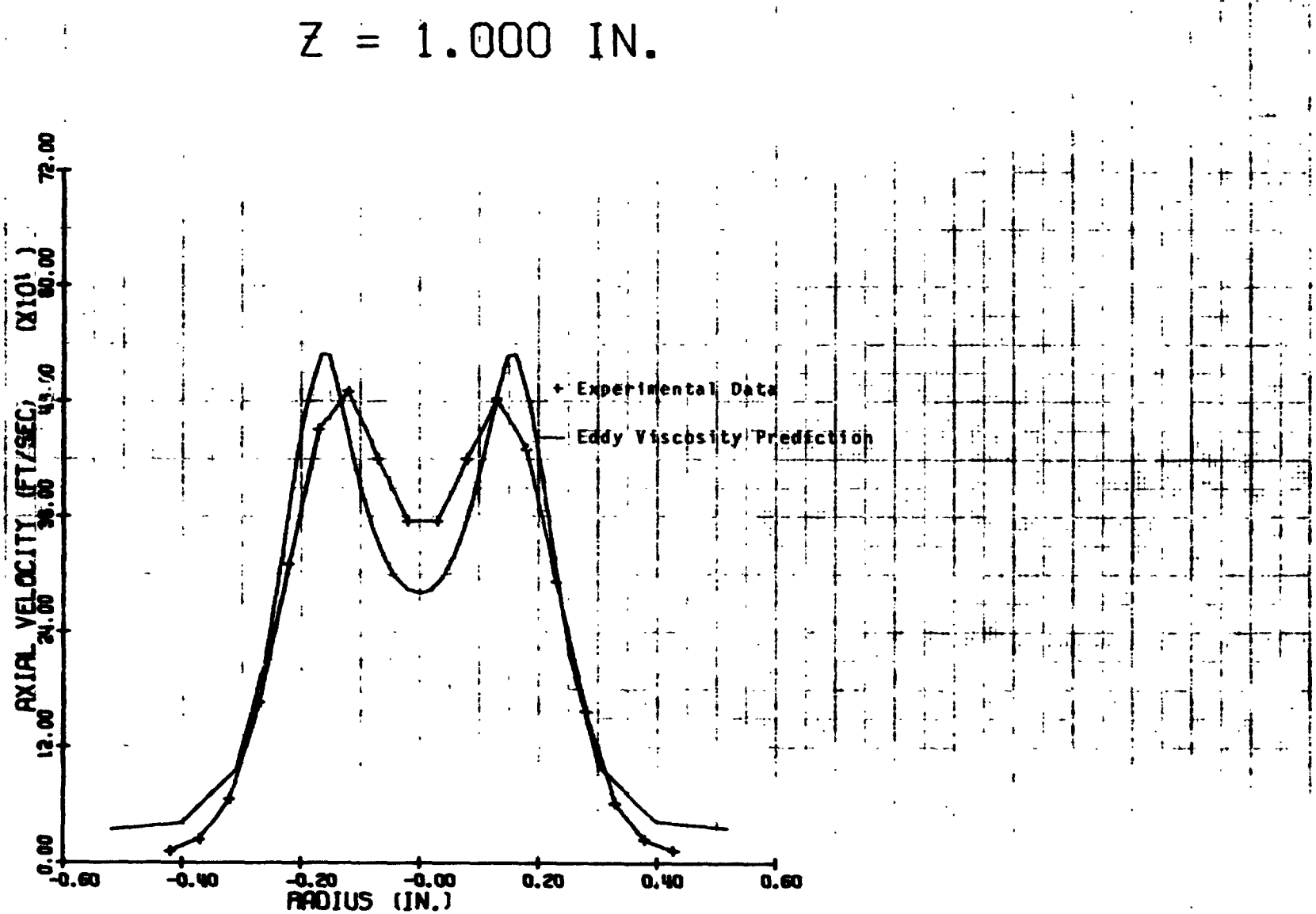

FIGURE 37. COMPARISON OF EXPERIMENTAL AND PREDICTED MEAN AXIAL VELOCITY PROFILES, z = 1.000 in.

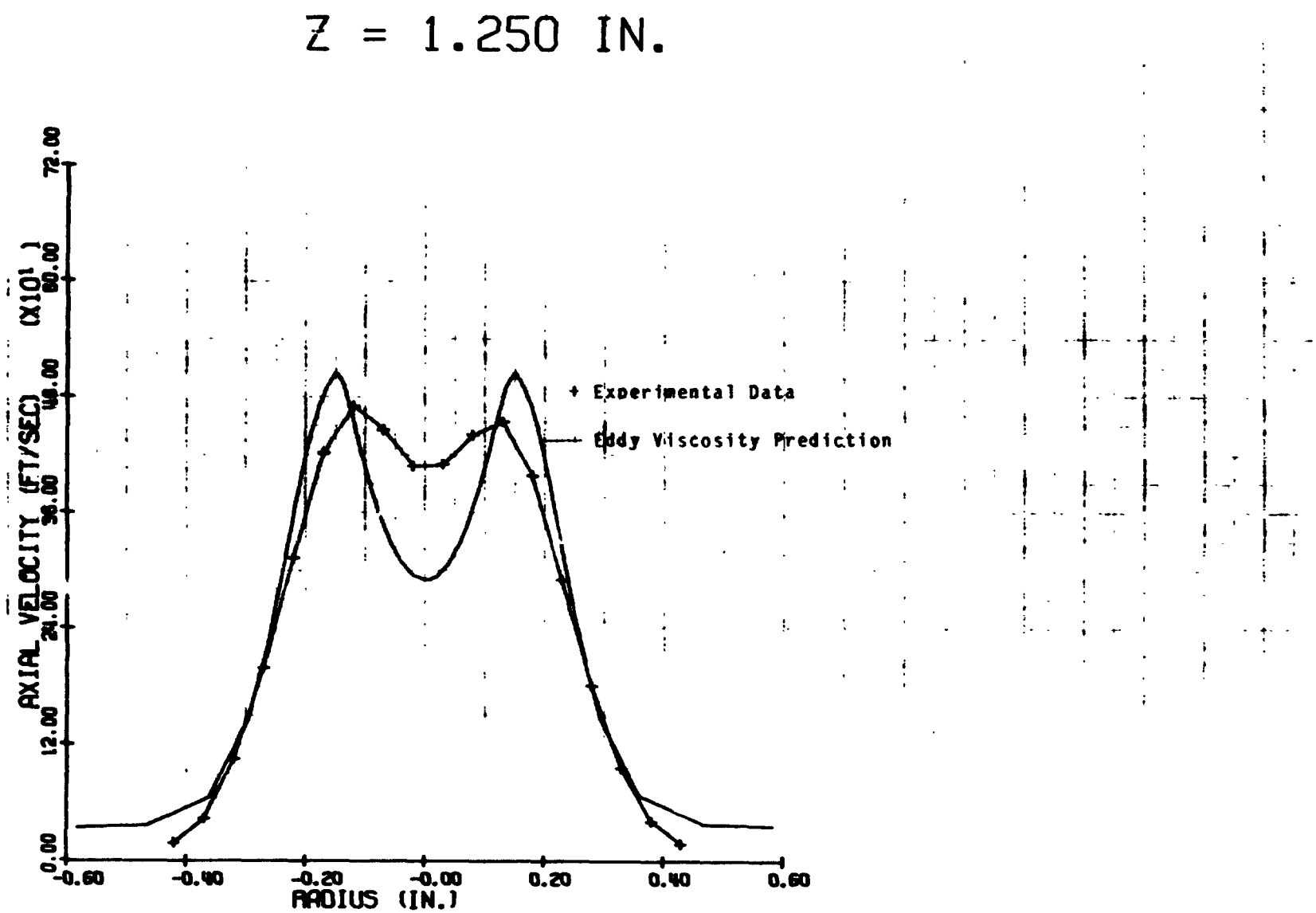

FIGURE 38. COMPARISON OF EXPERIMENTAL AND PREDICTED MEAN AXIAL VELOCITY PROFILES, z = 1.250 in.

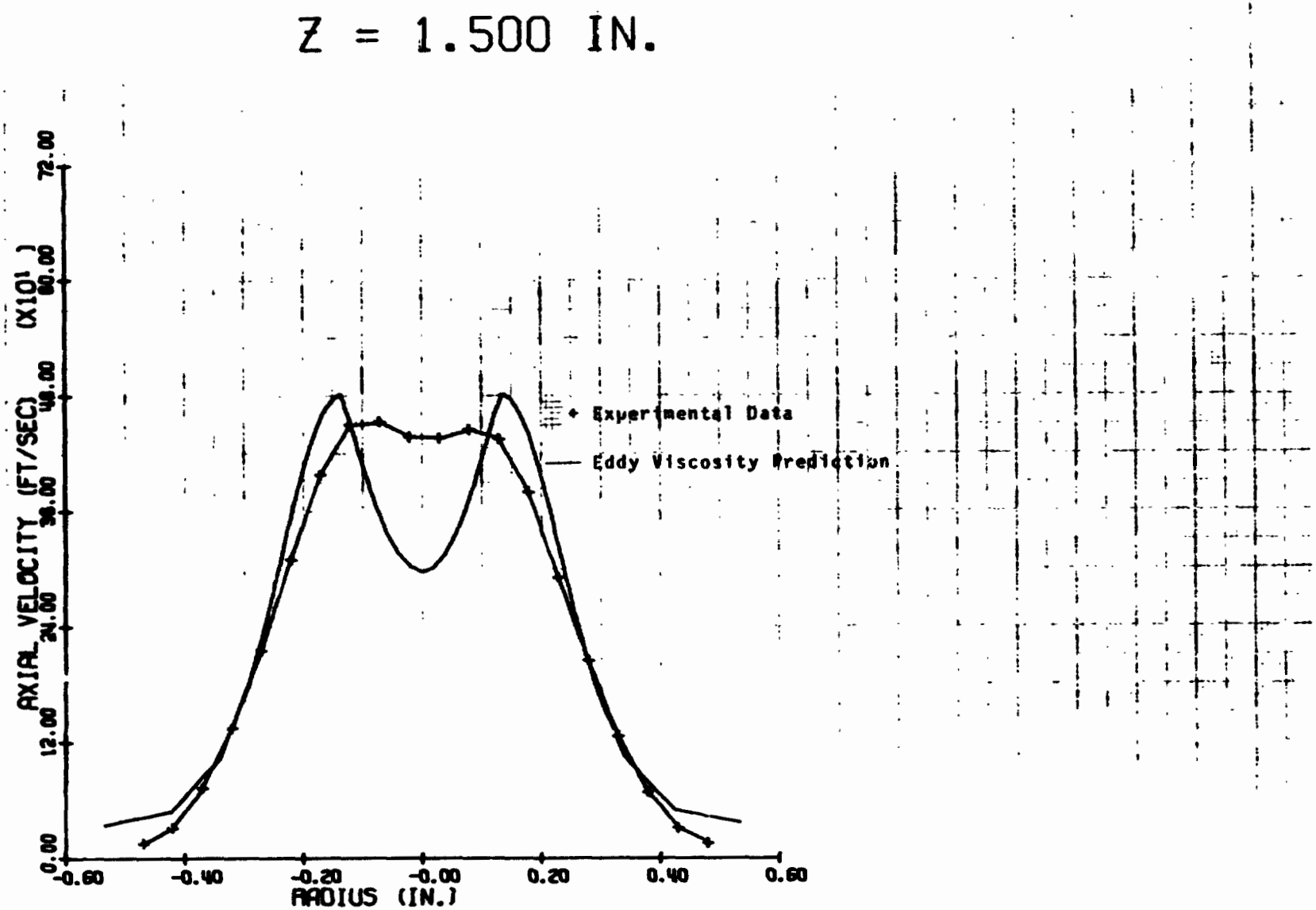

FIGURE 39. COMPARISON OF EXPERIMENTAL AND PREDICTED MEAN AXIAL VELOCITY PROFILES, z = 1.500 in.

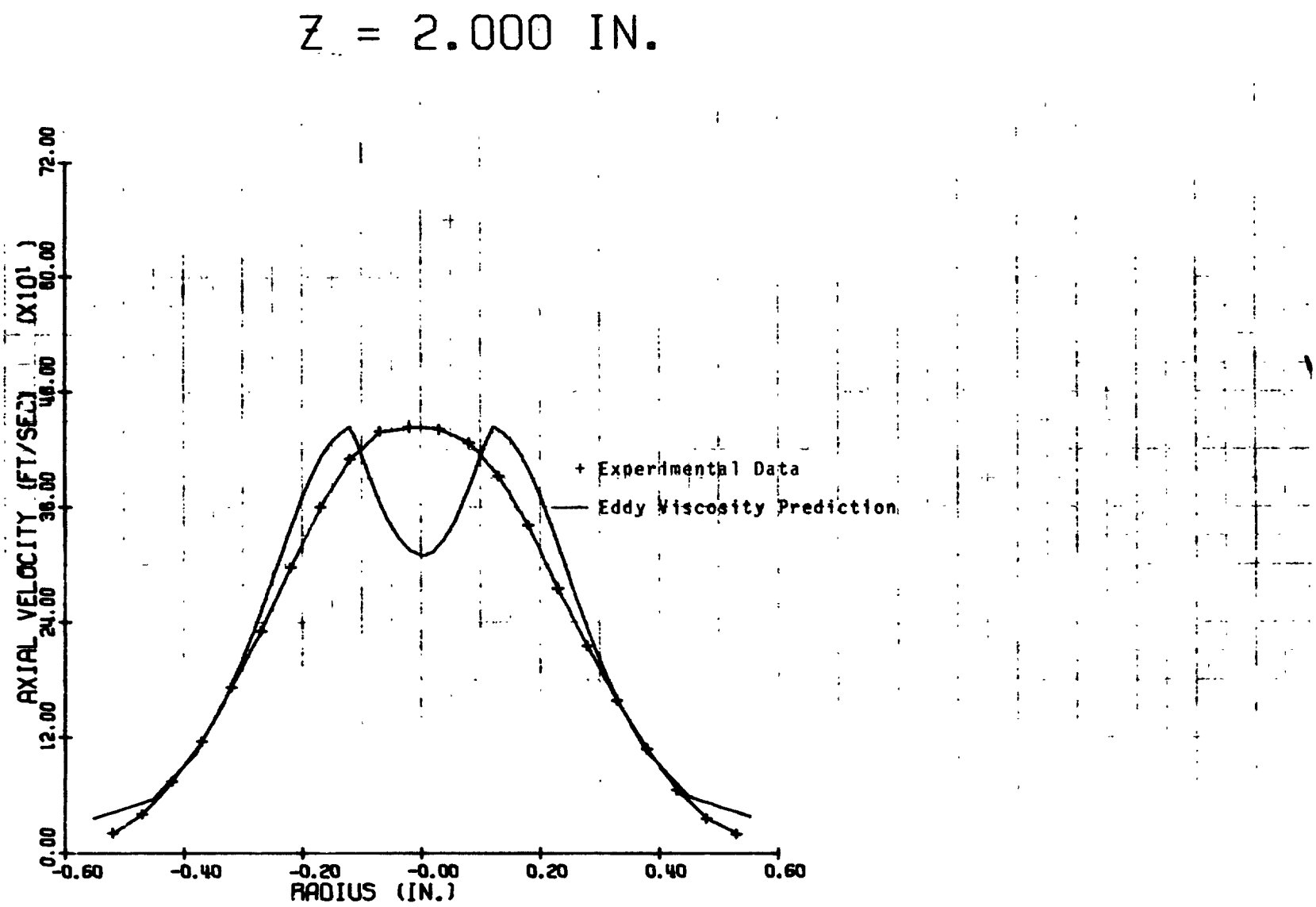

FIGURE 40. COMPARISON OF EXPERIMENTAL AND PREDICTED MEAN AXIAL VELOCITY PROFILES, z = 2.000 in.

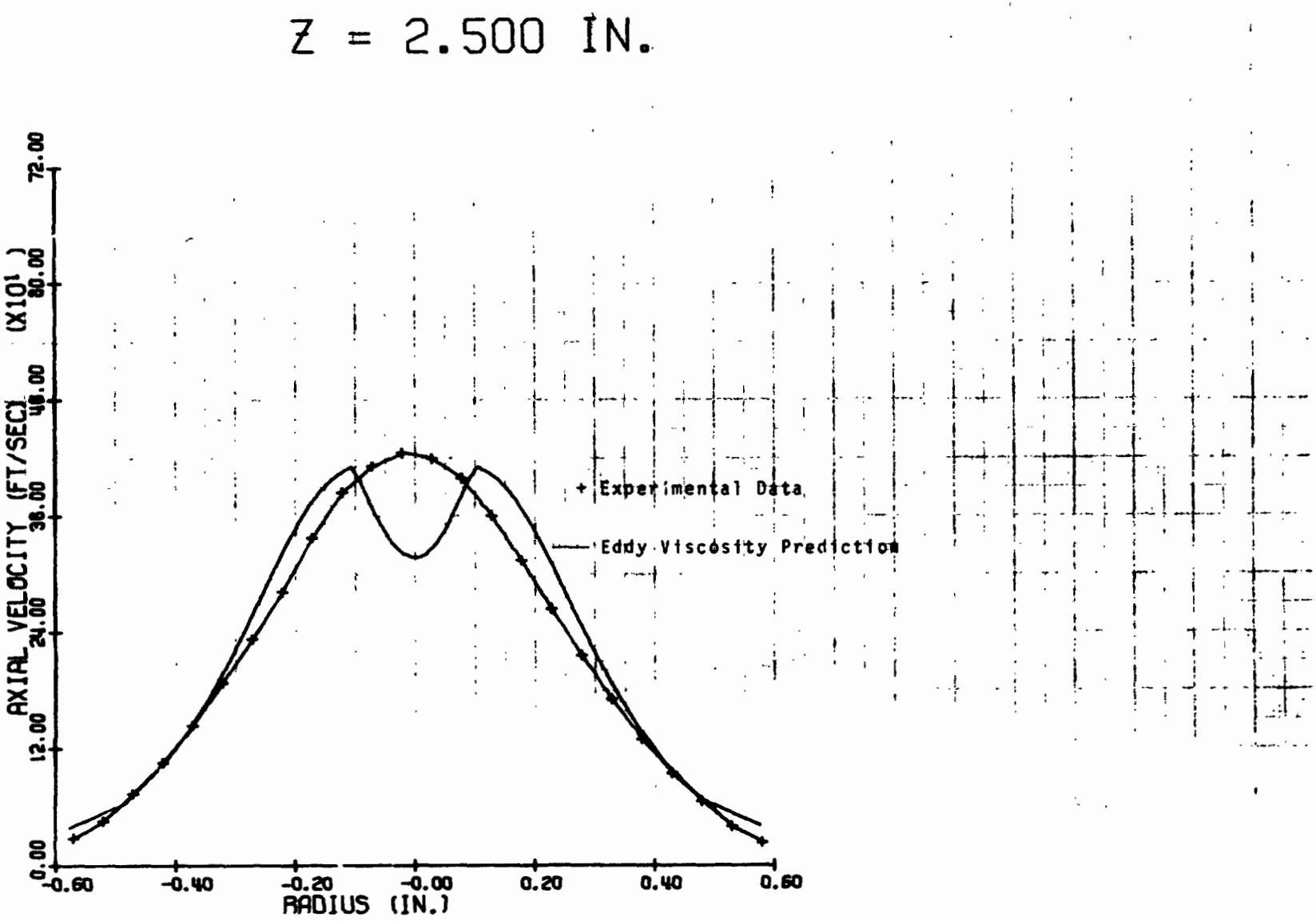

FIGURE 41. COMPARISON OF EXPERIMENTAL AND PREDICTED MEAN AXIAL VELOCITY PROFILES, z = 2.500 in.

APPENDIX A

GASEOUS HYDROGEN/OXYGEN ROCKET PERFORMANCE CORRELATION AND PREDICTION PROGRAM

User's Manual for IBM 7090

Prepared by

O. H. Fortune
J. H. Morgenthaler
S. Feyl

APPENDIX A

GASEOUS HYDROGEN/OXYGEN ROCKET PERFORMANCE CORRELATION AND PREDICTION PROGRAM

1. Description of Program

The computer program used for the Gaseous H_2/O_2 Rocket Performance Correlation Prediction Calculations is similar to that described in detail in Ref. 8, i.e., it utilizes an explicit finite-difference numerical integration technique in which the governing shear layer equations (which are identical in form to the boundary layer equations) are solved in the von Mises coordinate system. The basic partial differential equations solved are:

Mass *

$$\frac{\partial \rho u y^N}{\partial x} + \frac{\partial \rho v y^N}{\partial y} =$$

Momentum

$$\rho u \frac{\partial u}{\partial x} + \rho v \frac{\partial u}{\partial y} = \frac{1}{y^N} \frac{\partial}{\partial y} \left[\mu y^N \frac{\partial u}{\partial y}\right] - \frac{dp}{dx}$$

Energy

$$\rho u \frac{\partial H}{\partial x} + \rho v \frac{\partial H}{\partial y} = \frac{1}{y^N} \frac{\partial}{\partial y} \left[\mu y^N \left\{\frac{\partial \frac{u^2}{2}}{\partial y} + \frac{1}{Pr}\left(\frac{\partial H}{\partial y} - \frac{\partial \frac{u^2}{2}}{\partial y}\right)\right.\right.$$

$$\left.\left. + \left(\frac{1}{Sc} - \frac{1}{Pr}\right) \sum_{y=1}^{n} h^j \frac{\partial \alpha^j}{\partial y}\right\}\right]$$

Diffusion

(a) Species (frozen and finite rate chemistry)

$$\rho u \frac{\partial \alpha^j}{\partial x} + \rho v \frac{\partial \alpha^j}{\partial y} = \frac{1}{y^N} \frac{\partial}{\partial y} \left[\frac{\mu}{Sc} y^N \frac{\partial \alpha^j}{\partial y}\right] + \dot{w}^j$$

*Nomenclature is consistent with that of Ref. 8.

(b) Elements (equilibrium chemistry)

$$\rho u \frac{\partial \tilde{\alpha}^k}{\partial x} + \rho v \frac{\partial \tilde{\alpha}^k}{\partial y} = \frac{1}{y^N} \frac{\partial}{\partial y} \left[\frac{\mu}{Sc} y^N \frac{\partial \tilde{\alpha}^k}{\partial y} \right]$$

where

$$N = \begin{cases} 0 = \text{Planar Two-Dimensional Flow} \\ 1 = \text{Axisymmetric Flow} \end{cases}$$

The equations are transformed from the physical plane to a stream function plane specified by

$$\psi^N \partial \psi = \rho u y^N \partial y \text{ and } \psi^N \partial \psi = \rho v y^N \partial x$$

In this plane, the Conservation Equations become:

Momentum

$$\frac{\partial u}{\partial x} = \frac{1}{\psi^N} \frac{\partial}{\partial \psi} \left[a \frac{\partial u}{\partial \psi} \right] - \frac{1}{\rho u} \frac{dp}{dx}$$

Energy

$$\frac{\partial H}{\partial x} = \frac{1}{\psi^N} \frac{\partial}{\partial \psi} \left[a \left\{ \frac{\partial \frac{u^2}{2}}{\partial \psi} + \frac{1}{Pr} \left(\frac{\partial H}{\partial \psi} - \frac{\partial \frac{u^2}{2}}{\partial \psi} \right) + \left(\frac{1}{Sc} - \frac{1}{Pr} \right) \sum_{j=1}^{n} h^j \frac{\partial \alpha^j}{\partial \psi} \right\} \right]$$

Diffusion

(a) Species

$$\frac{\partial \alpha^j}{\partial x} = \frac{1}{\psi^N} \frac{\partial}{\partial \psi} \left[\frac{a}{Sc} \frac{\partial \alpha^j}{\partial \psi} \right] + \frac{\dot{w}^j}{\rho u}$$

(b) Elements

$$\frac{\partial \tilde{\alpha}^k}{\partial x} = \frac{1}{\psi^N} \frac{\partial}{\partial \psi} \left[\frac{a}{Sc} \frac{\partial \tilde{\alpha}^k}{\partial \psi} \right]$$

where

$$a \equiv \rho u \mu \left(\frac{y^2}{\psi} \right)^N$$

2. Transformed Streamfunction Plane

The streamfunction transformation may be written as

$$\int_{\psi_a}^{\psi_b} \psi^N d\psi = \int_{y_a}^{y_b} \rho u y^N dy$$

$$N = \begin{cases} 0 - \text{Planar 2-D Flow} \\ 1 - \text{Axisymmetric Flow} \end{cases}$$

If the initial profile consists of two uniform streams; say hydrogen from $y_1 = 0$ to $y_2 = y_{H_2}$ and oxygen from y_2 to y_3, then the streamfunction can be computed as

$$\frac{\psi_2^{N+1} - \psi_1^{N+1}}{2} = \frac{(\rho u)_{H_2}(y_2^{N+1} - y_1^{N+1})}{2}$$

But $\psi_1 = y_1 = 0$, so that

$$\psi_2 = [(\rho u)_{H_2} y_2^{N+1}]^{\frac{1}{N+1}}$$

$$\psi_2 = y_2 (\rho u)_{H_2}^{\frac{1}{N+1}}$$

For the oxygen stream

$$\psi_3 = [\psi_2^{N+1} + (\rho u)_{O_2}(y_3^{N+1} - y_2^{N+1})]^{\frac{1}{N+1}}$$

Note that for planar 2-D flow, $\frac{1}{N+1} = 1$, the streamfunction is identical to the mass flow rate

$$\psi_2 = (\rho u)_{H_2} y_2(1) = \dot{m}_{H_2}$$

The proper way to model the initial potential core region is to put the bulk of the grid points in the stream for which $\psi_{H_2} = \psi_2$ or $\psi_{O_2} = \psi_3 - \psi_2$ is smallest. Also, it should be noted that ψ_1 may be > 0 and $\psi_{top} < \psi_3$ at the origin, and it is hence possible to concentrate initially on the interface region between the two streams.

The program computational grid will automatically spread out towards $\psi_t = 0$ and ψ_3 as the mixing process occurs downstream. Also, more than two streams may be modeled, as long as sufficient grid points are used; each stream should have a minimum of ten grid points. The interval between grid points, $\Delta\psi$, at $\psi = 0$ is determined by $\Delta\psi = \frac{\psi \text{ Smallest Stream}}{\text{Desired Number of Grid Points}}$.

3. Brief Description of Subroutines

The Flow Chart in Block Diagram form of the Bell Aerospace Combustor Correlation/Prediction Program is presented in Fig. A-1. The important Subroutines are described briefly below:

MAIN

MAIN is used to input the data for each case, initialize the necessary variables, and then to call the true Master subroutine of the program, MARCH. MAIN will also control the FCORE varying of the viscosity level and repetition of a calculation until it converges upon experimental results.

BEGIN

BEGIN is used to store the fits for the thermodynamic data for the chemical species.

PIF1

PIF1 is used to make linear interpolations between two one-dimensional arrays.

HEAT

HEAT is used to (a) compute the enthalpy from the specie mass fractions, thermodynamic fits, and temperature, or (b) invert to obtain the temperature from the enthalpy and specie mass fractions.

DENSE

DENSE is used to compute the mixture density, mass flux, and molecular weight at each point in the flow field.

SED

SED contains the viscosity models and employs the inout specified model.

MARCH

MARCH is the master controlling subroutine of the analysis, and specifies the sequence of operations performed for each step in the axial direction.

STEP

STEP contains the axial step size stability criteria, and computes the axial step size accordingly.

PRINT

PRINT prints out the radial profiles of the independent and dependent variables at all specified axial locations.

CONSRV

CONSRV solves the Conservation Equations for the change in the independent variables (H, u, α^J or $\tilde{\alpha}^k$) across each diffusion step.

GRID

GRID adds mesh grid points, and doubles the interval between grid points, as the calculation proceeds downstream.

BULK

BULK computes bulk properties across the flow field at each axial station

4. Input Format and Deck Organization for IBM 7090

The Input Format required for the Data Deck is shown in Table A-1. As many sets of data (cases) may be run as desired. Only one END card is needed following the last case. The organization of the complete deck for the IBM 7090 is illustrated in Fig. A-2. A sample input for the Bell Coaxial Injector Case 892, ready for key punching, is presented in Table A-2.

5. Output Format and Sample Case

The Output Format is given in Table A-3 and the computer printout obtained for the sample case above is shown in Table A-4. In this printout, ETA PRED computed at the initial axial

station (x=0) and final axial station (x=L) are each given along with F, and ETA for each iteration. When the value of F consistent with the experimental efficiency (ETA) is being determined, more than one iteration is generally required. When only a prediction is desired, the value of ETA must be set to zero and no iterations will be made. In such cases only one computation, which terminates at the axial station just beyond x=L will be made, and the values of ETA PRED are consistent with the input value of F. Note, that when iterations are required to determine the appropriate value of F, the number of the iteration printed out will not be changed in cases in which values of ETA PRED are greater than 99.99%. This procedure simplified considerably the counting procedure and rarely occurs.

6. Computations and Results

The calculations were always begun assuming slug (step) profiles and $Sc_T = 0.7$, $Pr_T = 1.0$. The initial Y_{O_2} profile used to start the computation (x=0) for Rocketdyne Case 12H, Ref. 9, is plotted in Fig. A-3 along with the Y_{O_2} profiles computed at intermediate and final stations of 0.5, 2.5, and 5 in., which were computed using the unreactive mixing calculation discussed in ANALYSIS. Note, that for the binary H_2/O_2 system considered, $Y_{H_2} \equiv 1 - Y_{O_2}$, so that the corresponding Y_{H_2} values can be obtained from the plots as well. The velocity profiles at these same stations are plotted in Fig. A-4. The initial step velocity profiles at x=0 are simply the bulk mean velocities computed using Eq. (9). The Y_{H_2O} profiles computed using either Eq. (5) or (6) are plotted in Fig. A-5 at the same axial stations. As explained in ANALYSIS the water was merely computed from either H_2 or O_2 concentrations (whichever was the limiting reagent), and played no role in the mixing calculation; of course, the Y_{H_2O} profiles were required for the computation of the combustion efficiency, η_{pred}, using Eq. (8). Although more sophisticated computations, e.g., including the finite rate chemistry, are within the capability of the computer program, the success achieved with the very simple approach suggested that expenditure of additional computer time was unwarranted - as long as only the combustion efficiency was to be predicted rather than details of the flow.

The H_2/O_2 mixing computations are well illustrated in Figs. A-3 to A-5. There is gradual mixing of both mass and momentum (stagnation temperature remains constant). As mass mixing proceeds, the computed water level grows, and hence, η_{pred} continually increases [Eq. (8)]. Starting with a given set of initial conditions, there is a one-to-one correspondence between the Y_{H_2O} profiles and η_{pred}. In the iteration to determine the appropriate value of F, the profiles at the final axial station, x=L, are "adjusted" until η_{pred} computed from Eq. (8) yields η_{exp} to within the desired tolerance, e.g., 0.1%.

Values of the turbulent viscosity, i.e., eddy viscosity, ε_η, used throughout the mixing computation for Rocketdyne Tests 12H, 14H, and 18H, Ref. 9, are plotted in Fig. A-6. Note that by assumption ε_η is <u>not</u> a function of radial position, and so is constant at each axial position. These particular test cases were selected because they covered the entire V_R range of the Rocketdyne Coaxial Injector test data; Test 14H is at the maximum of the curve of F vs V_R in Fig. A-7. For comparison, values of ε_{model} computed directly from Eq. (4) are presented in Fig. A-8. Of course, these values are directly proportional to the ε_η's plotted in Fig. A-6 [Eq. (1)]; however, their relative magnitudes are shifted because the F's vary (as do the η's). In view of the erratic behavior of these mixing coefficients, it is very surprising that useful correlations, such as those presented in Fig. A-7 were obtained; however, useful correlations have been obtained for every case to which the technique has been applied.

Table A-1
Bell Aerospace Combustor Correlation Input Format

CARD	NAME	DESCRIPTION	COL	FORMAT
1	TITLE	Input Run Designation, ID, etc	2-72	18A4
2	ETA†	Experimental Combustion Efficiency (%)	1-10	E10.8
	F	Input Correlation Factor	11-20	E10.8
	PC	Input Chamber Pressure (psia)	21-30	E10.8
	L††	Input Chamber Length (in.)	31-40	E10.8
	EL	Input No. of Injector Elements	41-50	E10.8
3	MDOTH2*	Input $\sum \dot{m}_{H_2}$ at Injector (lbm/sec)	1-10	E10.8
	AH2INJ	Input $\sum$ Area H_2 at Injector ($in.^2$)	11-20	E10.8
	TH2	Input $T_{H_2,total}$ (°R)	21-30	E10.8
4	MDOTO2	Input $\sum \dot{m}_{O_2}$ Injector (lbm/sec)	1-10	E10.8
	AO2INJ	Input $\sum$ Area O_2 Injector ($in.^2$)	11-20	E10.8
	TO2	Input $T_{O_2,total}$ (°R)	21-30	E10.8
5	END	Used to Indicate End of Data	1-4	A4

†If ETA=0 predict Combustion Efficiency using input value of the Correlation Factor, F. If ETA>0, e.g., 95%, a value of F consistent with the input ETA will be determined by iteration.

††Length From Injector to Nozzle Throat

*Film Coolant Flow Not Included

BAC 0949 REV. 2/67

COMPUTER INPUT FORM ☐ RUN ☐ HOLD

of _____

IDENT NO.

Table A-2
Sample Input Bell Aerospace Combustor Correlation Computer Program

1 2 3 4 5 | 6 | 7 8 9 10 11 12 13 14 15 16 17 18 19 20 21 22 23 24 25 26 27 28 29 30 31 32 33 34 35 36 37 38 39 40 41 42 43 44 45 46 47 48 49 50 51 52 53 54 55 56 57 58 59 60 61 62 63 64 65 66 67 68 69 70 71 72 | 73 74 75 76 77 78 79 80

4-8-74 BELL 892 COAX

90.9	.05	263.	9.5	19.0
.6987	1.287	523.		
1.8235	.8429	512.		

END

U-V

1 2 3 4 5 | 6 | 7 8 9 10 11 12 13 14 15 16 17 18 19 20 21 22 23 24 25 26 27 28 29 30 31 32 33 34 35 36 37 38 39 40 41 42 43 44 45 46 47 48 49 50 51 52 53 54 55 56 57 58 59 60 61 62 63 64 65 66 67 68 69 70 71 72 | 73 74 75 76 77 78 79 80

Table A-3
Bell Combustor Correlation and Prediction Program

OUTPUT FORMAT

LINE	NAME	FORMAT	DESCRIPTION
1	PROGRAM HEADING		
2	TITLE	18A4	Input Run Designation, ID, etc.
3	ETA	F15.6	Experimental Combustion Efficiency (%)*
	F	F15.6	Input Correlation Factor
	PC	F15.6	Input Chamber Pressure (psia)
	L	F15.6	Input Chamber Length (in.)
	EL	F15.6	Input No. of Injector Elements
	VRINJ	F15.6	Velocity at H_2/Velocity O_2 Injector
	OFINJ	F15.6	O_2/H_2 Mass Flow Ratio at Injector
	R1IN	F15.6	Radius of Central Jet (effective radius if not axisymmetric injector)(in.)
4	MDOTH2	F15.6	Input $\sum \dot{m}_{H_2}$ at Injector (lbm/sec)
	AH2INJ	F15.6	Input $\sum$ Area H_2 at Injector ($in.^2$)
	TH2	F15.6	Input $T_{H_2,total}$ (°R)
	MDOTH2/EL	F15.6	$\sum \dot{m}_{H_2}$/Injector Element (lbm/sec-element)
	AH2INJ/EL	F15.6	$\sum$ Area H_2/Injector Element ($in.^2$/element)
	UH2INJ	F15.6	H_2 Jet Velocity (in annulus)(ft/sec)
5	MDOTO2	F15.6	Input $\sum \dot{m}_{O_2}$ Injector (lbm/sec)
	AO2INJ	F15.6	Input $\sum$ Area O_2 Injector ($in.^2$)
	TO2	F15.6	Input $T_{O_2,total}$ (°R)
	MDOTO2/EL	F15.6	$\sum \dot{m}_{O_2}$/Injector Element (lbm/sec-element)
	AO2INJ/EL	F15.6	$\sum$ Area O_2/Injector Element ($in.^2$/element)
	UO2INJ	F15.6	O_2 Jet Velocity (central jet)(ft/sec)
6	X	F15.4	Axial Station (in.)
	L	F15.2	Input Chamber Length (in.)
	F	F15.6	Input Correlation Factor
	ETA PRED	F15.3	Computed/Predicted Combustion Efficiency (%)
	ETA	F15.1	Experimental Combustion Efficiency (%) (repeated for comparison)
	ITER	I9	No. of iteration when input ETA>0; otherwise blank

*If ETA=0 predict Combustion Efficiency using input value of the Correlation Factor, F. If ETA>0, e.g., 95%, a value of F consistent with the input ETA will be determined by iteration.

Table A-4
Sample Printout

GASEOUS HYDROGEN/OXYGEN ROCKET PERFORMANCE CORRELATION AND PREDICTION PROGRAM

4-8-74 BELL H2 COAX

ETA	F	PC	L	EL	VRINJ	UFINJ	RIIA
0.909000	0.050000	203.000000	9.500000	19.000000	4.004524	2.009847	0.118769

MDOTH2	AH2INJ	TH2	MDOTH2/EL	AH2INJ/EL	LH2INJ
0.699700	1.287000	523.000000	0.036774	0.067737	827.362599

MDOTO2	AO2INJ	TO2	MDOTO2/EL	AO2INJ/EL	LO2INJ
1.823500	0.842000	512.000000	0.095974	0.044316	203.557165

X	L	F	ETA PREC.	ETA	ITER
0.		0.050000	0.		
9.5105	9.50	0.050000	88.287	90.9	0
0.		0.057121	0.		
9.5115	9.50	0.057121	90.595	90.9	1
0.		0.058112	0.		
9.5190	9.50	0.058112	90.937	90.9	2

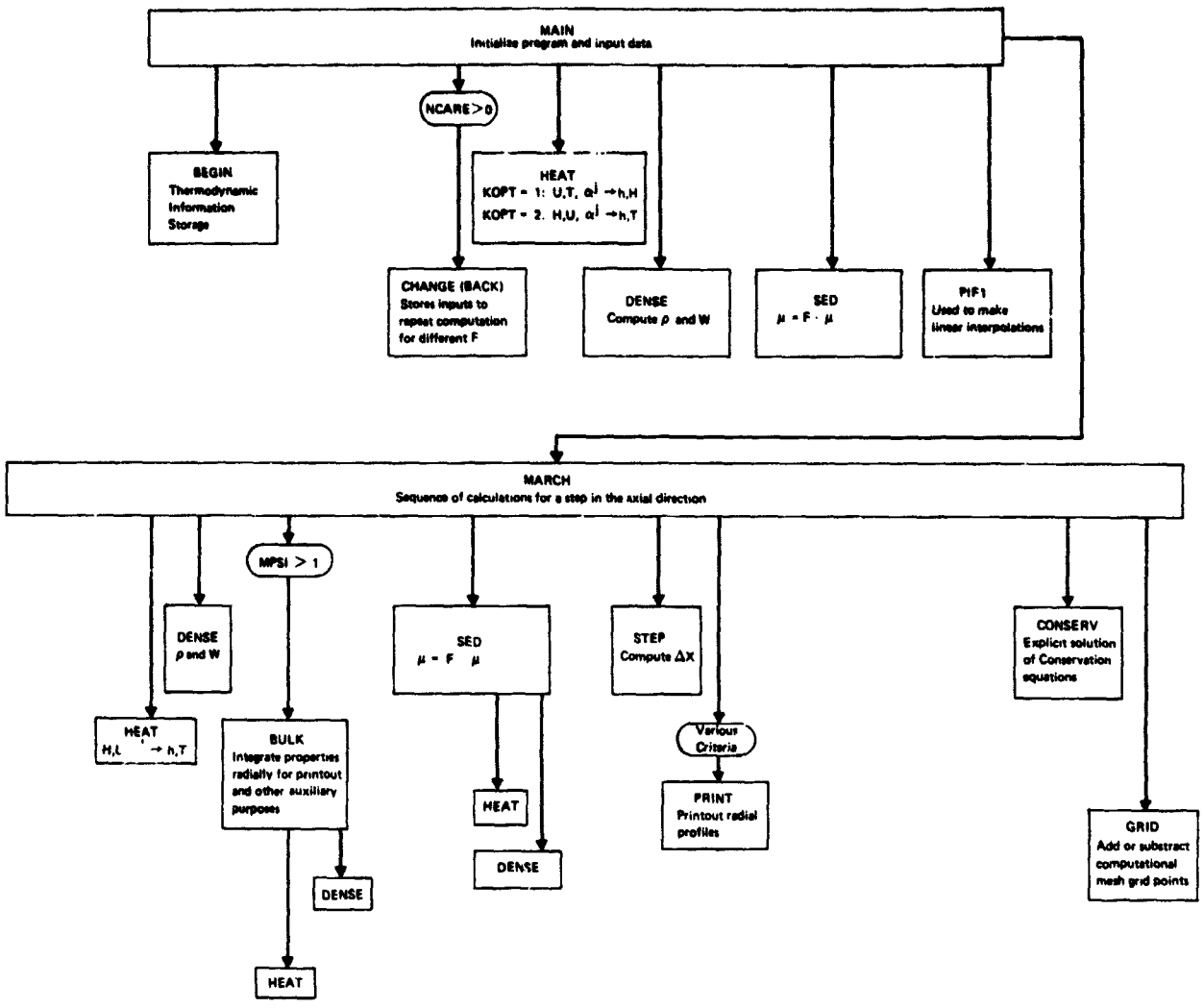

Figure A-1. Block Diagram - Bell Aerospace Combustor Correlation Computer Program

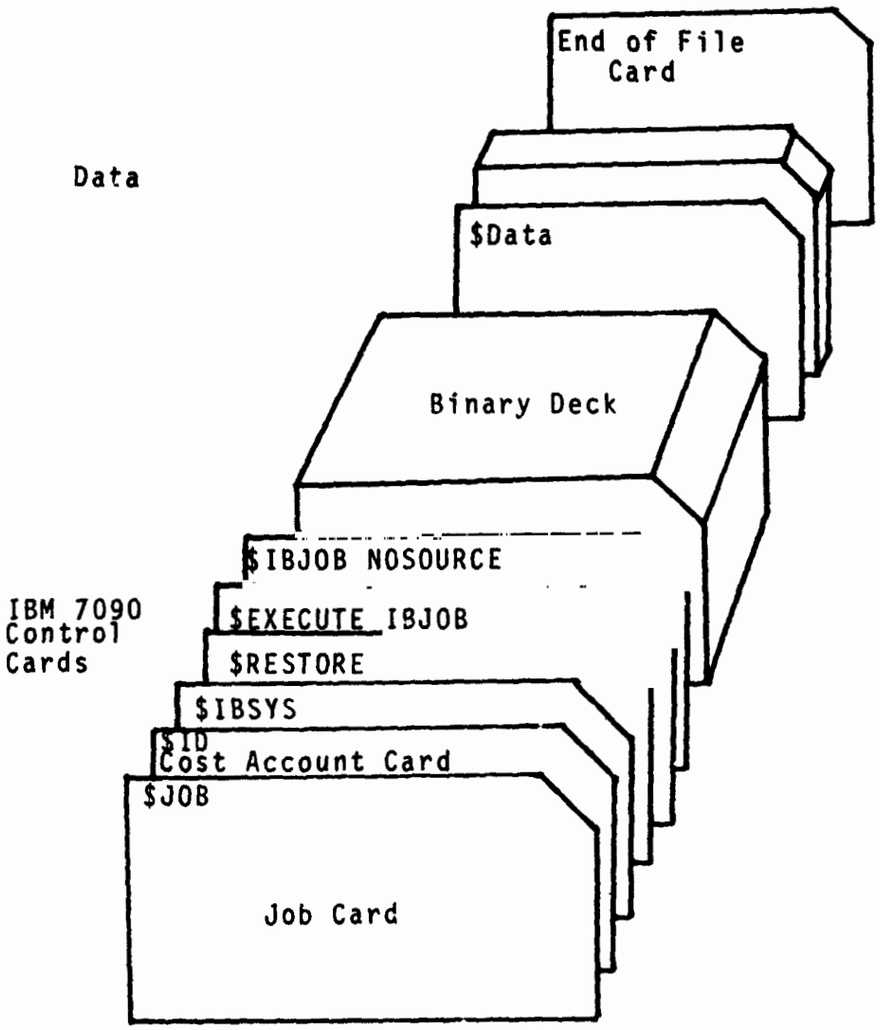

Figure A-2 - The Bell Aerospace Combustor Correlation Deck Organization for the IBM 7090

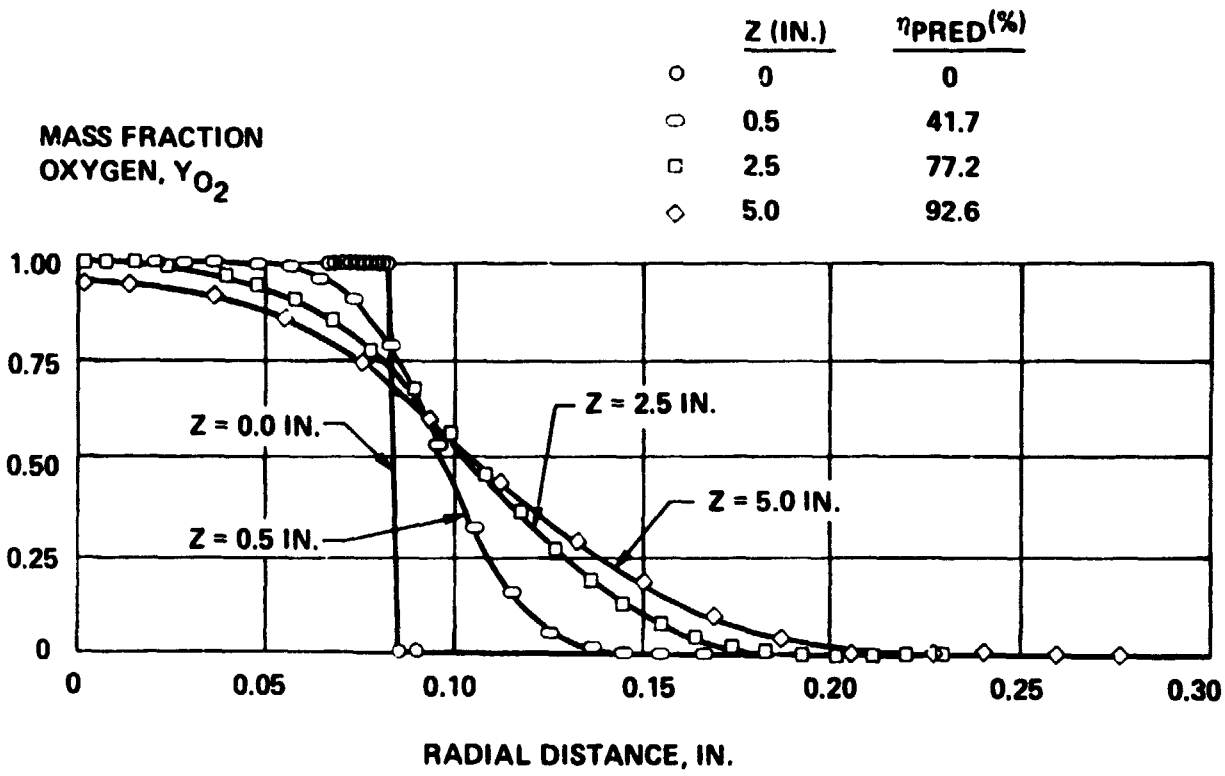

Figure A-3. Mass Fraction Oxygen at Various Axial Stations Computed using ϵ_η of Figure A-6 Rocketdyne Coaxial Injector Test 12H, Ref. 9

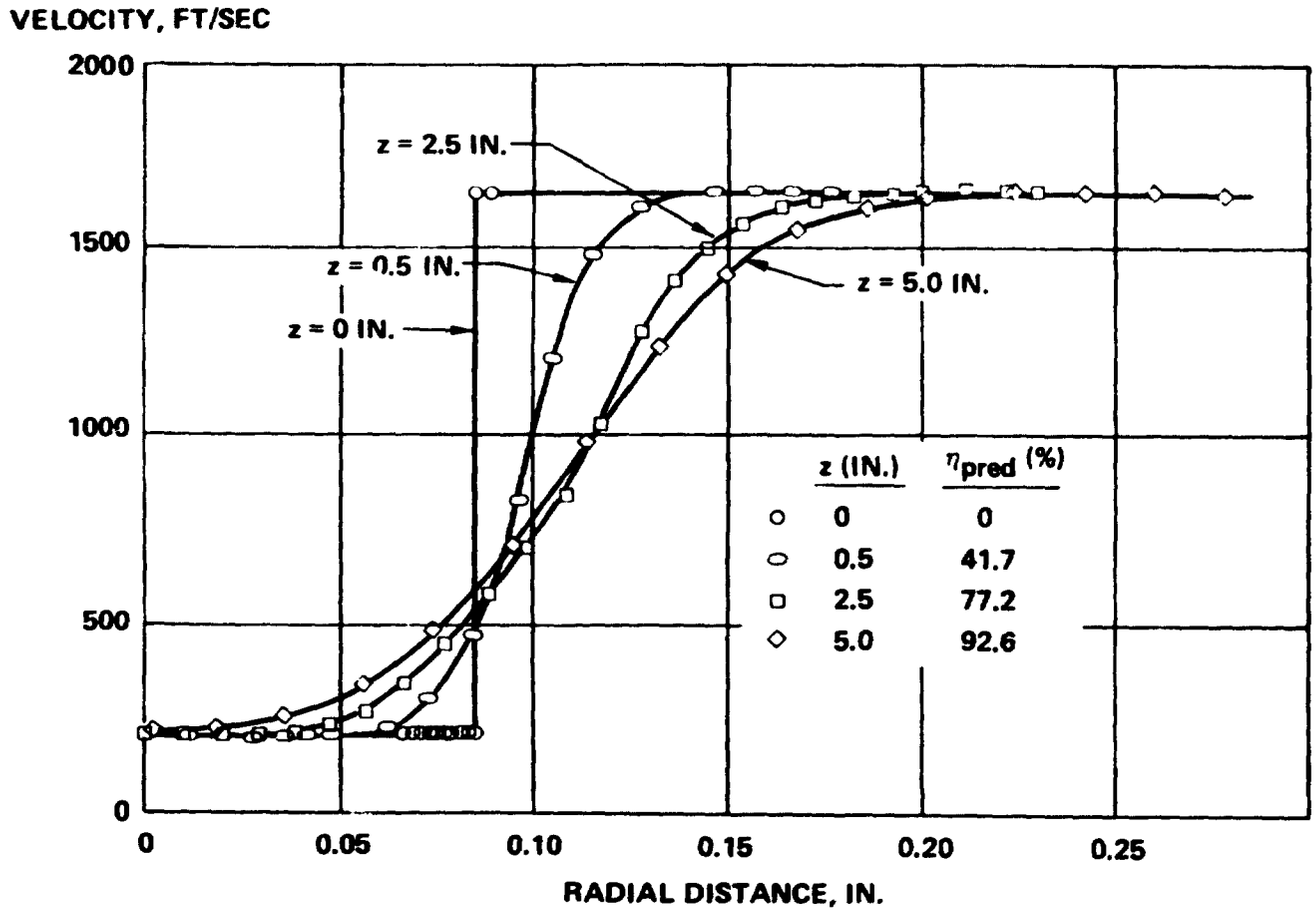

Figure A-4. Velocity Profiles at Various Axial Stations Computed using ϵ_η of Fig. A-6 Rocketdyne Coaxial Injector Test 12H, Ref. 9

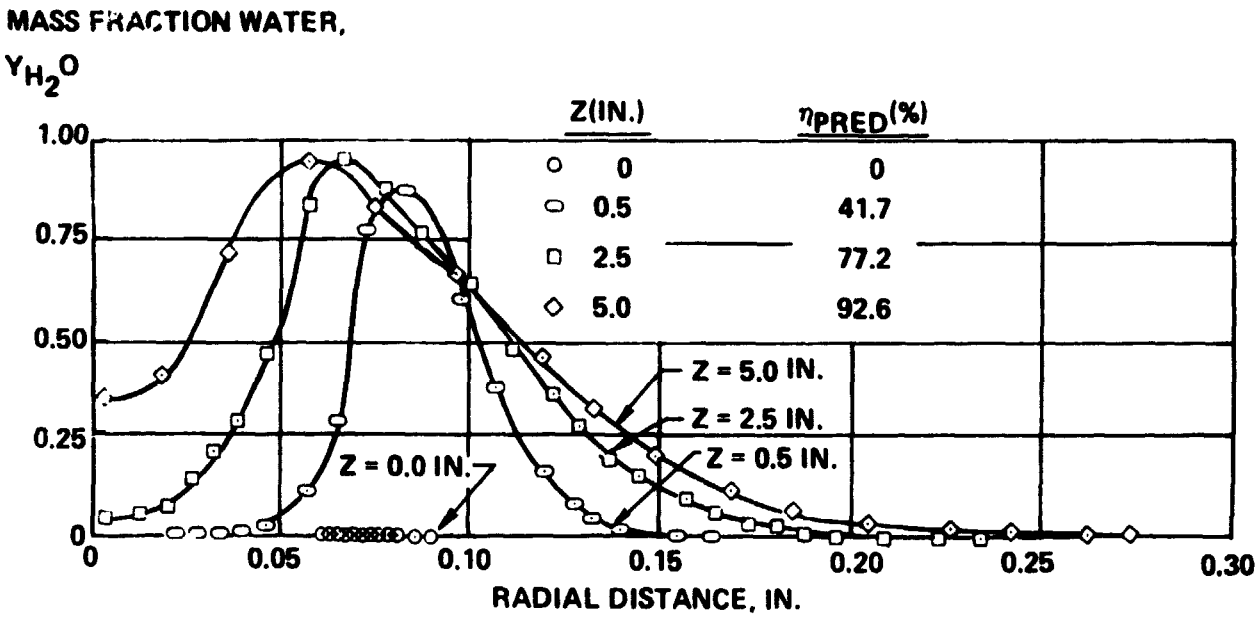

Figure A-5. Water Profiles at Various Axial Stations Computed using Eqs (5) and (6) - Rocketdyne Coaxial Injector Test 12H, Ref 9

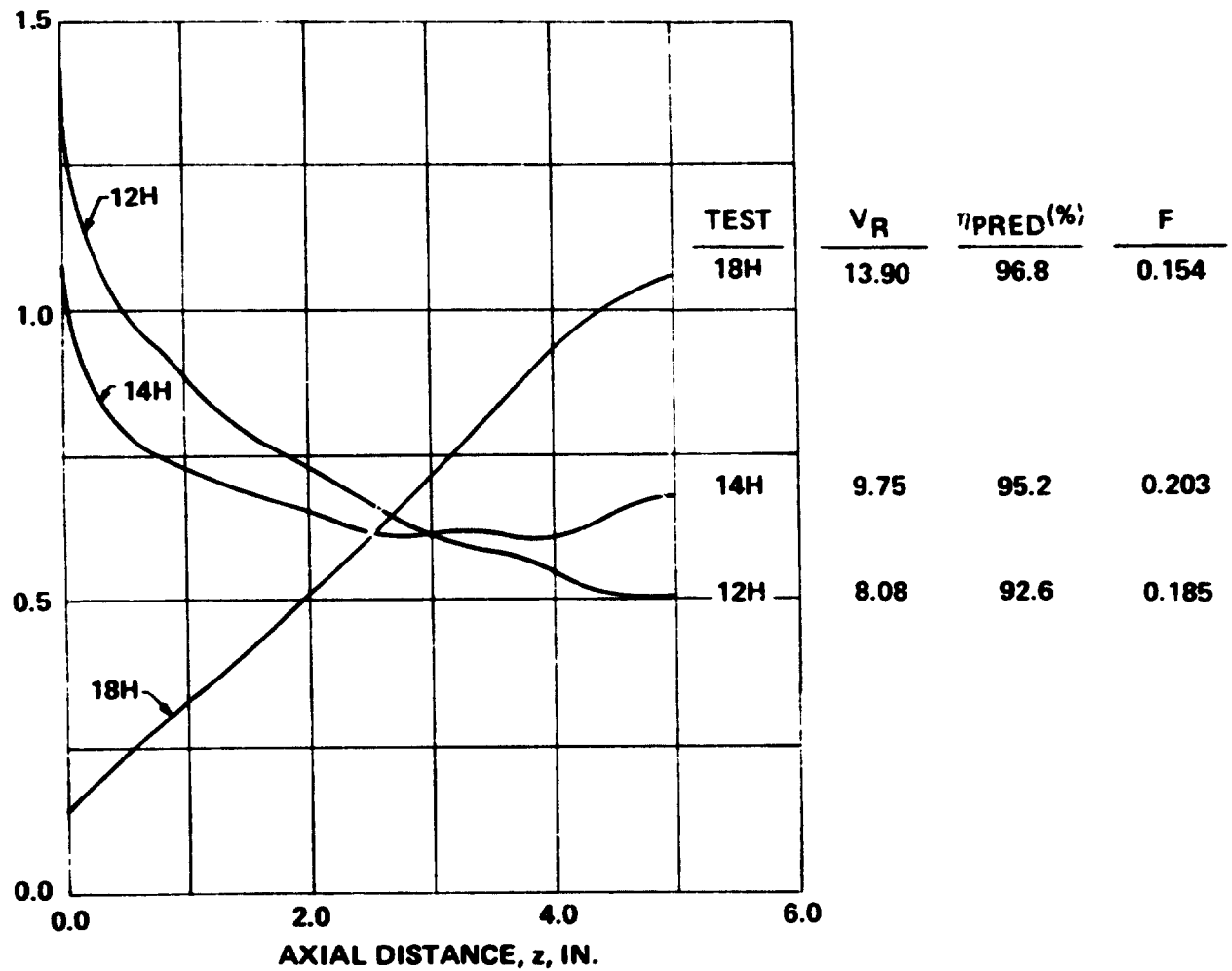

Figure A-6. Value of Turbulent (Eddy) Viscosity used in η Computation for Rocketdyne Coaxial Injector Tests 12H, 14H, and 18H. Ref. 9

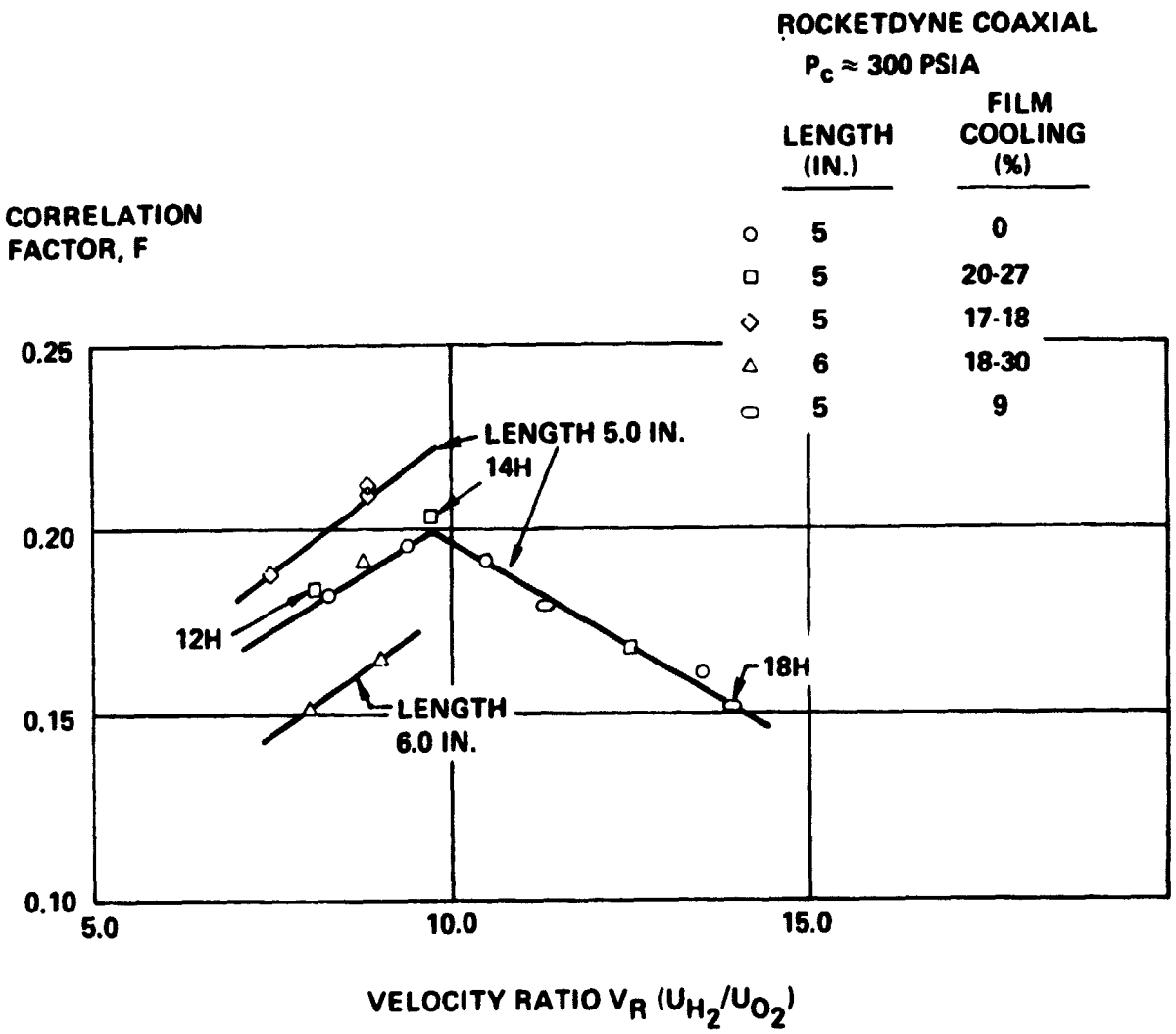

Figure A-7. Correlation of Rocketdyne Coaxial Injector Performance Data, Ref 9

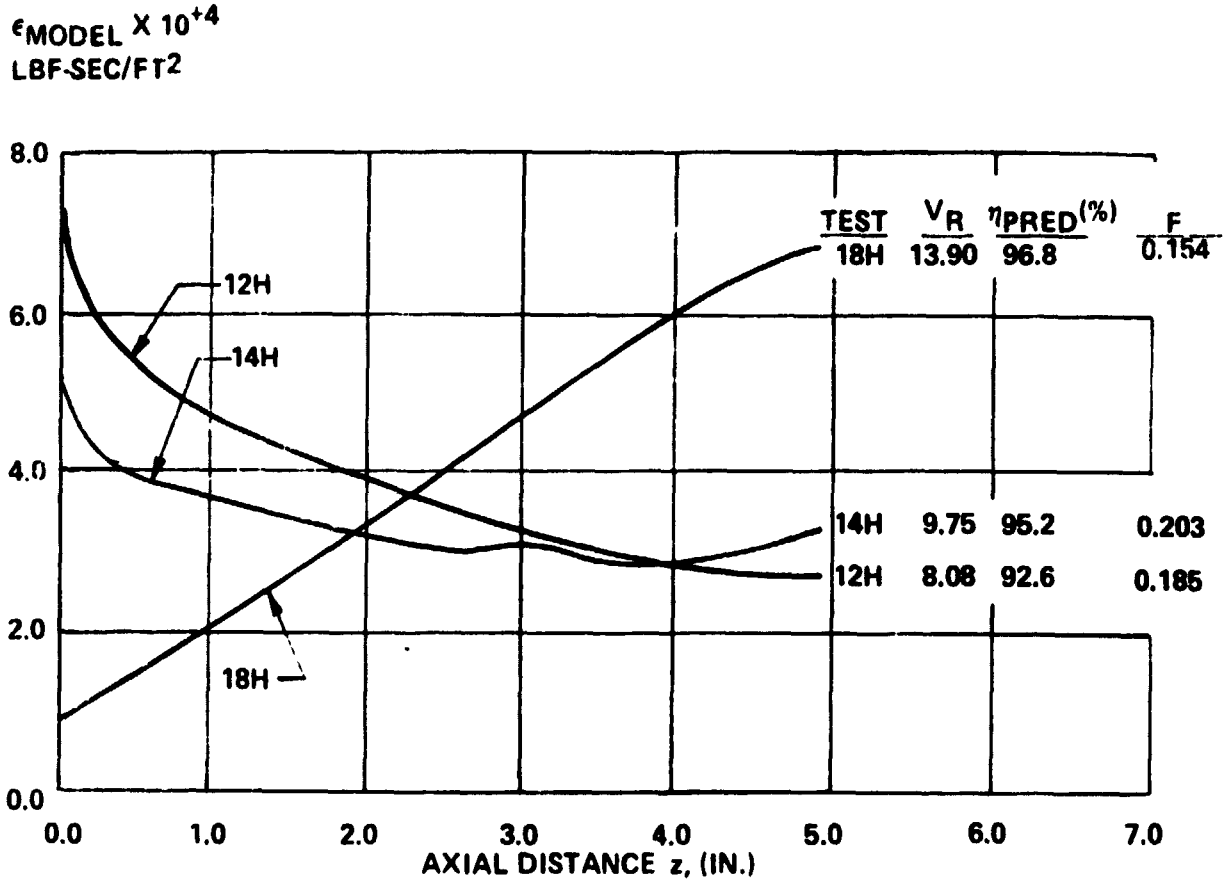

Figure A-8. Comparison of Predictions of Mixing Model, [Eq. (4)] for Rocketdyne Coaxial Injector Tests 12H, 14H, and 18H, Ref. 9

NOMENCLATURE

A	Area, ft^2
$\sum A$	Total injection area for a particular propellant, ft^2
D_ρ	Empirical density parameter ($\equiv \rho_u/\rho_{min}$)$^{1.5}$
EL	Number of injector elements
F	Correlation Factor ($\equiv \varepsilon_\eta/\varepsilon_{model}$)
f	Empirical length parameter ($\equiv 0.5 + 0.005\bar{z}$; $\bar{z} < 100$, and 1.0; $\bar{z} \geq 100$)
G	Total mass flow rate of gaseous propellant measured at injector, lbm/sec
L	Length of combustion chamber (injector to nozzle throat), ft
M	Mach number
MW	Molecular weight, lbm/lb-mole
$\dot{m}$	Computed mass flow rate, lbm/sec
P	Static pressure, lbf/ft^2
P_c	Chamber pressure, lbf/ft^2
P_c'	Static pressure during hot film calibration, lbf/ft^2
P_o	Total pressure, lbf/ft^2
Pr_T	Turbulent Prandtl number
R	Universal gas constant, 1545 ft-lbf/lb-mole-°R
R_1	"Effective" radius of central oxidizer injector, defined in Eq. (11), ft
R_2	"Effective" radius of annular fuel injector, defined in Eq. (12), ft
r	Radial coordinate, ft
Sc_T	Turbulent Schmidt number
T	Static temperature, °R

T_o	Total or stagnation temperature, °R
U	Axial velocity, ft/sec
$\bar{U}$	Time mean (average) velocity, ft/sec
$\sqrt{u^2}$	Turbulence intensity, ft/sec
$\bar{V}$	Indicated mean velocity (hot film), ft/sec
V_R	Velocity ratio ($\equiv U_{H_2}/U_{O_2}$)
Y	Mass fraction
z	Axial coordinate, ft
$\bar{z}$	Normalized axial coordinate ($\equiv z/2R_1$)
γ	Ratio of specific heats
ε_{model}	Turbulent (eddy) viscosity predicted by Eq. (4), lbm/sec-ft
ε_η	Turbulent (eddy) viscosity used in computation of η_{pred} ($\equiv F\varepsilon_{model}$), lbm/sec-ft
η_{exp}	Experimentally determined combustion efficiency
η_{pred}	Combustion efficiency predicted using computer program
ρ	Density, lbm/ft^3
ρ_c	Density during calibration of hot film, lbm/ft^3

Subscripts

e	External or freestream conditions
i	Central or inner
L	Splitter plate or land
o	Annular or outer
u	Condition at velocity half radius where $\bar{U} \equiv 0.5(U_{max} + U_{min})$
∞	Freestream condition

REFERENCES

1. Swithenbank, J., "The Unknown Fluid Mechanics of Combustion," Fluid Mechanics of Combustion, American Society of Mechanical Engineers, New York, May 1974, pp. 1-6.

2. Morgenthaler, J. H., "Turbulent Mixing and Reacting Flow Characterization," Fluid Mechanics of Combustion, American Society of Mechanical Engineers, New York, May 1974, pp. 21-34.

3. Zelazny, S. W., Morgenthaler, J. H., and Herendeen, D. L., "Reynolds Momentum and Mass Transport in Axisymmetric Coflowing Streams," Proceedings of the 1970 Heat Transfer and Fluid Mechanics Institute, Stanford University Press, June 1970, pp. 135-152.

4. Morgenthaler, J. H., Zelazny, S. W., "Predictions of Axisymmetric Free Turbulent Shear Flows Using a Generalized Eddy-Viscosity Approach," Free Turbulent Shear Flows, Vol. I - Conference Proceedings, NASA SP-321, July 1972, pp. 277-326.

5. Zelazny, S. W., Morgenthaler, J. H., and Herendeen, D. L., "Shear Stress and Turbulence Intensity Models for Coflowing Axisymmetric Streams," AIAA Journal, Vol. 11, No. 8, August 1973, pp. 1165-1173.

6. Morgenthaler, J. H., Zelazny, S. W., and Herendeen, D. L., "Combustor Correlation Technique," AIAA Paper No. 72-1074, AIAA/SAE 8th Joint Propulsion Specialist Conference, New Orleans, Louisiana, November 1972.

7. Morgenthaler, J. H. and Rudinger, G., "High Speed Turbulent Mixing and Combustion," AFOSR-TR-74-0228, November 1973.

8. Zeiberg, S. L. and Bleich, G. D., "Finite Difference Calculation," AIAA Journal, Vol. 2, No. 8, 1964, pp. 1396-1402.

9. "Hydrogen-Oxygen APS Engines, Volume I: High Pressure Thruster," Rocketdyne Final Report, February 1973, NASA CR-120805 (R-8837-1).

10. "Hydrogen-Oxygen Auxiliary Propulsion for the Space Shuttle, Volume I: High Pressure Thrusters," Aerojet Liquid Rocket Company Final Report, 30 January 1973, NASA CR-120895.

11. "High Pressure Reverse Flow APS Engine," Bell Aerospace Report No. 8636-950004, November 1972, NASA CR-120881.

12. "Hydrogen-Oxygen Catalytic Ignition and Thruster Investigation," Volume I - Catalytic Ignition and Low Pressure Thruster Evaluation, NASA CR-120869, Volume II - High Pressure Thruster Evaluations, NASA CR-120870, TRW Final Reports, November 1972.

13. "O_2/H_2 Coaxial Injector, 1000 lb-F, 250 P_c," BAC IR&D Report Model 8618, 21 May 1970, & "Low P_c Gaseous O_2/H_2 Performance Evaluation Program," BAC IR&D Report, Model 8616, 12 May 1970.

14. "Space Shuttle Hypergolic Bipropellant RCS Engine Design Study," May 1974, Contract NAS9-12996, Bell Aerospace Report No. 8701-910041.

15. "Bell Aerospace Company Monthly progress Report No. 14 for Space Shuttle Orbit Maneuvering Engine, Reusable Thrust Chamber Program," Contract NAS9-12803, Bell Aerospace Report No. 8693-933014, September 1973.

16. Stark, S. B., "Mixing of Gas Streams in a Flame," Zhurnal Tecknicheskoy Fisiki, Vol. 23, No. 10, 1953, p. 1802.

17. Arutyunov, V. A., "Concerning Mixing Processes in Coaxial Turbulent Streams," Izvestiya Vysshikh Uchebnykh Zavedeniy, Vol. 11, 1963, p. 207.

18. Chigier, N. A., and Beer, J. M., "The Flow Region Near the Nozzle in Double Concentric Jets," Journal of Basic Engineering, Trans. ASME, Series D, Vol. 86, No. 4, December 1963, p. 797.

19. Champagne, F. H., and Wygnanski, I. J., "An Experimental Investigation of Co-Axial Jets," International Journal of Heat and Mass Transfer, Vol. 14, 1971, p. 1445.

20. Durao, D. and Whitelaw, J. H., "Turbulent Mixing in the Developing Region of Coaxial Jets," ASME Paper No. 73-FE-19, June 1973.

21. Schlichting, H., Boundary Layer Theory, McGraw-Hill, 1960, p. 504.

22. Ricou, F. D., Spalding, D. B., "Measurements of Entrainment by Axisymmetrical Turbulent Jets," Journal of Fluid Mechanics, Vol. 11, No. 21, 1961.

23. Edelman, R., and Fortune, O., "An Analysis of Mixing and Combustion in Ducted Flows," AIAA preprint 68-114, 1968.

24. Peters, C. E., Phares, W. J., and Cunningham, T. H. M., "Theoretical and Experimental Studies of Ducted Mixing and Burning of Coaxial Streams," AIAA preprint 69-85, 1969.

25. Bradshaw, P., Ferris, D. H., and Atwell, N. P., "Calculation of Boundary-Layer Development Using the Turbulent Energy Equation," Journal of Fluid Mechanics, Vol. 28, No. 3, 1967, pp. 593-616.

26. Lee, S. C., and Harsha, P. T., "The Use of Turbulent Kinetic Energy in Free Mixing Studies," AIAA preprint 69-683, 1969.

27. Donaldson, C. duP., and Rosenbaum, H., "Calculation of Turbulent Shear Flows Through Closure of the Reynolds Equations by Invariant Modeling," ARAP Inc., Report 127, 1968.

28. Gosman, A. D. et al, Heat and Mass Transfer in Recirculating Flow, Academic Press, London, 1969.

29. Launder, B. E., Morse, A., Rodi, W., and Spalding, D. B., "Prediction of Free Shear Flows - A Comparison of the Performance of Six Turbulence Models," Free Turbulence Shear Flows, Volume I - Conference Proceedings, pp. 361-422, NASA SP-321, July 1972.

30. Zelazny, S. W., "Modeling of Turbulent Axisymmetric Co-flowing Streams and Quiescent Jets: A Review and Extension," PhD Dissertation, University of Buffalo, September 1972.